UNIVERSIDADE DA BEIRA INTERIOR
Engenharia

Cellular Planning and Optimization for 4G and 5G Mobile Networks

Anderson Rocha Ramos

Dissertação para obtenção do Grau de Mestre em

Engenharia Eletrotecnica e Computadores

(2º ciclo de estudos)

Orientador: Prof. Doctor Fernando J. Velez

Covilhã, Junho de 2019

I would like to dedicate this dissertation to my family, especially to my mother, Angelita Silva da Rocha and my sister Selma Rocha Ramos, who helped in every step of my journey and supported me in the moments of need. It was only thanks to their help that I could get where I am today.

Acknowledgements

I would like to thank my adviser, Dr. Fernando J. Velez, for all the knowledge and guidance he provided during this journey. I also want to thank several friends that helped me with the work that will be presented in the following pages and highlight that this work would not be possible without their help. First of all I would like to thank the engineer Rui Paulo for the support, friendship, and for his help with the work involving the LTE-Sim, for the knowledge he shared and for the codes he provided that made it possible to perform most of the simulations done with LTE-Sim. To Bruno Cruz for his friendship during all my time in Portugal and for the help he provided with the code he developed that were key to the results that will be shown in this thesis. To my great Brazilian friend Rooderson Andrade, who not only helped me with the knowledge about MIMO but also supported me in all moments. To Marisa Lourenço, my college at the Instituto de Telecomunicações who helped a lot with the work performed with Matalab.To Emanuel Teixeira for his support in several aspects of this work, specially with the work involving Matlab. To Emanuel Mahina, another college from the Instituto de Telecomunicações whose friendship and insights were of paramount importance. To all the teachers I had during this Master course and that guided me through the different areas of knowledge that contributed to this work. Finally, I would like to thank the Instituto de Telecomunicações for the opportunity, and for the scholarship supported by National Founding from FCT through CONQUEST (CMU/ECE/$030/2017$), for the support provided via National Founding from FCT through the UID/EEA/50008/2013, and as well as for the equipment provided by ORCIP (CENTRO-01-0145-FEDER-022-141) and for the support from COST CA 15104.

Abstract

Cellular planning and optimization of mobile heterogeneous networks has been a topic of study for several decades with a diversity of resources, such as analytical formulations and simulation software being employed to characterize different scenarios with the aim of improving system capacity. Furthermore, the world has now witnessed the birth of the first commercial 5G New Radio networks with a technology that was developed to ensure the delivery of much higher data rates with comparably lower levels of latency. In the challenging scenarios of 4G and beyond, Carrier Aggregation has been proposed as a resource to allow enhancements in coverage and capacity. Another key element to ensure the success of 4G and 5G networks is the deployment of Small Cells to offload Macrocells. In this context, this MSc dissertation explores Small Cells deployment via an analytical formulation, where metrics such as Carrier plus Noise Interference Ratio, and physical and supported throughput are computed to evaluate the system´s capacity under different configurations regarding interferers positioning in a scenario where Spectrum Sharing is explored as a solution to deal with the scarcity of spectrum. One also uses the results of this analyses to propose a cost/revenue optimization where deployment costs are estimated and evaluated as well as the revenue considering the supported throughput obtained for the three frequency bands studied, i.e., 2.6 GHz, 3.5 GHz and 5.62 GHz. Results show that, for a project life time of 5 years, and prices for the traffic of order of 5€ per 1 GB, the system is profitable for all three frequency bands, for distances up to 1335 m. Carrier Aggregation is also investigated, in a scenario where the LTE-Sim packet level simulator is used to evaluate the use of this approach while considering the use of two frequency bands i.e., 2.6 GHz and 800 MHz to perform the aggregation with the scheduling of packets being performed via an integrated common radio resource management used to compute Packet Loss Ratio, delay and goodput under different scenarios of number of users and cell radius. Results of this analysis have been compared to a scenario without Carrier Aggregation and it has been demonstrated that CA is able to enhance capacity by reducing the levels of Packet Loss Ratio and delay, which in turn increases the achievable goodput.

Keywords

4G, 5G, HetNet, LTE, propagation model, Small Cell, Spectrum Sharing

Resumo

O planeamento e otimização de redes de redes celulares heterogéneas tem sido um tópico de investigação por várias décadas com diversas abordagens que incluem formulações analíticas e softwares de simulação, sendo aplicados na caracterização de diferentes cenários, com o objetivo de melhorar a capacidade de sistema. Além disso, o mundo testemunhou o nascimento das primeiras redes 5G New Radio, com uma tecnologia que foi desenvolvida com o objetivo de garantir taxas de transferência de dados muito superiores, com níveis de latência comparativamente inferiores. Neste cenário de desafios pós-4G, a agregação de Espectro tem sido proposta como uma solução para permitir melhorias na cobertura e capacidade do sistema. Outro ponto para garantir o sucesso das redes 5G é a utilização de Pequenas Células para descongestionar as Macro células. Neste contexto, esta dissertação de mestrado explora a utilização de Pequenas Células através de uma formulação analítica, onde se avaliam métricas como a relação portadora-interferência-mais-ruído, débito binário e débito binário suportado, sob diferentes configurações de posicionamento de interferentes em cenários onde a partilha de espectro é explorada como uma solução para enfrentar a escassez de espectro. Os resultados dessa análise são também considerados para propor uma otimização de custos/proveitos, onde os custos de implantação são estimados e avaliados, assim como os proveitos ao se considerar o débito binário suportado obtido para as três bandas de frequência em estudo, a saber, 2.6 GHz, 3.5 GHz e 5.62 GHz. Os resultados demonstram que, para um tempo de vida do projeto de 5 anos, e para preços de tráfego de cerca de 5 € por GB, o sistema é lucrativo para as três bandas de frequência, para distâncias até 1335 m. Também se investiga a agregação de espectro recorrendo ao simulador de pacotes LTE-Sim para avaliar o uso de duas bandas de frequência, a saber, 2.6 GHz e 800 MHz, considerando agregação com a calendarização de pacotes por meio de um gestor comum de recursos de rádio integrado, utilizado para computar a taxa de perda de pacotes, o atraso e o débito binário na camada de aplicação, em cenários com diferentes valores de número de utilizadores e raios das células. Os resultados dessa análise foram comparados com o desempenho de um cenário sem agregação. Foi demonstrado que a agregação é capaz de aumentar a capacidade de sistema, ao reduzir os níveis de perda de pacotes e do atraso, o que por sua vez possibilita a elevação dos níveis de débito binário atingidos.

Palavras-chave

4G, 5G, HetNet, LTE, Modelos de propagação, Pequenas Células, Partilha de Espectro

Table of Contents

List of Figures

List of Tables

List of Acronyms

1G	First Generation
3G	Third Generation
4G	Fourth Generation
5G	Fifth Generation
3GPP	Generation Partnership Project
AMF	Access Mobility Functions
AMPS	Advance Mobile Phone System
ARIB	Association of Radio Industries and Businesses
ATIS	Alliance for Telecommunications Industry Solutions
BER	Bit Error Rate
BMBS	Basic Multi-Band Scheduler
BS	Base Station
CA	Carrier Aggregation
CBR	Constant Bit Rate
CC	Carrier Component
CCSA	China Communications Standards Association
CDMA	Code Division Multiple Access
CNIR	Carrier to Noise plus Interference Ratio
CoMP	Coordinated Multipoint Transmission and Reception
COST	European Cooperation in Science and Technology
CP	Cyclic Prefix
CP-OFDM	Cyclic Prefix Orthogonal Frequency Division Multiplexing
CQI	Channel Quality Indicator
CSI	Channel State Information
CSI-RS	Channel State Information Reference Signal
CT	Core Network and Terminals
DL	Downlink
DM-RS	Demodulation Reference Signal
DwPTS	DL Pilot Time Slot
eICIC	enhanced Inter-Cell Interference Coordination
eLAA	enhanced Licensed Assisted Access
eLTE	enhanced Long Term Evolution

EMBS	Enhanced Multi Band Scheduler
eNB	evolved Node B
EPC	Evolved Packet Core
ePDCCH	enhance Physical Downlink Control Channel
EPS	Evolved Packet System
ETIS	European Telecommunications Standards Institute
E-UTRA	Evolved Universal Terrestrial Radio Access
FDD	Frequency Division Duplexing
FDTD	Finite-Difference Time-Domain
FR1	Frequency Range 1
FR2	Frequency Range 2
gNB	Next Generation Node B
GMBS	General Multi Band Scheduler
GP	Guard Period
GSM	Global System for Mobile Communications
HetNets	Heterogeneous Networks
IEEE	Institute of Electrical and Electronics Engineers
IGP	Integer Programing
IMT	International Mobile Telecommunications
IoT	Internet of Things
IP	Internet Protocol
IPv4	Internet Protocol version 4
IPv6	Internet Protocol version 6
IT	Instituto de Telecomunicações
ITU	International Telecommunication Union
LBR	Low-Power Border Router
LTE	Long Term Evolution
LTE-A	Long Term Evolution -Advanced
LTE-U	Long Term Evolution -Unlicensed
MCN	Macro Cell Network
MCS	Modulation Code Scheme
MIMO	Multiple Input Multiple Output
M-LWDF	Modified-Largest Weighted Delay First
mmWave	Millimeter Wave
NB-IoT	Narrowband IoT

NF	Network Functions
NMT	Nordic Mobile Telephone
NR	New Radio
NTT	Nippon Telephone and Telegraph
OFDM	Orthogonal Frequency Division Multiplexing
OFDMA	Orthogonal Frequency Division Multiple Access
PDCCH	Physical Downlink Control Channel
PDU	Protocol Data Unit
PDSCH	Physical Downlink Shared Channel
PF	Profit Function
PLMN	Public Land Mobile Network
PLR	Packet Loss Ratio
PUCCH	Physical Uplink Control Channel
PUSCH	Physical Uplink Shared Channel
QoS	Quality of Service
RAN	Radio Access Network
RAT	inter-Radio Access Technology
Rel	Release
RF	Radio Frequency
RS	Reference Signal
SA	Systems Aspects
SSB	Single Band Side
SSC	Session and Service Continuity
SC	Small Cell
SCS	Sub Carrier Spacing
SINR	Signal to Interference and Noise Ratio
SMF	Section Management Function
S-NSSAI	Single - Network Slice Selection Assistance Information
SRS	Sounding Reference Signal
TBS	Transport Block Size
TDD	Time Division Duplexing
TDMA	Time Division Multiple Access
TNL	Transport Network Layer
TSDS	Telecommunications Standards Development Society
TTA	Telecommunications Technology Association

TTC	Telecommunication Technology Committee
UE	User Equipment
UL	Uplink
UMTS	Universal Terrestrial Mobile System
UpPTS	UL Pilot Time Slot
USIM	Universal Subscriber Identity Module
VoIP	Voice over IP
VPLMN	Visited Home Public Land Mobile Network
WLAN	Wireless Local Area Network

Chapter 1

Introduction

1.1 Motivation

The exponential growth of machine-to-machine communications and the continuous development of bandwidth-demanding applications have created a scenario where the cellular networks are approaching their edge [1]. This scenario has created in increasing interest in researches about the deployment of Small Cell (SC) access points to ensure extended coverage and link budget. In this scenario of Heterogeneous Networks (HetNets) there is a variety of small range cells that underlays the Macro Cell Network (MCN) and this approach can enhance coverage and spatial reuse allowing cellular systems to deliver higher data rates preserving mobility and connectivity. Carrier Aggregation (CA) has been adopted for operator to address the growing challenges surrounding high data demand in mobile communications and it can be deployed in both Frequency-Division Duplexing (FDD) and Time-Division Duplexing (TDD) frame structure allowing for the increase of transmission bandwidth over those that can be supported by a single channel or carrier. CA plays a key role in the Long Term Evolution Advanced (LTE-A) meeting requirements for large transmissions width (40 MHz-100 MHz) and high peak data rates of 500 Mbps in the uplink (UL) and 1 Gbps in the downlink (DL) [2]. Also, in 2018 the 3^{rd} Generation Partnership Project (3GPP) finished the technical specifications for 5G New Radio (NR), and the first commercial 5G networks started to operate in the first semester of 2019. The technology of 5G NR will allow for significantly more faster wireless communication and will greatly improve the subscriber's experiences, by delivering much higher data rates in both uplink and downlink direction. New Radio is expected to make extensive use of CA and SC deployment as well as Multiple Input Multiple Output (MIMO) alongside other technologies, what brings further importance to the study of SCs deployment scenarios. All this context motivates the research presented in this master thesis, where one CA and SCs deployment are investigated through analytical formulations and simulations. The technical specifications 5G are also explored as a first step towards the expansion of the research performed by IT in the direction of the upcoming technology.

1.2 State of the Art

1.2.1 Evolution of Mobile Communications

In the study of the evolution of mobile communications, the cellular wireless generation (G)is a term used to characterize the changes in the services provided by the operators and incorporation of new technologies, such as new frequency bands or frame structures [3]. In this sense, one can sumarize the steps in this evolution process as follows:

- First Generation (1G) characterized by the use of analog networks;
- Second Generation (2G) with the introduction of digital multiple access technologies;
- Third Generation (3G) with support to multimedia services;
- Fourth Generation (4G);
- Fifth Generation (5G) New Radio.

The first cellular system of what would latter be known as 1G began its operation in 1979 in Tokyo, Japan, deployed by Nippon Telephone and Telegraph (NTT). It was characterized by the use of analog communication systems to transmit voice data, using Frequency-Division Multiple Access (FDMA) to modulate signals in frequencies of about 150 MHz [4]. Several 1G standards were adopted across the globe such as the Nordic Mobile Telephone (NMT) for the Nordic countries and the Advanced Mobile Phone System (AMPS) in the United States which adopted a 40 MHz bandwidth and 800 to 900 MHz as operating frequencies with a reuse pattern (k) of 7.
The second generation, or 2G was introduced in the late 1980s bringing with it new technologies such as Time Division Multiple Access (TDMA) and Code Division Multiple Access (CDMA) [5]. This new generation brought a series of improvements when compared to 1G, such as better data services and higher spectral efficiency, and some operators also offered Short Message Service (SMS). The first 2G networks based on the Global System for Mobile Communications (GSM) were launched in Finland in 1991.
The third generation had its first commercially available network deployed in Japan by NTT in 2001 [6]. This generation offers a wide range of services that the covers the possibilities of the previous generations but also improves upon it by offering more advanced resources such as video calls and broadband wireless data, all with improved spectral efficiency. The development of the 3G was not uniform, varying according to the region [7] what gave birth to several standards such as Universal Terrestrial Mobile System (UMTS) in Europe [8] or the CDMA2000, which is the American variety of 3G [9].

The first tests of what would be known as 4G were conducted in Tokyo, Japan in 2005 where field trials demonstrated that the new technology was able to achieve speeds up to 1 Gbps in the downlink direction. 4G improves upon the technology of 3G offering high quality audio and video streams

The initial specifications for the fifth generation of cellular communications, or 5G NR were completed by the the 3GPP in June of 2018, starting the non-standalone phase of the technology, where it is expected to work alongside the existing 4G/LTE infrastructure, offering retro-compatibility with existing services [10]. By the time this work is being written, the first commercial 5G networks are already operating in some regions of the world, namely South Korea [11], United States [12] and Uruguay [13].

1.2.2 3GPP

The 3rd Generation Partnership Project covers cellular telecommunications network technologies that include radio access, core transport network and service capabilities [14]. This project includes telecommunications organizations (ARIB, ATIS CCSA, ETSI, TSDSI, TTA, TTC) that cooperate in the development of standards and specifications for the underlying technologies and it is composed of three technical specifications groups: Radio Access Network (RAN), Services and Systems Aspects (SA) and Core Network and Terminals (CT).

Rel.14 of 3GPP started the work on critical enhancements such as LTE support for V2x services, enhanced Licensed Assisted Access (eLAA) and 4 band carrier aggregation while **Rel.15** brought the first 5G specifications and continued the maturing process of LTE-Advanced Pro. The proposed 3GPP time line for 5G in Figure 2.7.

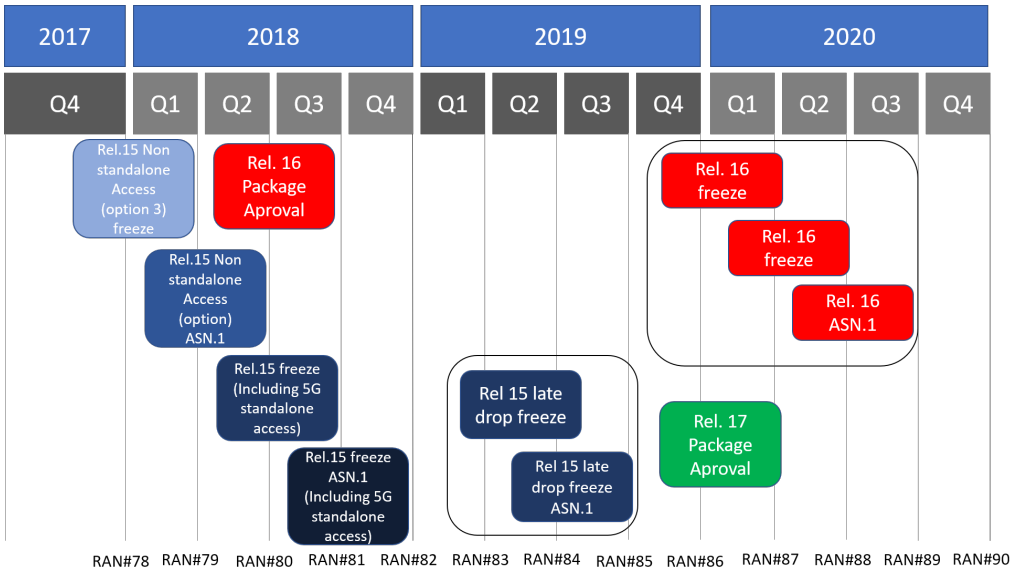

Figure 1.1: Tentative timeline for 3GPP 5G, adapted from [15]

Rel.10 introduced the first specifications for LTE-Advanced to meet International Telecommunication Union (ITU)/International Mobile Telecommunications (IMT)-Advance requirements, such as high speed higher achievable speeds to UEs compared to the specifications of Rel.8. This release also introduced some key features that would be further explored in the following releases, such as:

- Use of 8x8 MIMO communications in DL and 4x4 MIMO in the UL direction [16];
- The introduction of CA to allow the use of the fragmented spectrum inside the same frequency band or across different bands, what allows for an increase in throughput. LTE-Advanced allows the use of bandwidths up to 100 MHz using up to five CCs with the possibility of aggregating contiguous and non contiguous carriers [17];
- As Rel.10 brought the first specifications for the design of HetNets, it also included the Inhenced Inter-Cell Interference Coordination (eICIC) to deal with interference is these networks;
- This release first proposed the use of relay nodes as a resource to extend tho coverage area of a evolved NodeB (eNB), with the relays usually being low-power eNBs.

With the introduction of LTE-Advanced, **Rel.11** brought some important enhancements to the standard previously established. For example, CA was further enhance with the introduction of non contiguous intra-band CA, multiple timing advances in the UL communication. It also introduced mechanism to allow a UE to reduce energy consumption by informing the network when it needs to run in battery saving mode, mainly due to data consumption by applications and process running in background. Other key features introduce by Rel.11 are:

- Network based positioning;
- Coordinated Multipoint Transmission and Reception (CoMP);
- Enhance Physical Downlink Control Channel (ePDCCH) [18].

For **Rel.12**, enhancements to CA were brought with the possibility of applying CA between co-located TDD and FDD carriers. Also, integration of LTE and Wifi was introduced, to allow operator to have more control in aspects related to traffic control.
Rel.15 phase 1 of 3GPP corresponds to NR phase 1, while **Rel.16** will cover the second phase for this technology. Even though the set of frequencies for 5G NR is firmly established, there is a convergence in use and other bands, such as 24.25 GHz and 33.4 GHz are being studied for use in this technology. The technology involved in the development of the 5G NR is expected to make extensive use Multiple Input Multiple Output (MIMO) communications with which is possible to

achieve up to 2 Gbps of DL speed, as shown in test scenarios [19]. Also, **Rel.15** lists a set of technologies related to 5G NR:

- LTE-U/LAA ;
- Multifire;
- LTE-Wireless Local Area Network (WLAN) aggregations;
- Citizen Broadband Radio Service / Licensed Shared Access;

The development of 5G standard was divided in two phase i.e., NR phase 1 in **Rel.15** and NR phase 2 in **Rel.16**. Even though in NR phase 1 there is a series of common elements between LTE and NR, the approach proposed by 3GPP was established to allow the use o existing hardware by considering a non-standalone version in which the LTE core is still present while in the standalone version NR core will work independently from LTE [20].

1.2.3 Heterogeneous Networks

One can define Heterogeneous Network as a network composed of a mix of low-power nodes and macrocells where some devices may be configured with directives of restrict access while others may lack a wired connections structures [21]. The study of cellular HetNets have become of paramount importance to researches over the last few decades, especially when one considers the exponential growth of mobile subscribers, and the uneven distribution of spectrum as well as its increasing scarcity, what makes mobile operators look for solutions to better use the available spectrum, usually deploying a series of devices with different transmit power, coverage or capacity, to ensure the quality of communication.
In the context of LTE broadband network deployment, one usually has scenarios of heavily dense urban areas or very remote areas, where a diversity of frequency bands is employed, with different propagation characteristics, alongside an accentuated heterogeneity in terms of devices [22].
One common element in HetNets is the Small Cell which is deployed with the aim of increasing the capacity of a network per unit of area offloading the macrocells and improving indoor coverage and cell-edge user performance. SCs are classified as follows [23]:

- Microcells, also known as micro Base Stations (BSs) or serving microcells, usually have the same interface as a typical BS, but operate at a much lower transmit power. They are most commonly operator-deployed and one of its most common applications is to serve as outdoors hotspots, with its coverage usually limited up to 1 mile and controlled by its transmit power.

- Picocells are low-power SCs, usually operator-installed and have the same the same back-haul features of the BS, but operate at a much smaller transmitter power, usually around (30 dBm) [24], with a cell radius ranging from 100 to less than 299 m. This cells can be equipped with omnidirectional antennas or with a different directionality, offering coverage up to 100 users.

- Femtocells also kwon as home base stations, are small low-power BSs which are usually consumer-deployed [25], commonly connected to their own wired back-haul, being designated as Home evolved NodeB (HeNB) in LTE. This cells can be deployed indoors or outdoors, but the first option is usually the most common.

1.2.4 Narrowband IoT

NB-IoT was first introduced by 3GPP in Rel.13 [26] starting the work to ensure wide-are coverage within the context of the Internet of Things(IoT). The idea behind this release was to first address some of the main challenges found in the deployment of IoT-based use cases, such as:

- Battery life time;

- Deployments with massive number of devices;

- Flexibility;

- Mobility;

- Significant coverage extension.

The technology proposed for NB IoT, even though not completely backwards compatible with previous releases, makes extensive use of LTE-based technologies and standardizations. It employs downlink Orthogonal Frequency-Division Multiple-Access (OFDMA) alongside the same channel coding, rate matching, and interleaving [26]. One of the main characteristics proposed by 3GPP for NB-IoT is that it uses narrow bandwidth, what makes it possible to re-farm chunks of available spectrum from other technologies. It also employs the support to repetition of signals, make it possible to boost signals from low-power devices, thus reducing the levels of Packet Loss Ratio (PLR) [27]. Figure 1.2 shows some of the possible applications of NB-IoT, which are usually common to classical IoT devices, while 1.3 shows some applications deployment scenarios in the DL direction.

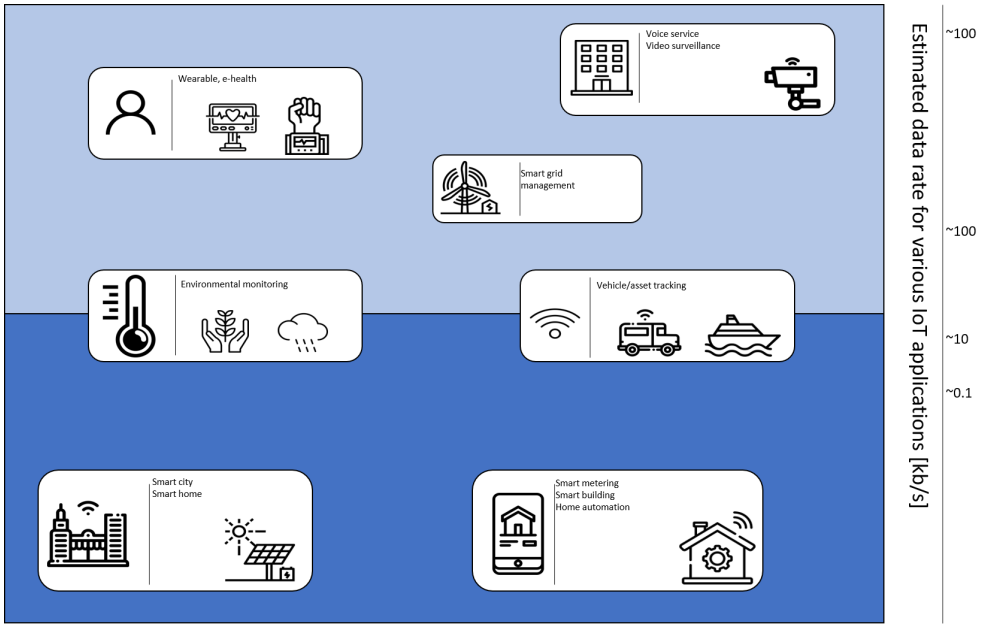

Figure 1.2: Examples of NB-IoT deployment and typical required data rate, adapted from [26]

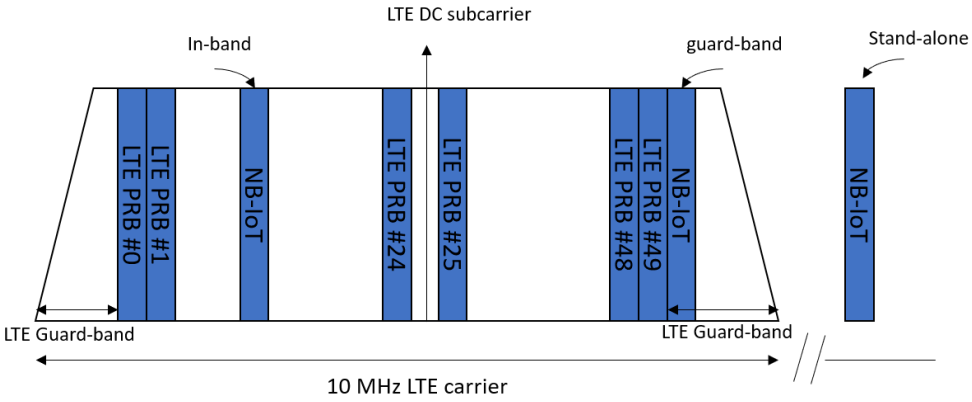

Figure 1.3: Examples of NB-IoT deployment in downlink, adapted from [26]

1.3 Objectives and Approach

This MSc dissertation proposes the study of carrier Carrier Aggregation evaluating scenarios with and without Small Cells deployment to study the behavior of the of mobile networks under different parameters such as cell radius, number of User Equipment (UE) and interferers.The proposal is to make use of the LTE-Sim packet level simulator and the packet schedulers previously developed by researchers from the Instituto de Telecomunicações-Covilhã to investigate the system´s capacity by considering the 2.6 GHz and 800 MHz frequency bands, and also to construct the framework necessary to allow the deployment of Small Cells in different locations and with different radius. To allow a comparative analysis of the results obtained, the framework used also performs the simulation of scenarios without CA, which can be compared with results from the scenarios that consider aggregation with and without SCs. Another objective of

this dissertation is to address spectrum sharing at the SC layer of the HetNet. Spectrum sharing assumes that two or more mobile operators/carriers have dedicated spectrum for macro cellular layer while SCs will use exclusive shared spectrum (by paying a fee) or share the access to non-licensed spectrum in an opportunist manner. To achieve this goal, a analytical formulation is used considering different assumptions ("cases") for the sharing scenario in the SC layer i.e., no sharing case scenario, where operators use the same frequency band or sharing with interferers positioned at different geographical locations. In this context, one considers a mapping between Modulation Code Schemes (MCSs) and minimum CNIR to obtain the physical throughput following the specifications of 3GPP to LTE networks. Supported throughput and average Carrier to Noise plus Interference Ratio (CNIR) are also computed by considering different cell radius and distances between Base Station and User Equipment. One also considers the specifications of 5G New Radio to compute the metrics proposed for studying, by updating the Matlab code while considering a maximum modulation order of six.

1.4 Contributions

The main contributions of this MSc dissertation are the analytical computation of the average Carrier Plus Noise Interference Ration (CNIR) and physical and supported throughput under the technical specifications of LTE and 5G New Radio, considering the two slope propagation model and Small Cells deployment, for the Ultra High Frequency/Super High Frequency (UHF/SHF), presented in chapter 2. This study follows the research on Small Cells deployment from Insituto de Telecomunicações - Covilhã.
Another fundamental contribution is the study of Carrier Aggregation with the LTE-Sim packet level simulator and the implementation of Aggregation with Small Cells, give contributions to the research started at the Instituto de Telecomunicações. The results of this research are presented in Chapter 3, where one evaluates the system´s capacity under several metrics, such as PLR, goodput, delay and Signal plus Noise Signal-to-Interference-plus-Noise Ratio (SINR).
The contributions of this work have already been presented in the following venues:

- One paper accepted for publications under the title "Techno-Economic Trade-off of Small Cell 5G Networks", to be presented in the 11^{th} Conference on Telecommunications (Conftele 2019);
- Two Temporary Documents $TD(19)10063$ and $TD(19)10065$ in the 10^{th} MC meeting and 10^{th} technical meeting of the COST CA 15104 held in Oulu, Finland from 27 to 29 of May 2019.

Also, in the context of the research carried out by the member within IT-Covilhã team, the

development of energy efficient routing protocols has been addressed for applications on IoT scenarios. This research topic has been presented on the following venues:

- One paper accepted for publication under the title ”Performance Evaluation of Source Routing Minimum Cost Forwarding Protocol over 6TiSCH Applied to the OpenMote-B Platform”, in proceeding of The Urb-IoT 2018 - 3^{rd} EAI International Conference on IoT in Urban Space, Guimarães, Portugal, Nov. 2018;
- One paper accepted for publications under the title ”Source Routing Minimum Cost Forwarding Protocol over 6TiSCH Applied to the OpenMote-B Platform”, to be presented in the 2019 IEEE 30^{th} Annual International Symposium on Personal, Indoor and Mobile Radio Communications (PIMRC), Istanbul, Turkey, Sep. 2019;
- One Temporary Documents $TD(19)09082$ in the 9^{th} MC meeting and 9^{th} technical meeting of the COST CA 15104 held in Dublin, Ireland, 16 - 18 of Jan 2019;
- One Temporary Documents $TD(18)07052$ in the 8^{th} MC meeting and 8^{th} technical meeting of the COST CA 15104 held in Cartagena, Spain, May 16 - Jun. 1 of 2019.

1.5 Outline of the Dissertation

The first part of this master thesis gave a brief state of the art covering topics such as the evolution of mobile communications, the Third Generations Partnership Project and the contributions of its technical releases to the standardization of mobile technologies, Heterogeneous Networks, Carrier Aggregation and Small Cells.
Then, in chapter 2 a scenario for spectrum sharing is studied, making use of a analytical formulation to evaluate physical and supportable throughput as well as average Carrier Plus Noise Interference Ration by considering a deployment case based in Small Cells with a central cell, 6 co-channel cells, one cell from a different mobile operator and and a central cell.For the study presented in chapter two one considers the technical specifications of LTE and 5G New Radio, evaluating the system´s capacity by considering different cell radii and User Equipment distances. A cost/revenue analysis is also presented in chapter two, where the values obtained for the supported throughput obtained via the analytical formulation are used to estimate the economic tradeoff of Small Cells deployment.
In chapter 3 the LTE-Sim packet level simulator is used to implement and evaluate Carrier Aggregation considering deployment scenarios with and without Small Cells.One considers two different frequency bands and the system´s capacity is evaluated in terms of goodput, PLR, delay, and Signal plus Interference noise ratio.

Finally, chapter 4 draws conclusions to the work, with a brief overview of the results obtained and suggestions for future work. In appendices A, B, and C, further results are presented for the analytical formulation developed in chapter 2, as well as the code used with 5G New Radio and the analytical formulation for the average CNIR . Appendix D describes the work performed on the implementation of a 4G network with OpenLTE/srsLTE.

Chapter 2

Cellular Radio and Network Optimization: Analytical Study

2.1 General Aspects of the Long Term Evolution

The Long Term Evolution is the radio interface standardized by 3GPP and had its first specification brought by Rel.8, offering support for FDD and TDD. It was first proposed to offer a framework for communication with delays lower than 5 ms and possibilities for data rates achieving peaks of 300 Mbps [28].

Since its first release, LTE underwent a series of changes provided by the new releases of 3GPP with the aim of improving the technology to match the growing number of mobile subscribers, heterogeneity of mobile networks and demand for higher data rates and quality of service. New paradigms have been incorporated, such as the introduction of NB-IoT [29], the exploration of unlicensed spectrum [30] or the use of Unnamed Aerial Vehicles (UAVs) [31]. LTE has now reached Rel.15, where not only 5G New Radio had its first complete standardization, but improvements were also introduced to allow enhancements in network capacity mainly aiming at ensuring backwards compatibility of the existing infrastructure and new the technologies proposed by NR [32].

2.1.1 Downlink Physical Channels and Physical Layer Procedures

The modulation scheme adopted in LTE is based on the use Orthogonal Frequency Division Multiplexing (OFDM) and it was first chosen due to its robustness against the effects of multi-path fading. It is also capable of performing multiplexing through the use of OFDMA offering a set of available bandwidths that goes from 1.4 MHz to 20 MHz. In the DL direction, the physical channels can transport information that are originated at higher layers or physical signals that are transmitted for the use of the physical layer.

An important element in LTE is the Physical Resource Block (PRB) and its allocation is handled by a scheduling algorithm, usually managed by the eNodeB in a network. Each LTE frame is constructed to have a duration of 10 ms and it is usually divided in 10 sub-frames of 1 ms each containing 2 slots with a length of 0.5 ms in the time domain. The number of resource blocks assigned to each slot depends on the operative bandwidth of the channel, e.g., 100 resource

blocks for a bandwidth of 20 MHz. Each resource block will be composed of 12 sub-carriers corresponding to each OFDM symbol, and the total number of OFDM symbols may be 7 for a normal cyclic prefix OFDM or 6 in long prefix. Figure 2.1, summarizes the formation of resource grids in the DL direction, where a resource element is the smallest possible unit for assignment of resources.

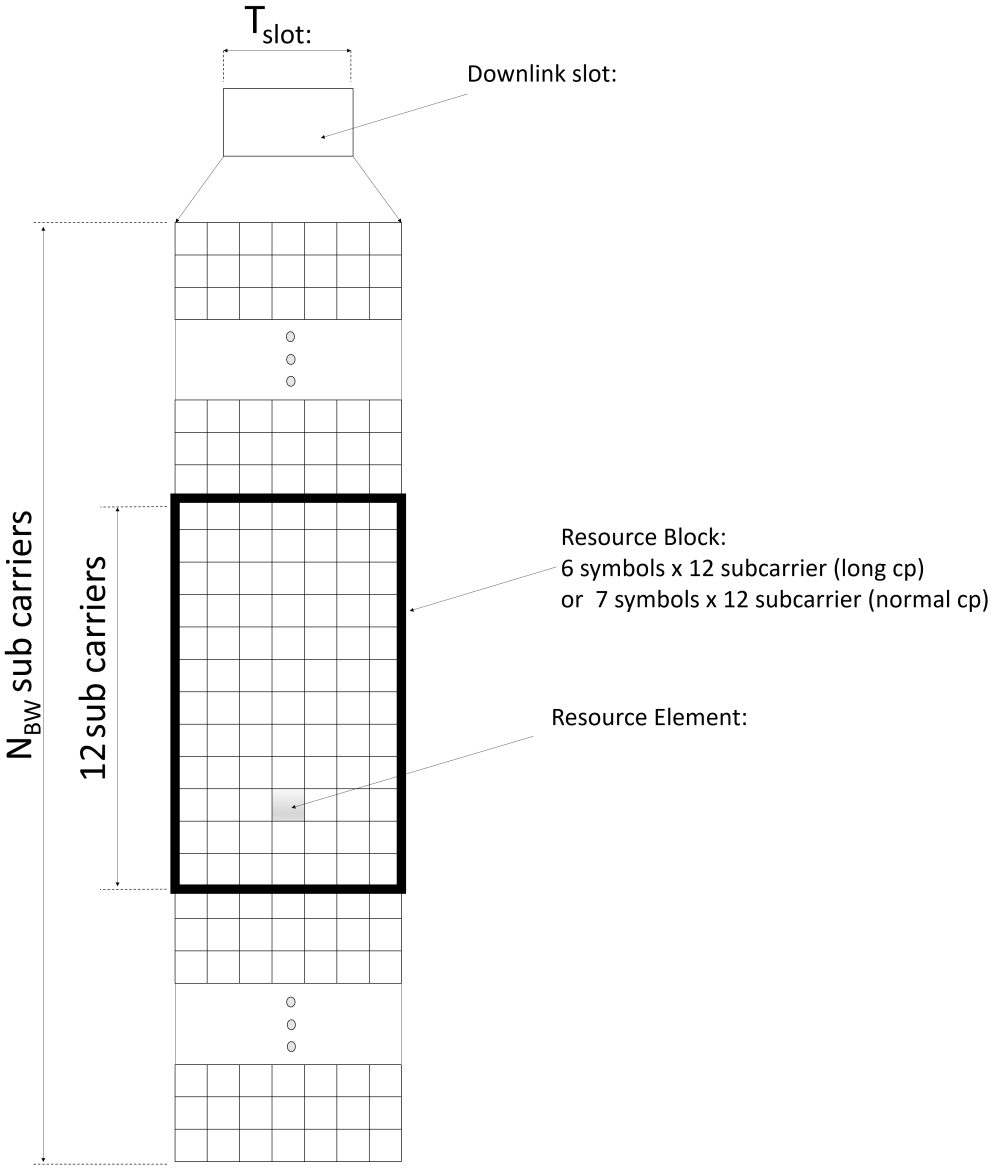

Figure 2.1: Resource grid in downlink, adapted from [33]

In cases when transmissions are based in more than one physical channel, the processing of the physical channel is performed according to the following 6 steps [33], which are summarized above and illustrated in figure 2.2.

- The first step consists in the scrambling of the code bits in each code word to be transmitted;

- In the second step, scrambled bits are modulated to produce complex values;
- In the third step, the complex values are mapped to one or more transmission layers;
- Complex-valued symbols are then precoded in the fourth step, for transmission over the antenna ports;
- In step five, the complex modulated values are mapped to resource elements, for each antenna port;
- Finally, in step 6, time-domain complex-valued OFDM signals are generated for each antenna port.

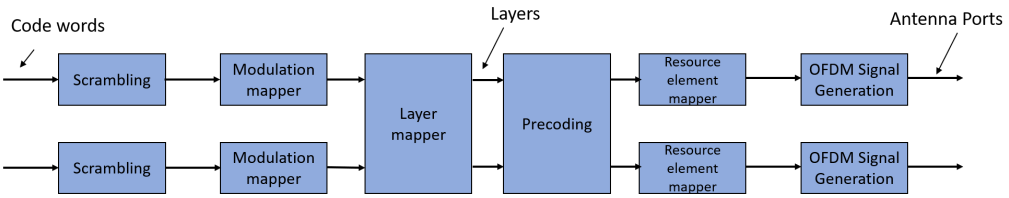

Figure 2.2: Physical channel processing procedures, adapted from [33]

2.2 5G New Radio Physical Layer

The general description of 5G NR given by Rel.15 allows for the deployment of a complete commercial network with a service based architecture employing the concept of modularity [34], where the elements of the architecture are called Network Functions (NFs) and offer their services via a common framework, as shown in figure 2.3.

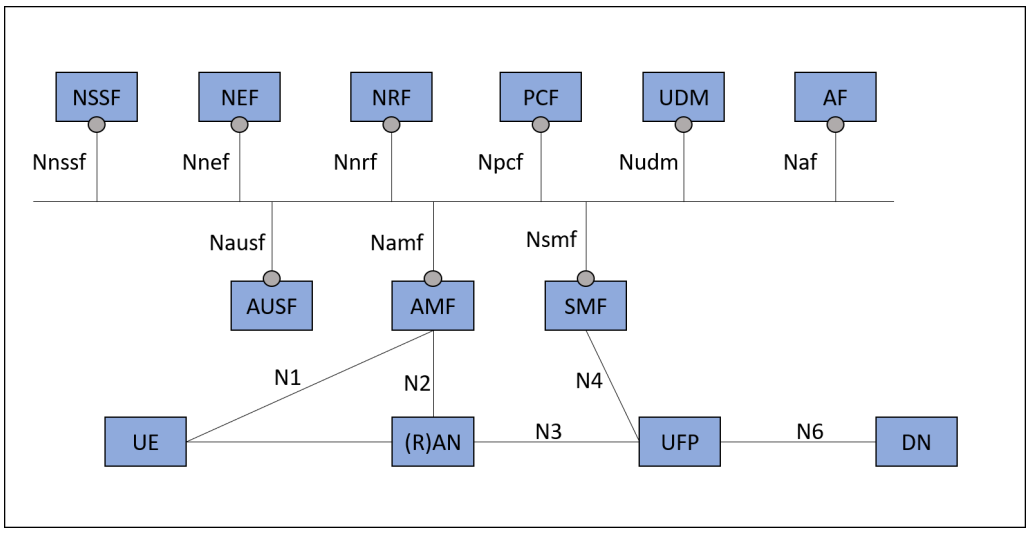

Figure 2.3: Non-roaming 5G system architecture, adapted from[35]

The system presented above defines Access Mobility Functions (AMF) and Session Management Functions (SMF) that operate separately to ensure the modularity of the architecture. The technology of 5G NR in terms of connectivity allows for services based on Protocol Data Unit (PDU) sessions of various types, such as Internet Protocol (IP) versions 4 (IPv4), and 6 (IPv6), Ethernet and Unstructured. To ensure the capability of providing IP addresses, the system provides the traditional Session and Service Continuity (SSC) and also brings new modules such as SSC mode 3. In this context, Quality of Service (QoS) is approached on a flow based framework, with the options of having QoS without signaling, based on standardized packet marking, or QoS signaling based, for more flexibility [36]. It also provides congestion and overload control, control plane load control, Transport Network Layer (TNL), AMF load balancing, SMF and AMF overload control.

In NR, UE's accesses attempts to the network are categorized into access categories, via unified Access Control. This feature gives the network the possibility of restricting accesses with policies based on categories. Furthermore, the technology allows for congestion control by means of DNN, Single - Network Slice Selection Assistance Information (S-NSSAI) and mobility management. Also, configurations into the Universal Subscriber Identity Module (USIM) card of a UE can be used to provide a list of preferred Public Land Mobile Network (PLMN) via access technology combinations monitoring roaming in a Visited Home Public Land Mobile Network (VPLMN).

NR is expected to make intensive use of MIMO communications in the different scenarios of deployment. Rel.15 specifies the support for multi-layer transmissions with the possibility of a maximum of four transmission layers in the UL direction and eight transmission layers in the DL directions. In this sense, scheduling procedures in NR consider the use of large numbers of multi-user MIMO users with Physical Downlink Shared Channel (PDSCH)/Physical Uplink Shared Channel (PUSCH) demodulation, and DL Channel State Information (CSI) acquisition supporting CSI Reference Signal (CSI-RS), Sounding RS (SRS), and Demodulation RS (DM-RS). Figure 2.4 shows the structure of PDSCH repetition and dynamic signaling adopted by NR.

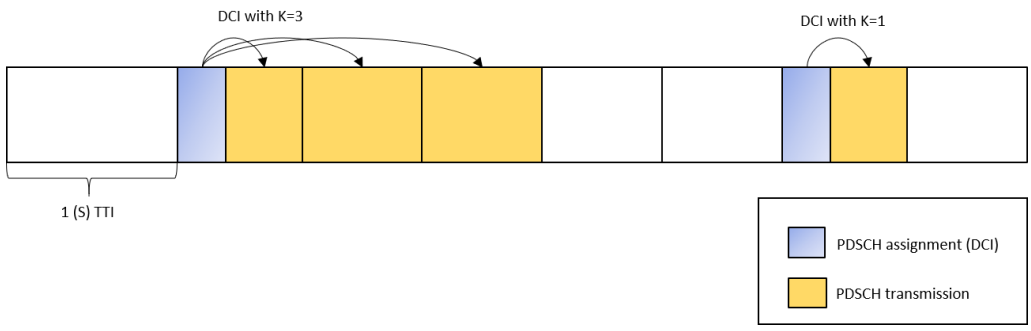

Figure 2.4: Illustration of PDSCH repetition and dynamic signaling of the number of PDSCH transmissions, adapted from [37]

2.2.1 NR Physical Layer Procedures

Bean management in the DL direction is performed by means of Single Band Side (SSB) and Channel State Information Reference Signal (CSI-RS), while SRS is used in the uplink direction where related procedures can be enhanced by the use of sweeping spatial filters at transmitter. UEs inside a network receive information about bean alignment on transmission beans for Physical Downlink Control Channel (PDCCH), Physical Uplink Control Channel (PUCCH) and PDSCH so that a UE can be able to identify and misalignment, transmitting information to inform the Next Generation nodeB (gNB). It also allows for the recovery of bean failure when misalignment between transmission/receptions beans occurs.

NR offers support codebooks for UL communications that allow for the deployment of networks with different implementations of transmitter phase coherence. Also, for the UL direction, there is possibility of employing non-codebook based transmissions with the gNB performing the selections of the appropriated transmissions layer by means of SRS resources transmitted by the UE.

5G NR is expected to allow for backward compatibly with LTE/LTE-A in the non-standalone phase, with the cells of both technologies offering different or the same coverage. Within NR deployment scenarios, it is possible to have a LTE/LTE-A eNB as a master node, offering an anchor carrier that can be boosted by a NR gNB, with data flow aggregated by the Evolved Packet Core (EPC) [36]. On the other hand, it is also possible to have a NR gNB as the master node, offering wireless services via the next generation core. In the latter case, an enhanced LTE (eLTE) eNB offers a booster carrier to the anchor node.

eLTE eNB can also be the master node in a standalone operation to offer wireless services. In this scenario, the eLTE eNB can work via the next generation core or have a collocated NR gNB to provide booster carriers. Finally, inter-Radio Access Technology (RAT) is expected to be applied in scenarios where the NR gNB is connected to the next generation core and the LTE-A eNB is connected to the EPC, to ensure handover between eNB and gNB. The possible deployment scenarios for 5G NR are presented in figure 3.4.

The numerologies of NR consider a Sub Carrier Spacing (SCS) that can assume values configured as subsets or super-sets of a 15 kHz spacing, with the possibility of inserting multiple cyclic prefix lengths for each sub-carrier. As the carrier frequencies of NR are higher than those of LTE/LTE-Advanced, one can expect these carrier frequencies to be more susceptible to the Doppler effect, but this effect can be mitigated by the employment of larger SCS.

2.2.2 NR Frame Structure

As define by 3GPP Rel.15, the sub-frames of NR are composed of slots that comprise 14 OFDM symbols, with lengths of 1 ms and 15 kHz of SCS. NR also adopts mini-slots that can carry control signal and mark the beginning or end of OFDM symbols. This structure allows for the possibility of allocating small packet sizes and also brings the possibility of immediately allocating resources for urgent data arrivals. Figure 2.5 shows the basic frame structure of 5G NR.

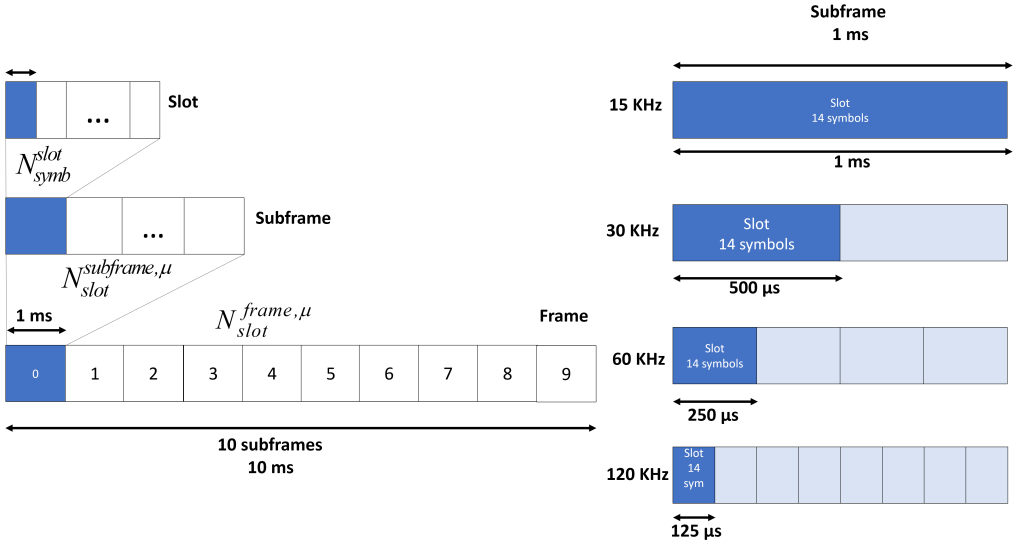

Figure 2.5: New Radio Frame Structure, adapted from [38]

It is possible to see from the representation in figure 2.5 that, when SCS is larger than 15 kHz, some of the OFDM symbols and CP lengths should be to the duration of one 15 kHz symbol duration, including CP length. Rel.15 of 3GPP has established two sets of frequency ranges identified as Frequency Range 1 (FR1) and Frequency Range 2 (FR2) as shown in figure 2.7. FR1 comprises the sub-6GHz frequency range (450-6000 MHz) while FR2 is the mmWave range (24250-52600 MHz).

Table 2.1 shows the complete set of frequency bands defined by Rel.15 that where identified considering marketing demand and also to allow the possibility of re-farming LTE bands. Considering this aspects, it is possible to identify, from 2.1 bands corresponding to their equivalents in LTE, such as band n7, while the bands in FR1 are new frequency bands introduced in 5G NR.

2.3 Propagation Model

The recent developments in wireless communications and the constant search for more efficient and reliable ways to ensure data delivery followed by the increasing number of mobile subscriber all around the world has led, in the past few years to the development of several propagation

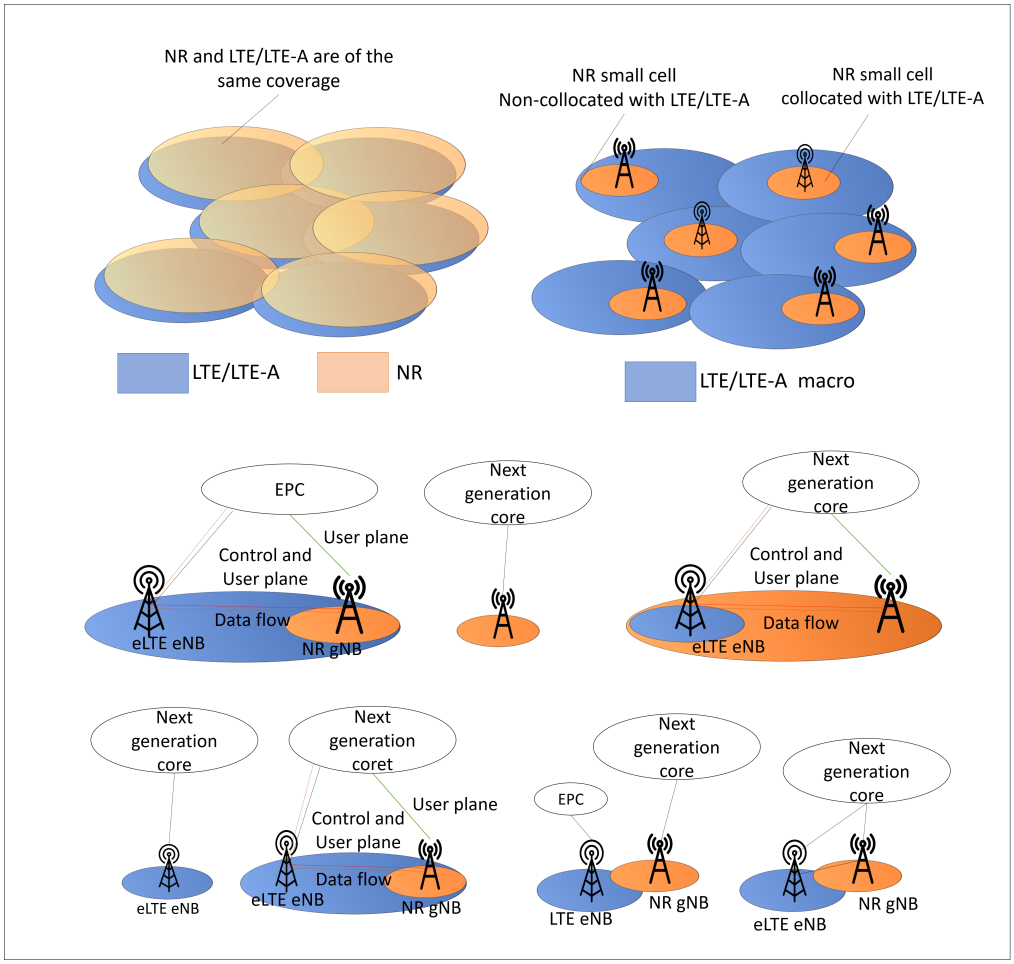

Figure 2.6: New Radio deployment scenarios, adapted from [39]

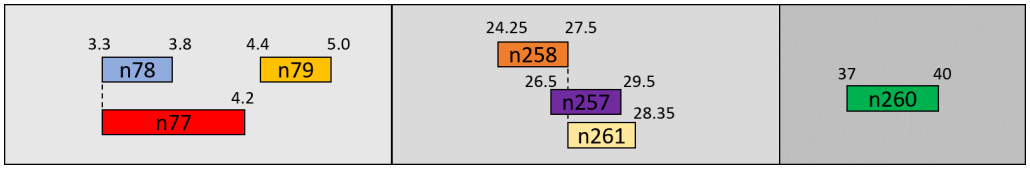

Figure 2.7: New Radio frequency bands defined by Rel. 15, adapted from [40]

models for applications in cellular mobile communications [41]. This models are of paramount importance to the correct characterization of the environment, system design, planning and testing [42].

Choosing a propagation model depends on several factors, such as environmental characteristics, type of application, frequencies to be applied, distances to be considered, and the computational cost of the chosen model.The large-scale propagation models are usually classified in four groups [43]:

- Empirical models;
- Semi-empirical models;
- Deterministic models;

Table 2.1: NR Frequency Bands, adapted from [40]

NR operating band	Uplink(UL) operating band	Downlink(UL) operating band	Duplex mode
n1	1920 MHz – 1980 MHz	2110 MHz – 2170 MHz	FDD
n2	1850 MHz – 1910 MHz	1930 MHz – 1990 MHz	FDD
n3	1710 MHz – 1785 MHz	1805 MHz – 1880 MHz	FDD
n5	824 MHz – 849 MHz	869 MHz – 894 MHz	FDD
n7	2500 MHz – 2570 MHz	2620 MHz – 2690 MHz	FDD
n8	880 MHz – 915 MHz	925 MHz – 960 MHz	FDD
n12	699 MHz – 716 MHz	729 MHz – 746 MHz	FDD
n20	832 MHz – 862 MHz	791 MHz – 821 MHz	FDD
n25	1850 MHz – 1915 MHz	1930 MHz – 1995 MHz	FDD
n28	703 MHz – 748 MHz	758 MHz – 803 MHz	FDD
n34	2010 MHz – 2025 MHz	2010 MHz – 2025 MHz	TDD
n38	2570 MHz – 2620 MHz	2570 MHz – 2620 MHz	TDD
n39	1880 MHz – 1920 MHz	1880 MHz – 1920 MHz	TDD
n40	2300 MHz – 2400 MHz	2300 MHz – 2400 MHz	TDD
n41	2496 MHz – 2690 MHz	2496 MHz – 2690 MHz	TDD
n51	1427 MHz – 1432 MHz	1427 MHz – 1432 MHz	TDD
n66	1710 MHz – 1780 MHz	2110 MHz – 2200 MHz	FDD
n70	1695 MHz – 1710 MHz	1995 MHz – 2020 MHz	FDD
n71	663 MHz – 698 MHz	617 MHz – 652 MHz	FDD
n75	N/A	1432 MHz – 1517 MHz	SDL
n76	N/A	1427 MHz – 1432 MHz	SDL
n77	3300 MHz – 4200 MHz	3300 MHz – 4200 MHz	TDD
n78	3300 MHz – 3800 MHz	3300 MHz – 3800 MHz	TDD
n79	4400 MHz – 5000 MHz	4400 MHz – 5000 MHz	TDD
n80	1710 MHz – 1785 MHz	N/A	SUL
n81	880 MHz – 915 MHz	N/A	SUL
n82	832 MHz – 862 MHz	N/A	SUL
n83	703 MHz – 748 MHz	N/A	SUL
n84	1920 MHz – 1980 MHz	N/A	SUL
n86	1710 MHz – 1780MHz	N/A	SUL
n257	26500 MHz – 29500 MHz	26500 MHz – 29500 MHz	TDD
n258	24250 MHz – 27500 MHz	24250 MHz – 27500 MHz	TDD
n260	37000 MHz – 40000 MHz	37000 MHz – 40000 MHz	TDD
n261	27500 MHz – 28350 MHz	27500 MHz – 28350 MHz	TDD

- Hybrid models.

Empirical models are based on measurements which make them very specific to each type of application. They are also usually simple, with a smaller number of parameters when compared to other models, what makes this models less complex in term of computational cost. One of the most widely none empirical models is the COST 231 One Slope Model, described by equation 2.1:

$$PL = L_0 + 10nlog(d) \quad \textbf{(2.1)}$$

where d is the distance between transmitter and receiver, L_0 is an empirical parameter that

characterizes the general losses of the system and n is the path loss exponent.

While empirical models offer less computational cost, they are also less accurate when compared to other models. Semi-empirical models, on the other hand offer a trade-off between complexity and accuracy offering higher accuracy by introducing deterministic factors. Some examples of this type of propagation models are the COST 231 Walfisch-Ikegami model [44], the Multiwall model [45], and COST 231 [46] penetration model.

Deterministic models also take into account information specific to the site of application, but are usually less complex in terms of computational cost when compared to empirical models. They are usually subdivided into finite-difference time-domain models (FDTD) and geometry models.

The work developed in this thesis considers the propagation model presented in [47] which is a two slope model applied to Urban Micro (UMi) scenarios line of sight (LoS). The UmiLoS model considers a range $d \geq 10$ but it is also analyzed for smaller distances in this work.

Considering the existence of a break point distance d'_{BP} described by equation 2.2, the pathloss is given by equation 2.3:

$$d'_{BP} = \frac{4h'_{UE}h'_{BS}f}{c} \quad (2.2)$$

$$\begin{aligned} PL1 &= 22\log_{10}(d) + 28 + 20\log_{10}(f), when\ d \leq d'_{BP} \\ PL2 &= 40\log_{10}(d) + 7.8 - 18\log_{10}(h'_{BS}) - 18\log_{10}(h'_{UE}) + 2\log_{10}(f), when\ d > d'_{BP} \end{aligned} \quad (2.3)$$

where $c = 3.0 * 10^8$ m/s is the propagation velocity in free space and f is the frequency in GHz. h_{BS} is the height of the base station in m, h_{UE} is the height of the User Equipment in m, (h_{BS} and both parameters can be obtained following the relation $h'_{UE} = h_{UE} - 1$ and $h'_{BS} = h_{BS} - 1$ and h_{UE}). For 2.6 GHz the breakpoint distance is 156 m and for 3.5 GHz is 210 m and for 5.85 GHz is 351 m.

The Friis equation 2.4 is used to compute the received power at the receiver:

$$P_R = P_E + G_E + G_R - PL \quad (2.4)$$

where P_R is the received power given in dBW, P_E is the transmitter power given in dBW, G_E and G_R are the transmitter and receiver gains of the antennas in dBi respectively and PL is the

pathloss values given in dB.

2.4 Cellular Topology and Spectrum Sharing

5G NR networks are expected to provide very high data rates while ensuring the delivery of QoS, what will cause a significant increase in the demand for spectrum [48]. In this context, SCs deployment with spectrum sharing is presented as a solution offering the possibility of offloading the traffic from the macro cell and also to ensure coverage [49]. The exploration of LTE-Unlicensed is also of particular interest for the planning process and to perform experimental research.

This section gives a general description of the chosen cellular topology. Considering a hexagonal cellular hexagonal topology, as the one shown in figure 2.8, with a frequency reuse distance, $D = \sqrt{3k}R$, where R is the radius of the hexagonal cell, the users will be moving in the direction of the cell's edge $5 \leq d \leq R$, starting from the cell´s center. The carrier-to-noise ratio, $\frac{C}{I}$, is given by:

$$\frac{C}{I} = \frac{1}{2(rcc+1)^{-\gamma} + 2(rcc)^{-\gamma} + 2(rcc-1)^{-\gamma}} \quad (2.5)$$

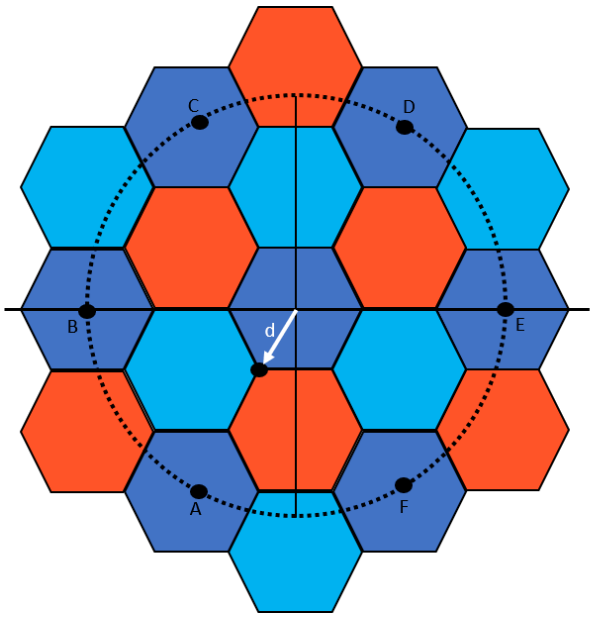

Figure 2.8: Scenario with $k = 3$, where first interference ring with six interferers are represented

In a scenario considering shared spectrum, coordinates of UE for the worst case scenario are $(\frac{-R}{2}; \frac{-\sqrt{3}R}{2})$, while for a general scenario are $(\frac{-d}{2}; \frac{-\sqrt{3}d}{2})$. With this information, one can obtain the distance between UEs and interferes as follows:

$$d = \sqrt{(x - x_0)^2 + (y - y_0)^2} \quad (2.6)$$

The first case analized in this section considers one interference ring, and so one has six interferes (SC eNBA, SC eNBB, SC eNBC, SC eNBD, SC eNBE, SC eNBF) as shown in figure 2.8. We also consider a reuse pattern $k = 3$. The distances for the worst case scenario can be summarized as follows:

- For the interferent SC eNBA the coordinates are $(\frac{-3R}{2}; \frac{-3\sqrt{3}R}{2})$;
- For the interferent SC eNBB the coordinates are $(-3R; 0)$;
- For the interferent SC eNBC the coordinates are $(\frac{-3R}{2}; \frac{3\sqrt{3}R}{2})$;
- For the interferent SC eNBD the coordinates are $(\frac{3R}{2}; \frac{3\sqrt{3}R}{2})$;
- For the interferent SC eNBE the coordinates are $(3R; 0)$;
- For the interferent SC eNBF the coordinates are $(\frac{3R}{2}; \frac{-3\sqrt{3}R}{2})$.

The distance between SC eNBA and UE is give by:

$d = \sqrt{(\frac{-R}{2} + \frac{3R}{2})^2 + (\frac{-\sqrt{3}R}{2} + \frac{3\sqrt{3}R}{2})^2}$

$d = \sqrt{R^2 + (\sqrt{3}R)^2}$

$d = 2R$

Defining the distance as $D + xR$ we have:

$3R + xR = 2R$

$x = -1$

$d = D - R$

The distance between SC eNBB is:

$d = \sqrt{(\frac{-R}{2} + 3R)^2 + (\frac{-\sqrt{3}R}{2} - 0)^2}$

$d = \sqrt{7}R$

Expressing this distance as $D + xR$, as in the previous case, gives us:

$3R + xR = \sqrt{7}R$

$x = -0.35$

$d = D - 0.35R$

For the distance between UE and SC eNBC:

$d = \sqrt{(\frac{-R}{2} + \frac{3R}{2})^2 + (\frac{-\sqrt{3}R}{2} - \frac{3\sqrt{3}R}{2})^2}$

$d = \sqrt{13}R$

that defined as a function of $D + xR$ gives:

$3R + xR = \sqrt{13}R$

$x = 0.61$

$d = D + 0.61R$

For SC enBD:

$d = \sqrt{(\frac{-R}{2} + \frac{-3R}{2})^2 + (\frac{-\sqrt{3}R}{2} - \frac{3\sqrt{3}R}{2})^2}$

$d = 4R$

As we need to define distance as $D + xR$ we have:

$3R + xR = 4R$

$x = 1;$

$d = D + R$

The distance between interferers SC eNBE, SC eNBF and the UE are equal to the distance between interferers SC eNBC and SC eNBB. Hence the result of the calculated distances is shown in figure 2.9.

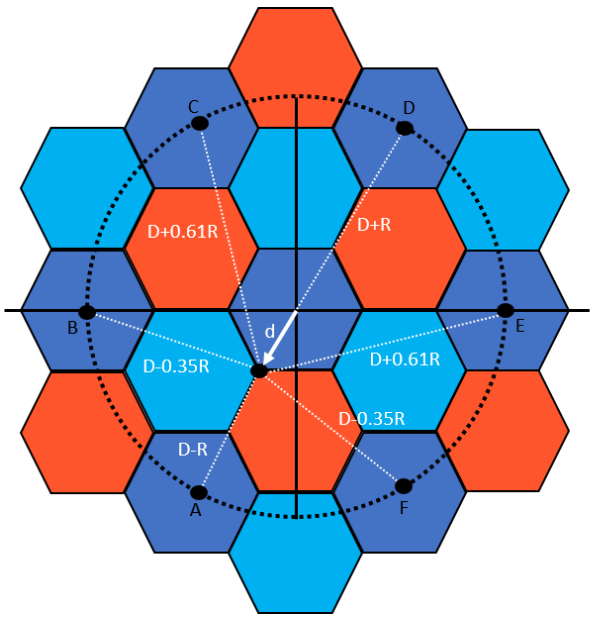

Figure 2.9: Cell planning for $k = 3$ with distance calculated for the worst case scenario

So the CIR formula for the worst case scenario, user at the cell edge, is as follows:

$$\frac{C}{I} = \frac{1}{2(D - 0.35R)^{-\gamma} + (D + R)^{-\gamma} + (D - R)^{-\gamma} + 2(D + 0.61R)^{-\gamma}} \quad (2.7)$$

The general CIR formula without sharing is as follows:

$$\frac{C}{I} = \frac{1}{2(d_{UB})^{-\gamma} + (D+d)^{-\gamma} + (D-d)^{-\gamma} + 2(d_{UE})^{-\gamma}} \quad \textbf{(2.8)}$$

where d_{UB} is the distance between the user and the co-channel SC eNBB and d_{UE} is the distance between the user and the co-channel SC eNBE. These distances are given by:

$$d_{UB} = \sqrt{(\frac{-d}{2} - 3R)^2 + (\frac{-\sqrt{3}d}{2})^2} \quad \textbf{(2.9)}$$

$$d_{UE} = \sqrt{(\frac{-d}{2} + 3R)^2 + (\frac{-\sqrt{3}d}{2})^2} \quad \textbf{(2.10)}$$

For a reuse a distance pattern $k = 4$, where the cellular topology is represented in the figure 2.10, we have the six interferers. The UE coordinates are the same as for $k = 3$, and we also obtain the distance for the worst case scenario:

- For the interferent SC eNBA the coordinates are $(-3R; R\sqrt{3})$;
- For the interferent SC eNBB the coordinates are $(-3R; -R\sqrt{3})$;
- For the interferent SC eNBC the coordinates are $(0; -2R\sqrt{3})$;
- For the interferent SC eNBD the coordinates are $(3R; -R\sqrt{3})$;
- For the interferent SC eNBE the coordinates are $(3R; R\sqrt{3})$;
- For the interferent SC eNBF the coordinates are $(0; 2R\sqrt{3})$.

The computation of the distance between UE and SC eNBA is as follows:

$d = \sqrt{(\frac{-R}{2} + 3R)^2 + (\frac{-\sqrt{3}R}{2} - R\sqrt{3})^2}$
$d = \sqrt{\frac{25R^2}{4} + (\frac{27R^2}{4})^2}$
$d = \sqrt{13}R$
As the reuse distance is $D + xR$, we have:
$\sqrt{12}R + xR = \sqrt{13}R$
$x = 0.14$
Therefore, one obtains $d = D + 0.14R$

The computation of the distance between UE and SC eNBB is as follows:

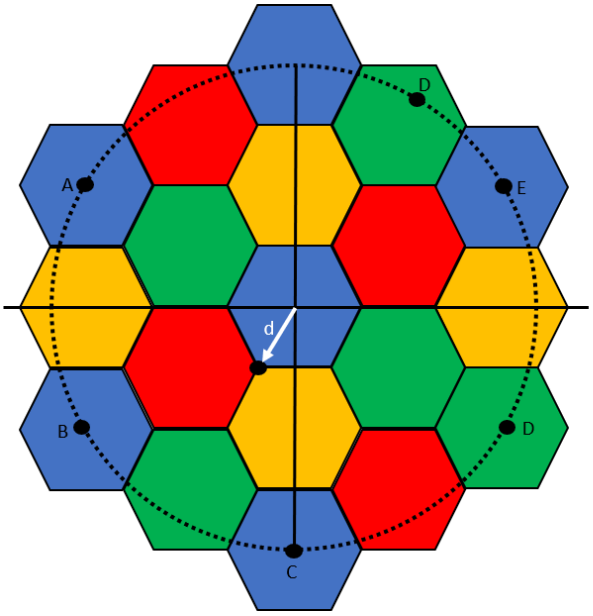

Figure 2.10: Scenario with $k = 4$, first interference ring and six interferers

$d = \sqrt{(\frac{-R}{2} + 3R)^2 + (\frac{-\sqrt{3}R}{2} + R\sqrt{3})^2}$

$d = \sqrt{\frac{25R^2}{4} + (\frac{3R^2}{4})^2}$

$d = \sqrt{7}R$

As we need to define distance as $D + xR$ one has::

$\sqrt{12}R + xR = \sqrt{7}R$

$x = -0.81$

So, one obtains $d = D - 0.81R$

The computation of the distance between UE and SC eNBE is as follows:

$d = \sqrt{(\frac{-R}{2} - 3R)^2 + (\frac{-\sqrt{3}R}{2} - \sqrt{3}R)^2}$

$d = \sqrt{\frac{49R^2}{4} + (\frac{27R^2}{4})^2}$

$d = \sqrt{19}R$

As we need to define distance as $D + xR$ we have:

$\sqrt{12}R + xR = \sqrt{19}R$

$x = 0.89$

Therefore, one obtains $d = D + 0.89R$

The distances to interferers SC eNBC, SC eNBD and SC eNBF are equal to the reuse distance to interferers SC eNBB, SC eNBA and SC eNBE so the result of the computed distances is shown in figure 2.11.

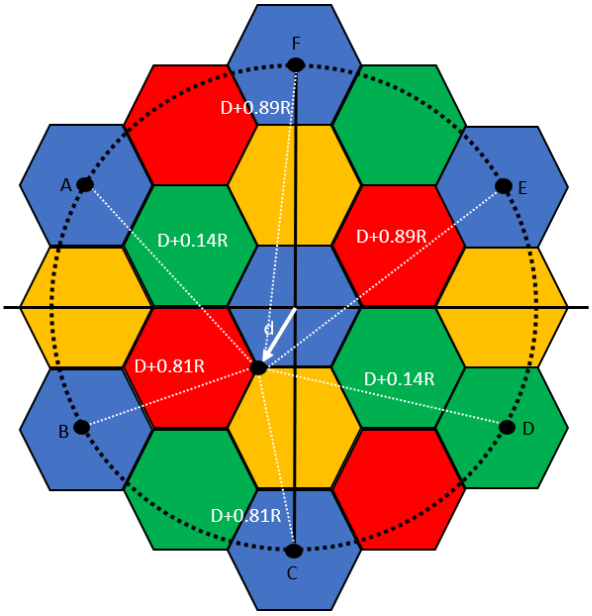

Figure 2.11: Cell planning for $k = 4$ with distance calculated for the worst case scenario

So, the CIR equation for the worst case scenario, with the user at the cell edge, is as follows:

$$\frac{C}{I} = \frac{1}{2(D+0.14R)^{-\gamma} + 2(D-0.81R)^{-\gamma} + 2(D+0.89R)^{-\gamma}} \quad (2.11)$$

While the general CIR equation without sharing is as follows:

$$\frac{C}{I} = \frac{1}{2(d_{UC})^{-\gamma} + 2(d_{UD})^{-\gamma} + 2(d_{UF})^{-\gamma}} \quad (2.12)$$

where d_{UC} is the distance between the user and the co-channel SC eNBC, d_{UD} is the distance between the user and the co-channel SC eNBD and d_{UF} is the distance between the user and the co-channel SC eNBF.

These distances are given as follows:

$$d_{UC} = \sqrt{(\frac{-d}{2})^2 + (\frac{-\sqrt{3}d}{2} + 2R\sqrt{3})^2} \quad (2.13)$$

$$d_{UD} = \sqrt{(\frac{-d}{2} - 3R)^2 + (\frac{-\sqrt{3}d}{2} + R\sqrt{3})^2} \quad (2.14)$$

$$d_{UF} = \sqrt{(\frac{-d}{2})^2 + (\frac{-\sqrt{3}d}{2} - 2R\sqrt{3})^2} \quad \textbf{(2.15)}$$

In this context, the deployment scenarios considers the existence of SCs placed close to each other, assigned to different Mobile Operators (MO), considered one by one in addition to the six co-channel interferes, in three different locations i.e. East, Northeast, and Southeast, as shown in figure 2.12.The positioning of interferes on the Northwest and West corners produces the same outcome in terms of interference, compared to the East and Southeast interferes, respectively and, for this reason, these two cases are not considered in the proposed analysis [50].

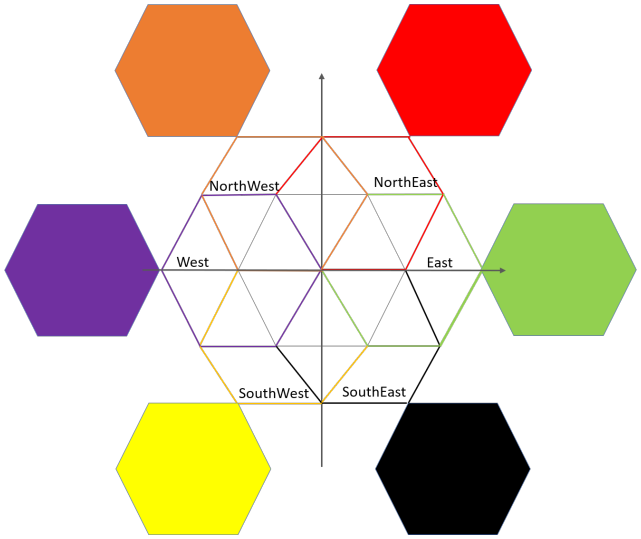

Figure 2.12: Positioning of interferes for the spectrum sharing scenario

Figure 2.13 represents the coverage area for the interferers and how the interference worsens the channel quality as the radius of cells increases.

Considering the analytical formulation presented, it is possible to evaluate the scenarios for spectrum sharing by considering the addition of the term $d_{sharing}$ to the CIR formula. $d_{sharing}$ can be obtained through equations 2.16, 2.17, 2.18, and 2.19, for the East, Northeast, Southeast and Southwest interferers, respectively:

$$\sqrt{(R + \frac{d}{2})^2 + (\frac{\sqrt{3}}{2})^2} \quad \textbf{(2.16)}$$

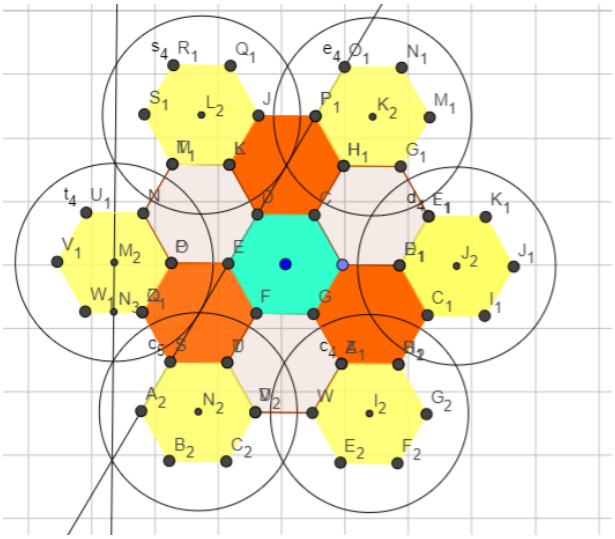

Figure 2.13: Positioning of interferes and representation of the respective cell radius, extracted from [51]

$$\sqrt{(\frac{R}{2}+\frac{d}{2})^2+(\frac{\sqrt{3}d}{2}+\frac{\sqrt{3}R}{2})^2} \quad (2.17)$$

$$R-d \quad (2.18)$$

$$\sqrt{(\frac{R}{2}+\frac{d}{2})^2+(\frac{\sqrt{3}d}{2}-\frac{\sqrt{3}R}{2})^2} \quad (2.19)$$

The general formulation for the CIR is given by equation 2.20 for a reuse pattern $k=3$ and by equation 2.21 for a reuse pattern $k=4$.

$$\frac{C}{I}=\frac{1}{2(d_{UB})^{-\gamma}+(D+d)^{-\gamma}+(D-d)^{-\gamma}+2(d_{UE})^{-\gamma}+d_{sharing}^{-\gamma}} \quad (2.20)$$

$$\frac{C}{I}=\frac{1}{2(d_{UC})^{-\gamma}+2(d_{UD})^{-\gamma}+2(d_{UF})^{-\gamma}+d_{sharing}^{-\gamma}} \quad (2.21)$$

2.5 Comparison of Parameters for Different Transmitter Powers

In this section one studies the proposed cellular topology for the 2.6 GHz, 3.5 GHz and 5.62 GHz frequency bands, by considering different transmitter powers. The 3.5 GHz frequency band has been adopted for operator in the recently deployed 5G networks alongside millimetre wavebands (mmWaves), manly 28 GHz, what gives a perspective about the possibilities for spectrum sharing within this new technology while comparing results with LTE-based networks. The 5.62 GHz frequency band is part of LTE-Unlicensed what brings possibilities for experimental research, being possible to compare the obtained results with licensed frequency bands, such as 2.6 GHz. In this sense,this study first considers different transmitter (Tx) power for each band, as shown in table 2.2. This assumptions are used to study the behavior of the three frequency bands regarding CNIR, physical throughput, Average CNIR/SINR, pathloss, and received power.

Table 2.2: Different transmitter powers considered for both frequencies

Tx power [dBW] (2.6 GHz)	Tx power [dBW] (3.5 GHz)	Tx power [dBW] (5.62 GHz)
-16	-10	-7
-13	-7	-4
-10	-4	-1
-7	-1	2
-4	2	5
-1	5	8
2	8	11

The results for CNIR and physical throughput for LTE, with a bandwidth of 20 MHz are shown in figures 2.14a, 2.14b, 2.14c, 2.15a,2.15b, and2.15c. It is possible to see that CNIR does not depend on the transmitter power, as has been previously established [50]. As the Physical throughput is dependent on the CNIR, it will be the same for different transmitter powers. The view graphs were plotted for a maximum value of d of 500 m because of the 5.62 GHz breakpoint distance.

CNIR and physical throughput are also analyzed for the assumptions of 5G NR, as shown in figures 2.16a, 2.16b, 2.16c, 2.17a, 2.17b, 2.17c.It is possible to observe that the general behavior of CNIR and throughput is preserved when considering higher bandwidth values and, as one would expect, the values obtained for the physical throughput for NR, considering the same bandwidth of 20 MHz, are considerable higher when compared to the results for LTE.

From the results in figures 2.18a and 2.18b it is possible to see that the pathloss is higher for the 5.62 GHz band, but the received power is lower for higher pathloss values. To determine the transmitter power to be used in each frequency band, one first considers the received power in the central cell, which is computed for the 3.5 GHz and 5,62 GHz with the transmitter power of -7 dBW and the breakpoint distance of the respective frequency band.

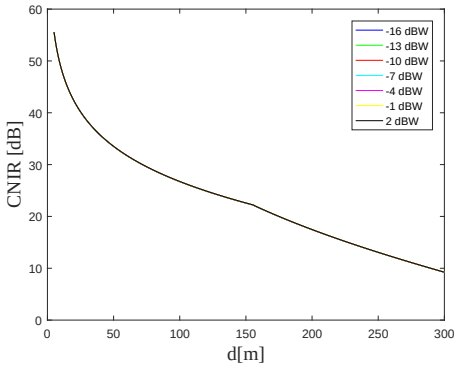

(a) 2.6 GHz

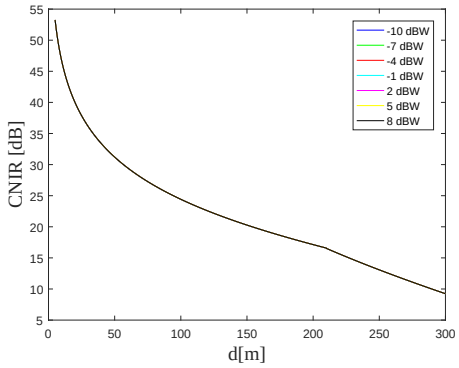

(b) 3.5 GHz

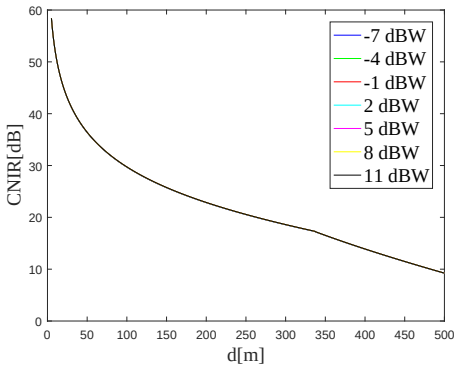

(c) 5.62 GHz

Figure 2.14: Different CNIR values for different transmitter powers

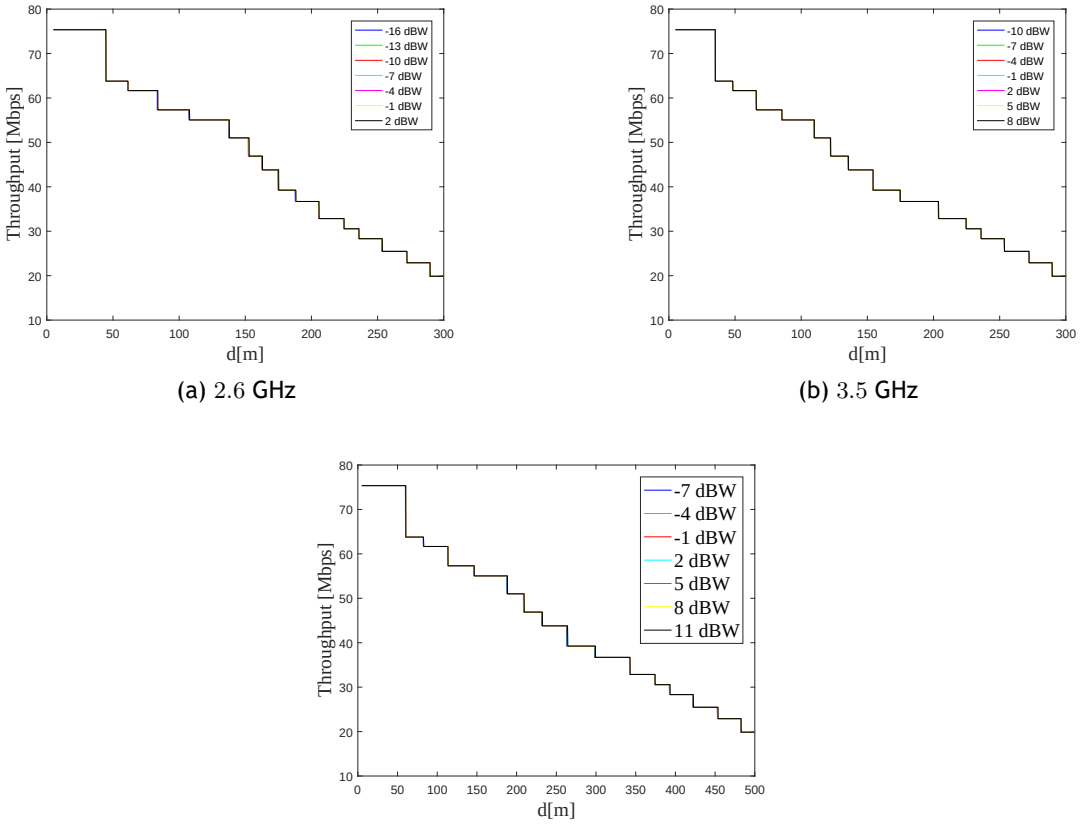

(a) 2.6 GHz

(b) 3.5 GHz

(c) 5.62 GHz

Figure 2.15: Different Physical throughput values for different transmitter powers in LTE

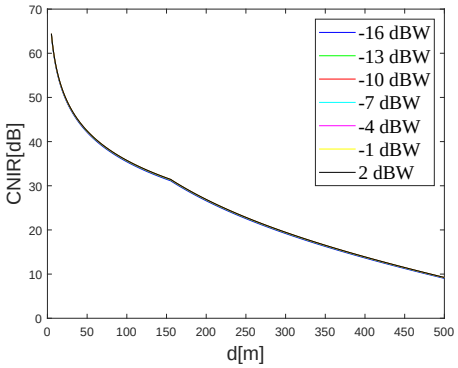

(a) 2.6 GHz

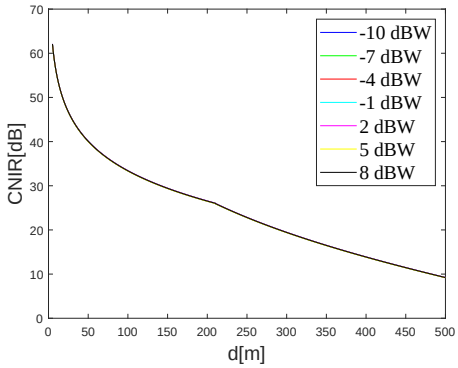

(b) 3.5 GHz

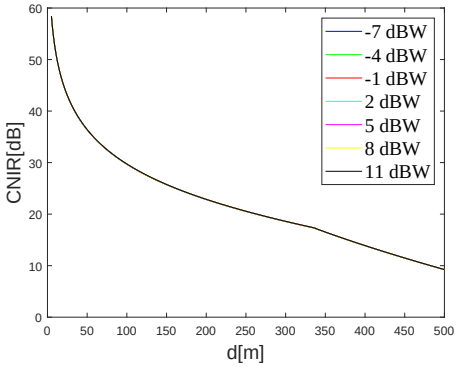

(c) 5.62 GHz

Figure 2.16: Different CNIR values for different transmitter powers for 5G New Radio

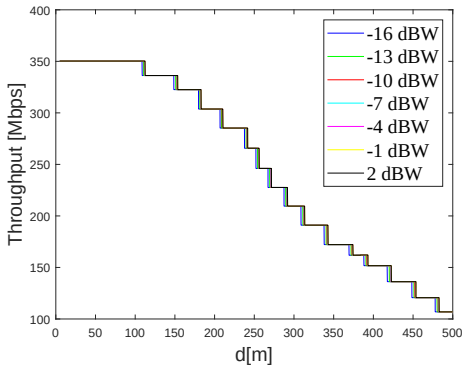

(a) 2.6 GHz

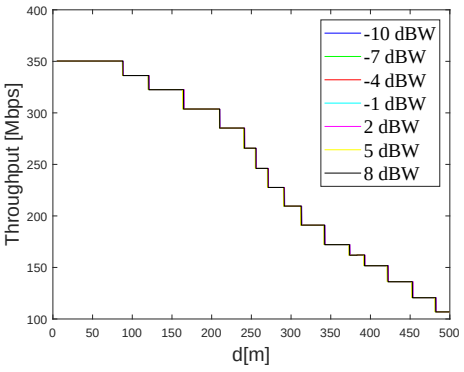

(b) 3.5 GHz

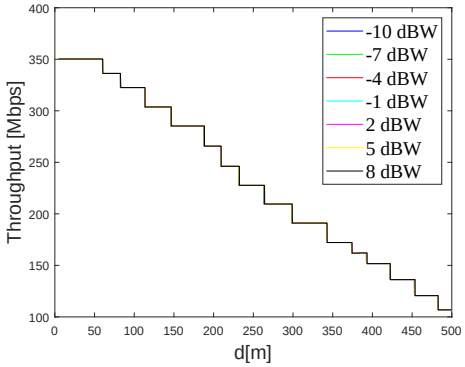

(c) 5.62 GHz

Figure 2.17: Different Physical throughput values for different transmitter powers in 5G New Radio

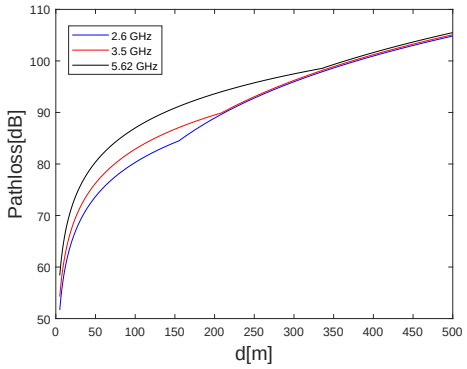

(a) Pathloss per distance comparison

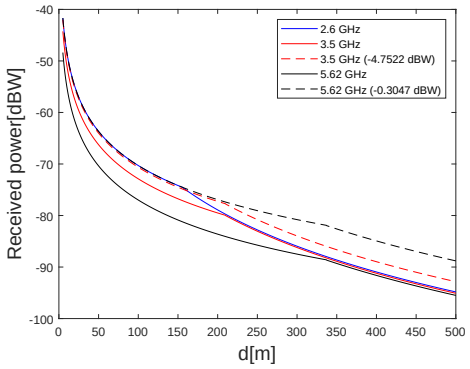

(b) Comparison of received power between 2.6 GHz, 3.5 GHz and 5.62 GHz

Figure 2.18: Pathloss and received power

Following the approach described, the results were computed to obtained the parameters to be used in the following sections, which are summarized in table 2.3.

Table 2.3: Parameters considered

Parameters	2.6 GHz	3.5 GHz	5.62 GHz
Transmitter power [dBW]	-7	-4.7522	-0.3047
Transmitter gain [dBi]	17	17	17
Receiver gain [dBi]	0	0	0
Bandwidth [MHz]	20	20	20
Noise figure [dB]	5	5	5
Height(Base Station) [m]	9	9	9
Height(User Equipment) [m]	0.5	0.5	0.5
Propagation exponent 1[γ]	$d < d_{BP}$, γ = 2.2	$d_{BP} < d$, γ = 2.2	$d_{BP} < d$, γ = 2.2
Propagation exponent 2[γ]	$d \geq d_{BP}$, γ = 4.0	$d_{BP} \geq d$, γ = 4.0	$d_{BP} \geq d$, γ = 4.0

2.6 CNIR and Physical Throughput Evaluation

In this section one proposes the computation of CNIR and PHY throughput under the technical specifications of 5G NR and LTE. According to the specifications from 3GPP to LTE, channel bandwidth can assume the values of 1.4, 3, 5, 10, 15 e 20 MHz. The available bandwidth is mapped into resource blocks (RB), following the values presented in table 2.4 [52].

Table 2.4: Resource Block Allocation in LTE

Bandwidth (MHz)	Number of Resource Blocks
1.4	6
3	15
5	25
10	50
15	75
20	100

The physical throughput in LTE can be determined by performing the mapping between the desired modulation code scheme and its corresponding transport block size (TBS), following the the specifications found in [53]. Once the desired TBS is chosen, its value can be multiplied by the considered transmission time interval (TTI) to determine the value of the physical throughput. If one considers a bandwidth of 20 MHz, by taken into account the RB allocation and a TTI= 1 ms, the respective mapping from MCS to TBS and the respective physical throughput is shown in table 2.5.

With the values from table 2.5 it is possible to study the interference between the co-channel cells, making use of the Matlab programs developed in [50]. We consider in this section reuse patterns (k) of $k = 3$ and $k = 4$ and the distance $5 \leq d \leq R$. The results of this analyzes are shown in figures 2.19a, 2.19b,2.20a, and 2.20b for k=3 and 2.21a, 2.21b, 2.22a, and 2.22b for

Table 2.5: Mapping into Physical throughput for 20 MHz bandwidth.

CNIR [dB]	CQI	MCS Index	Modulation Order	ITBS	Throughput [Mbps]
-4.63	1	0	2	0	2.797
-3.615	1	1	2	1	3.624
-2.6	2	2	2	2	4.584
-1.36	2	3	2	3	5.736
-0.12	3	4	2	4	7.224
-1.17	3	5	2	5	8.76
-2.46	4	6	2	6	10.296
-3.595	4	7	2	7	12.216
4.73	5	8	2	8	14.112
6.13	6	9	4	9	15.84
7.53	6	10	4	9	15.84
8.1	6	11	4	10	17.568
8.67	7	12	4	11	19.848
9.995	7	13	4	12	22.92
11.32	8	14	4	13	25.456
12.78	8	15	4	14	28.336
14.24	9	16	6	15	30.576
14.725	9	17	6	15	30.576
15.21	10	18	6	16	32.856
16.92	10	19	6	17	36.696
18.63	11	20	6	18	39.232
19.975	11	21	6	19	43.816
21.32	12	22	6	20	46.888
22.395	12	23	6	21	51.024
23.47	13	24	6	22	55.056
25.98	13	25	6	23	57.336
28.49	14	26	6	24	61.664
31.545	14	27	6	25	63.776
34.6	15	28	6	26	75.376

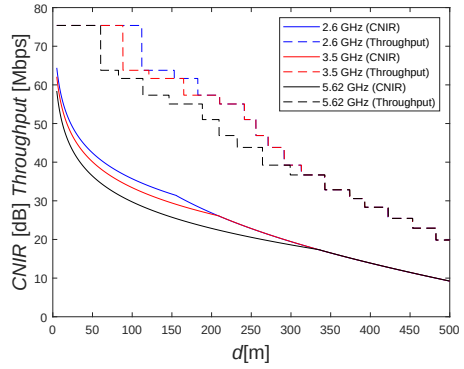

(a) No Interferer for the three bands with $k = 3$

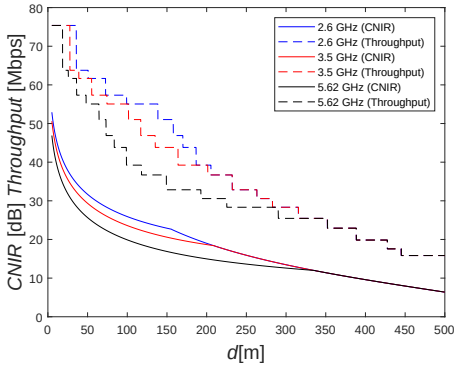

(b) East Interferer for the three bands with $k = 3$

Figure 2.19: CNIR and Physical throughput as a function of d for the No and East interferer scenario for $k = 3$

k=3.

The results obtained show that the physical throughput achieved at the 2.6 GHz frequency band is higher for the shortest distances, followed by the values for 3.5 GHz and 5.62 GHz. At the

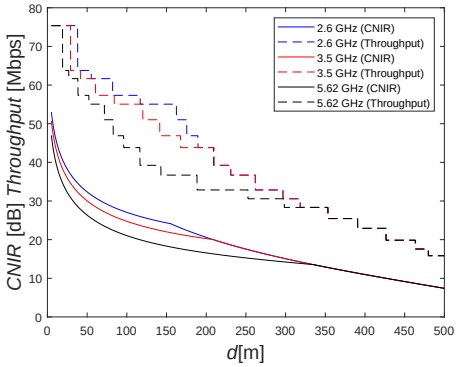

(a) Northeast Interferer for the three bands with $k = 3$

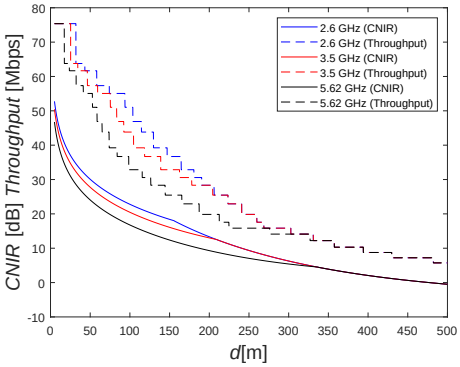

(b) Southeast Interferer for the three bands with $k = 3$

Figure 2.20: CNIR and Physical throughput as a function of d for the Northeast and Southeast interferer scenario for $k = 3$

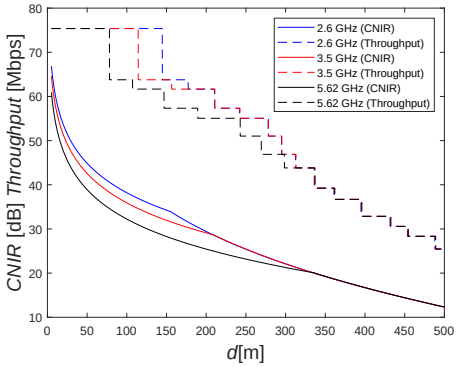

(a) No Interferer for the three bands with $k = 4$

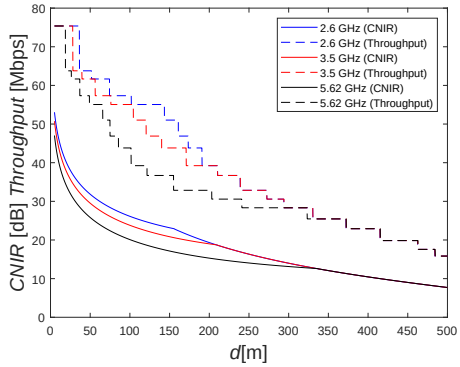

(b) East Interferer for both bands with $k = 4$

Figure 2.21: CNIR and Physical throughput as a function of d for the No and East interferer scenario for $k = 4$

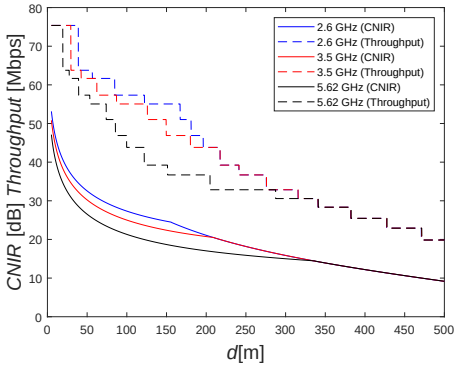

(a) Northeast Interferer for the three bands with $k = 4$

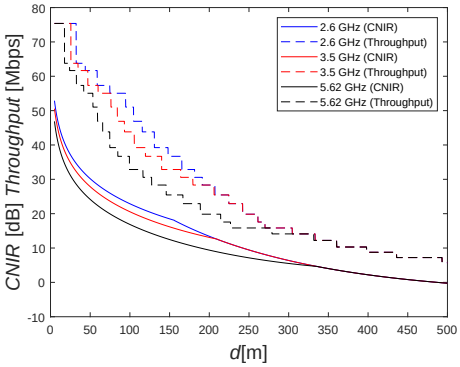

(b) Southeast Interferer for the three bands with $k = 4$

Figure 2.22: CNIR and Physical throughput as a function of d for the Northeast and Southeast scenario for $k = 4$

break point distance of 2.6 GHz, i.e., 156 m, the difference in the values for the PHY throughput between the 2.6 GHz and 3.5 GHz becomes less relevant, for the scenario with no interferer and at this same distance it is possible to observe a change on the shape of the curve for the CNIR, with the rate of decrease accelerating as the distances progress to higher values. The same behavior can be observed at the breakpoint distances for 3.5 and 5.62 GHz, which are 210 m and 337.2 m, respectively. At the point of the break point distance for the 5.62 GHz frequency band, the values achieved by the three frequency bands are already very similar when there is non interferer. The distances where the values for 2.6 GHz become more close to those of the other two frequency bands changes as one analyzes different interferer scenarios, being of approximately 200 m for the case the East interferer, for 2.6 and 3.5 GHz.

For all cases analyzed, the no interferer scenario is where the highest values of PHY throughput are achieved, followed by the scenarios for the East, NorthEast and SouthEast interferes, which show values for the physical throughput and for the CNIR that are very close.For the cases where one considers a reuse pattern $k = 4$, even though the maximum achievable PHY throughput remains the same, its decrease for the shortest distances is less accentuated when compared to the results with $k = 3$. Also, for the non interferer case, it possible to see that maximum achievable value for the CNIR is higher in comparison to its equivalent scenario with $k = 3$.

From the mapping between MCS and physical throughput, it is possible to represent the mapping results by means of 3D graphics, as the ones presented in this sections, obtained with a normalized distance, coverage radius and physical throughput for the three frequency bands considered so far. Results are shown in figures 2.23, 2.24, 2.25, 2.26, 2.27, 2.28, for all the frequency bands, with $k = 3$ and for the no interferer and NorthEast interferer case. Results for $k = 4$ are shown in Appendix A.

This representation allows for the visualization of the effect of distance of the UE upon the physical throughput while also considering the cell radius.

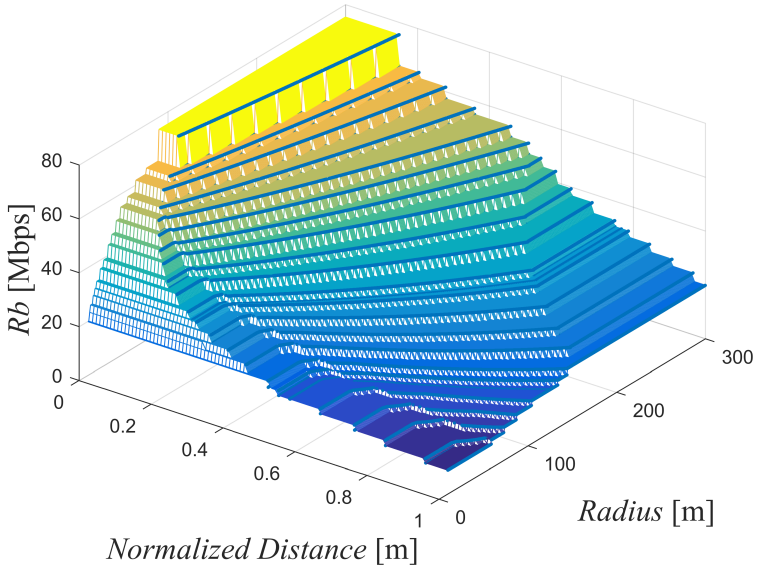

Figure 2.23: 3D View of the PHY throughput mapped into MCSs with No Interferer at the 2.6 GHz band with $k = 3$

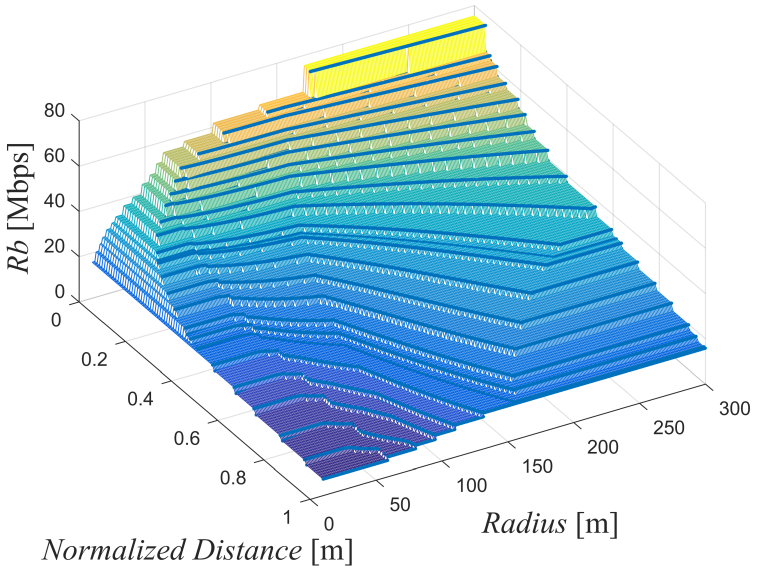

Figure 2.24: 3D View of the PHY throughput mapped into MCSs with Northeast Interferer ate the 2.6 GHz band with $k = 3$

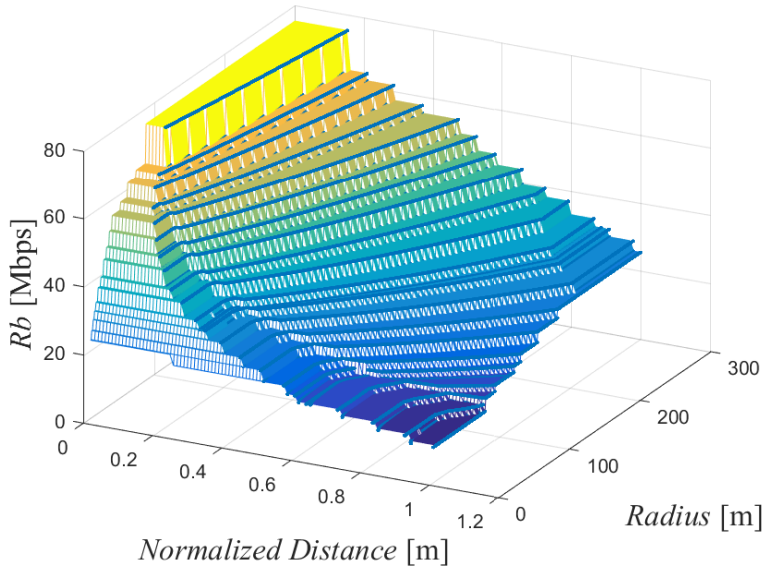

Figure 2.25: 3D View of the PHY throughput mapped into MCSs with No Interferer at the 3.5 GHz band with $k = 3$

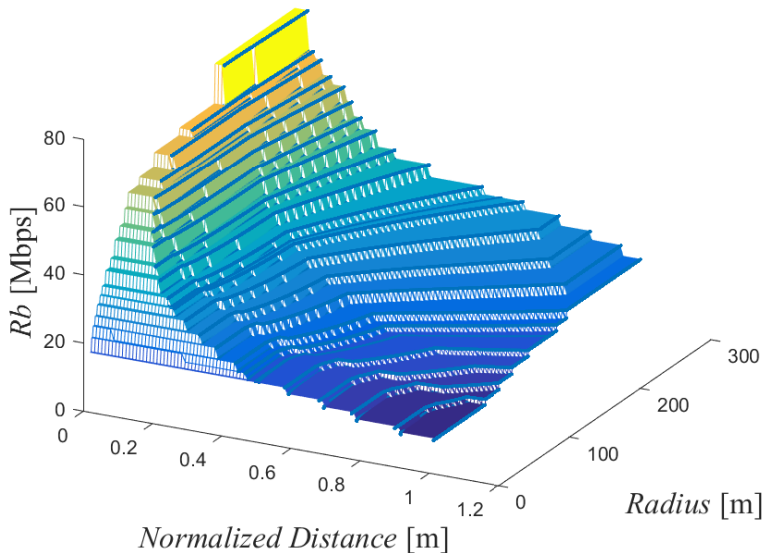

Figure 2.26: 3D View of the PHY throughput mapped into MCSs with Northeast Interferer at the 3.5 GHz band with $k = 3$

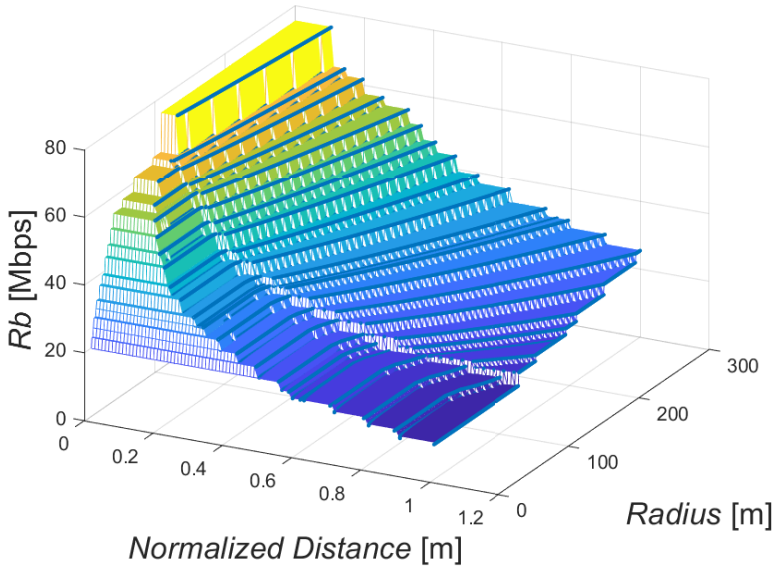

Figure 2.27: 3D View of the PHY throughput mapped into MCSs with No Interferer at the 5.62 GHz band with $k = 3$

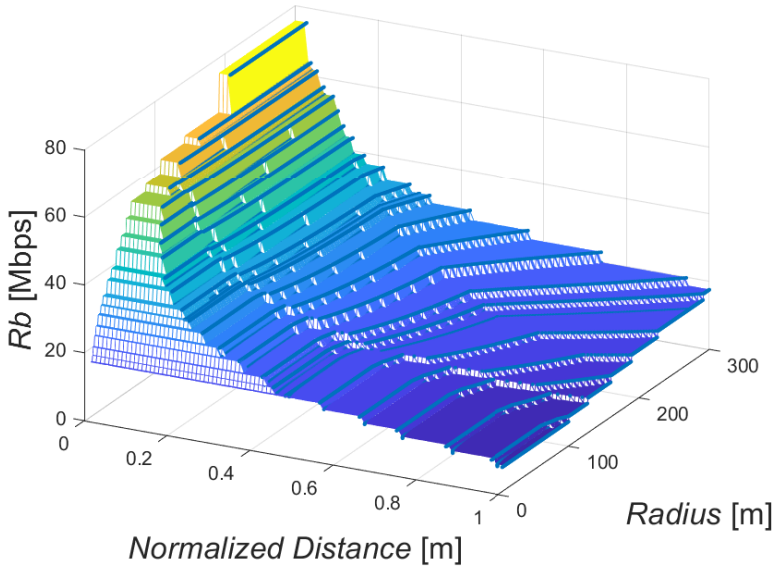

Figure 2.28: 3D View of the PHY throughput mapped into MCSs with Northeast Interferer at the 5.62 GHz band with $k = 3$

Figure 2.23 shows the mapping for the no interferer scenario, for the 2.6 GHz and $k = 3$, where it is possible to see how the available resources are concentrated as users are located near the center of the cell, especially for distances that are smaller than the break point distance. As expected for the NorthEast case scenario, resources are more dispersed throughput the cell´s radius, with the maximum values achieved near the center of the cell more concentrated in a smaller area, when compared to the no interferer scenario.

The process of determination of the physical throughput in 5G NR is less straightforward than in

LTE, since the RB choice takes into account the SCS alongside the bandwidth [19]. The possible combinations of SCS and bandwidth are shown in table 2.6.

Table 2.6: Transmission bandwidth configurations for 5G NR .Adapted from [40]

SCS (kHz)	5 MHz RB	10 MHz RB	15 MHz RB	20 MHz RB	25 MHz RB	30 MHz RB	40 MHz RB	50 MHz RB	60 MHz RB	80 MHz RB	90 MHz RB	100 MHz RB
15	25	52	79	106	133	160	216	270	N/A	N/A	N/A	N/A
30	11	24	38	51	65	78	106	133	162	217	245	273
60	N/A	11	18	24	31	38	51	65	79	107	121	135

From the values of the previous table, it is possible to choose the number of RBs according to the desired bandwidth and SCS. Using this information, it is possible to determine the physical throughput using the following equation:

$$DataRate\,(Mbps) = 10^{-6} \cdot \sum_{j=1}^{J} \left(\nu_{layers}^{(j)} \cdot Q_m^{(j)} \cdot f^j \cdot R \cdot \frac{N_{PRB}^{BW(j),\mu} \cdot 12}{T_s^{\mu}} \cdot \left(1 - OH^{(j)}\right) \right) \quad (2.22)$$

In equation 2.22, $\nu_{layers}^{(j)}$ is the maximum number o layers, $Q_m^{(j)}$ is the modulation order, f^j is the scaling factor which can assume the values 0.75 or 1, μ is the NR numerology which represents the SCS, J is the number of aggregated channels, R is the code rate, $N_{PRB}^{BW(j)}$ is the number of physical resource blocks, determined from table 2.6, T_s^{μ} is the average OFDM symbol, and $OH^{(j)}$ is the overhead configured by the higher layers, which can assume the values 0.14 for FR1 DL, 0.08 for FR1 UL, 0.18 for FR2 DL and 0.10 for FR2 UL.

Determining the TBS values in 5G New radio is also a very different process in comparison to LTE, where there are tables that summarize all the possible choices. The process starts by coputing the number of information allocated resources N_{RE} and information N_{info} as follows:

$$N_{RE} = N_{RE}^{'} \cdot N_{symb}^{sh} - N_{DMRS}^{PRB} - N_{oh}^{PRB} \quad (2.23)$$

where $N_{RE}^{'}$ is given by:

$$N_{RE}^{'} = N_{SC}^{RB} \cdot n_{PRB} \quad (2.24)$$

$$N_{info} = N_{RE} \cdot R \cdot Q_m \cdot \nu \quad (2.25)$$

In case $N_{info} \leq 3824$, one must determine $N_{info}^{'}$ through the following equations and than

consult table 2.7 to choose the appropriate TBS value:

$$N_{info}^{'} = max\left(24, 2^n \cdot \left[\frac{N_{info}}{2^n}\right]\right) \quad \textbf{(2.26)}$$

where the variable n is given by:

$$n = max\left(3, [log_2\left(N_{info}\right)] - 6\right) \quad \textbf{(2.27)}$$

Table 2.7: TBS for 5G for $N_{info} \leq 3824$, adapted from [37]

Index	TBS	Index	TBS	Index	TBS	Index	TBS
1	24	31	336	61	1288	91	3624
2	32	32	352	62	1320	92	3752
3	40	33	368	63	1352	93	3824
4	48	34	384	64	1416		
5	56	35	408	65	1480		
6	64	36	432	66	1544		
7	72	37	456	67	1608		
8	80	38	480	68	1672		
9	88	39	504	69	1736		
10	96	40	528	70	1800		
11	104	41	552	71	1864		
12	112	42	576	72	1928		
13	120	43	608	73	2024		
14	128	44	640	74	2088		
15	136	45	672	75	2152		
16	144	46	704	76	2216		
17	152	47	736	77	2280		
18	160	48	768	78	2408		
19	168	49	808	79	2472		
20	176	50	848	80	2536		
21	184	51	888	81	2600		
22	192	52	928	82	2664		
23	208	53	984	83	2728		
24	224	54	1032	84	2792		
25	240	55	1064	85	2856		
26	256	56	1128	86	2976		
27	272	57	1160	87	3104		
28	288	58	1192	88	3240		
29	304	59	1224	89	3368		
30	320	60	1256	90	3496		

For the cases when the condition $N_{info} \leq 3824$ is not satisfied, the values of n and $N_{info}^{'}$ are computed using equations 2.28 and 2.29:

$$n = log_2\left(N_{info} - 24\right) - 5 \quad \textbf{(2.28)}$$

$$N_{info}^{'} = 2_n \cdot round\left(\frac{N_{info} - 24}{2_n}\right) \quad \textbf{(2.29)}$$

If the value of R is less than or equal to $\frac{1}{4}$, the TBS value is give by:

$$TBS = 8 \cdot C \cdot \left(\frac{N_{info}^{'} + 24}{8 \cdot C}\right) \quad \textbf{(2.30)}$$

where C is given by:

$$C = \frac{N_{info}^{'} + 24}{3816} \quad \textbf{(2.31)}$$

For the cases when $R \geq \frac{1}{4}$, if $N_{info}^{'} \geq 8424$ the value of C must be calculated using equation 2.32, after what equation is 2.30 is used to determine the TBS value. For the same value of R, if $N_{info}^{'} \geq 8424$ the value of the TBS must then be determined by equation 2.33:

$$C = \frac{N_{info}^{'} + 24}{8424} \quad \textbf{(2.32)}$$

$$TBS = 8 \cdot \left(\frac{N_{info}^{'} + 24}{8}\right) \quad \textbf{(2.33)}$$

Table 2.8 shows the values of physical throughput for a configuration with SCS of 30 kHz and bandwidth of 20 MHz.

With the previous information, it was possible to update the Matlab programs used on the previous sections to compute the values of CNIR and physical throughput in the considered cellular topology. Once again, we consider the frequency bands of 2.6, 3.5, and 5,62 GHz with the previously described parameters, evaluating the system's capacity by considering $k = 3$ and $k = 4$.

The adoption of higher bandwidth values, the use of cyclic prefix OFDM and the possibility of

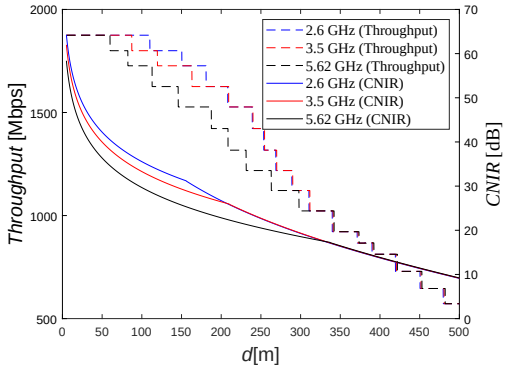

(a) No Interferer for the three bands with $k = 3$

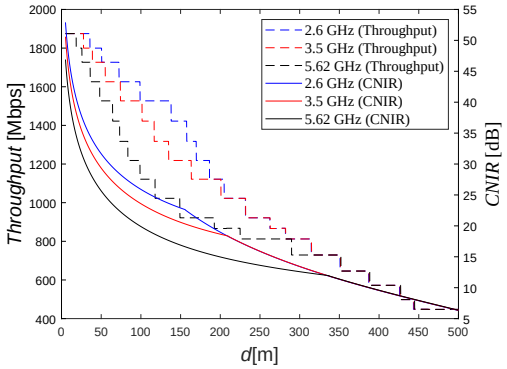

(b) East Interferer for the three bands with $k = 3$

Figure 2.29: CNIR and Physical throughput as a function of d for the No and East interferer scenario for $k = 3$ and bandwidth of 100 MHz

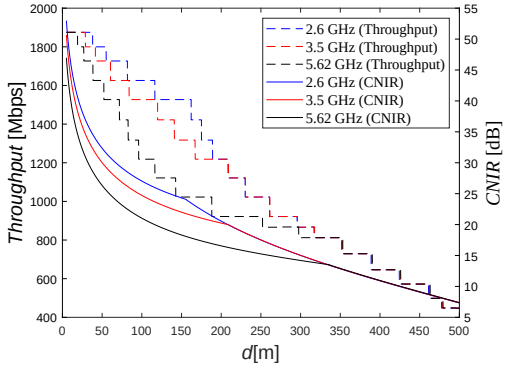

(a) Northeast Interferer for the three bands with $k = 3$

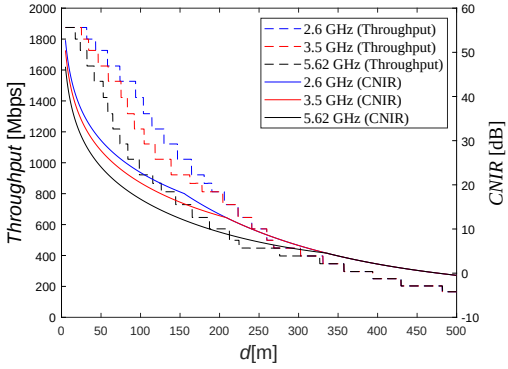

(b) Southeast Interferer for the three bands with $k = 3$

Figure 2.30: CNIR and Physical throughput as a function of d for the Northeast and Southeast interferer scenario for $k = 3$ and bandwidth of 100 MHz

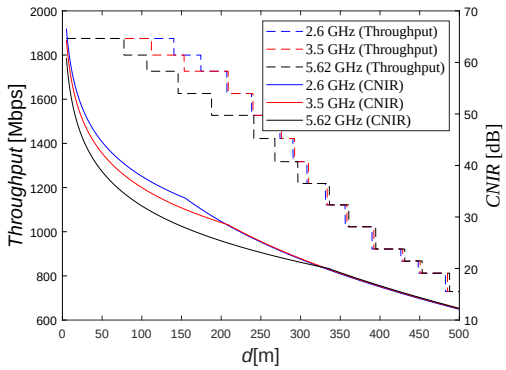

(a) No Interferer for the three bands with $k = 4$

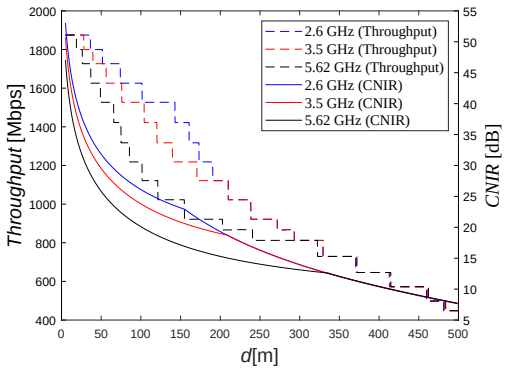

(b) East Interferer for the three bands with $k = 3$

Figure 2.31: CNIR and Physical throughput as a function of d for the No and East interferer scenario for $k = 4$ and bandwidth of 100 MHz

Table 2.8: NR UL Throughput for a bandwidth of 20 MHz and SCS of 30 kHz

MCS	Code Rate	Modulation Order	Max. Throughput (Mpbs)
0	120	2	14.78
1	193	2	23.77
2	308	2	37.93
3	449	2	55.30
4	602	2	74.15
5	378	4	93.11
6	434	4	106.91
7	490	4	120.70
8	553	4	136.22
9	616	4	151.74
10	658	4	162.09
11	466	6	172.18
12	517	6	191.03
13	567	6	209.50
14	616	6	227.61
15	666	6	246.08
16	719	6	265.67
17	772	6	285.25
18	822	6	303.72
19	873	6	3225.69
20	682.5	8	336.24
21	711	8	350.28
22	754	8	371.47
23	797	8	392.65
24	841	8	414.33
25	885	8	436.00
26	916.5	8	451.52
27	948	8	467.04

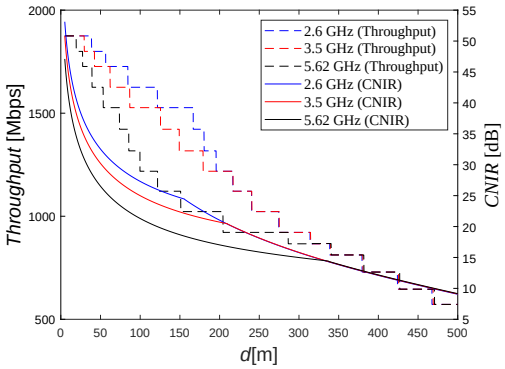

(a) Northeast Interferer for the three bands with $k = 4$

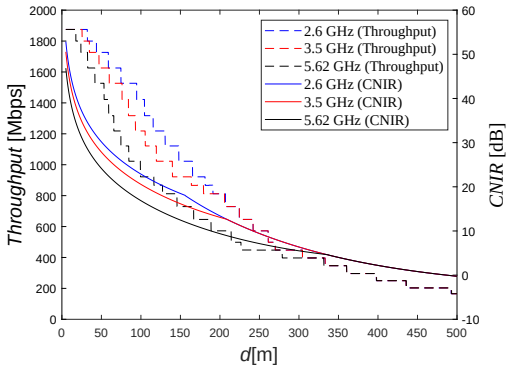

(b) Southeast Interferer for the three bands with $k = 4$

Figure 2.32: CNIR and Physical throughput as a function of d for the Northeast and Southeast interferer scenario for $k = 4$ and bandwidth of 100 MHz

allocating higher values of resource blocks and TBSs over different SCSs ensure much higher values of PHY throughput in NR, comparing the obtained results with those in the previous subsection. For the non interferer case with $k = 3$, the PHY throughput achieves a maximum of 1800 Mbps, for all the frequency bands, for the shortest distances. As the computations of

results for 5G NR and LTE considers the same maximum achievable modulation order, the values for the CNIR are not significantly grater for the cases where 5G NR assumptions are considered.

Even though the capacity of the system is significantly improved in NR, the behavior of the curves regarding the breakpoint distance an the position of the interferes is very similar for the LTE scenario, with the point where the achievable throughput for the 2.6 and 3.5 GHz frequency bands becomes the same occurring at a slightly greater distance for the East interferer case, shown in figure 2.29 b).

Following the same approach proposed for the LTE scenarios, one presents a 3D view of the physical throughput mapped into modulation code schemes considering the assumptions of 5G New Radio. The results presented here consider a SCS of 60 kHz and bandwidth of 100 MHz.The representations cover the scenario where there is no interferer and also the scenarios, NorthEast interferers. Results considering $k = 3$ are presented in figures 2.33, 2.34, 2.35, 2.36, , and 2.38.

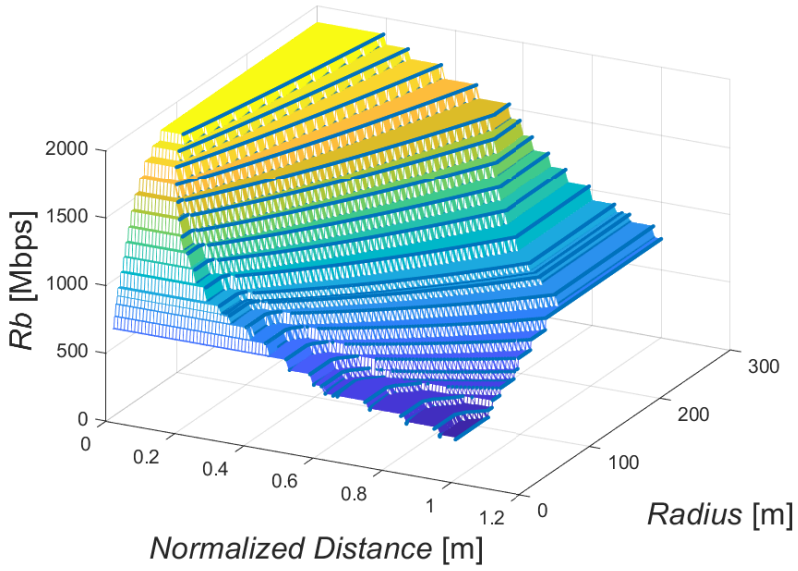

Figure 2.33: 3D View of the PHY throughput mapped into MCSs with No Interferer at the 2.6 GHz band with $k = 3$

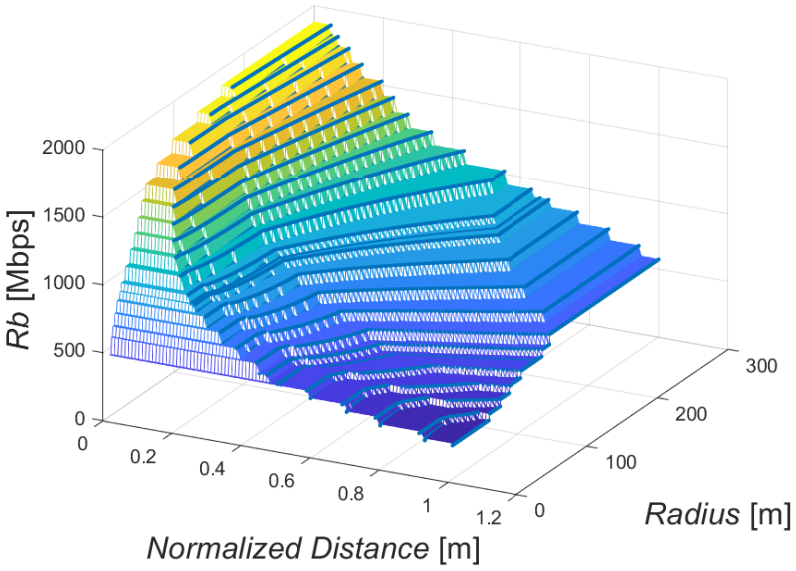

Figure 2.34: 3D View of the PHY throughput mapped into MCSs with Northeast Interferer at the 2.6 GHz band with $k = 3$

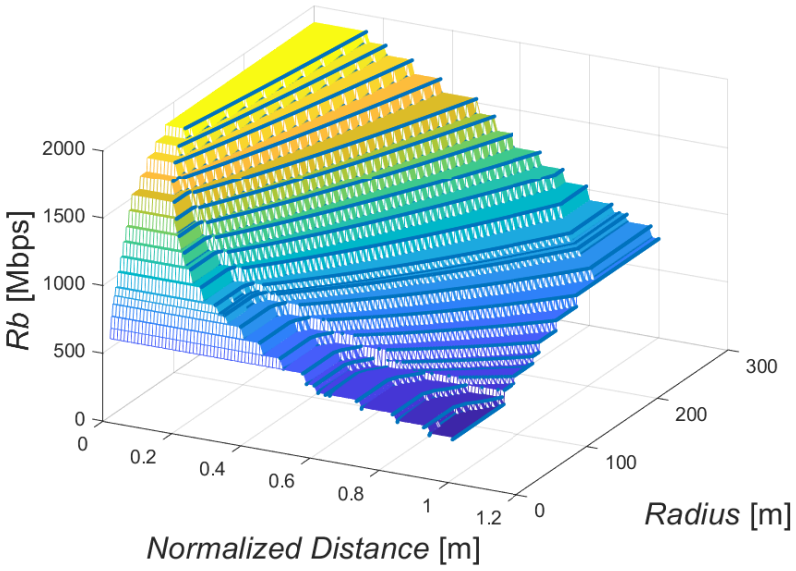

Figure 2.35: 3D View of the PHY throughput mapped into MCSs with No Interferer at the 3.5 GHz band with $k = 3$

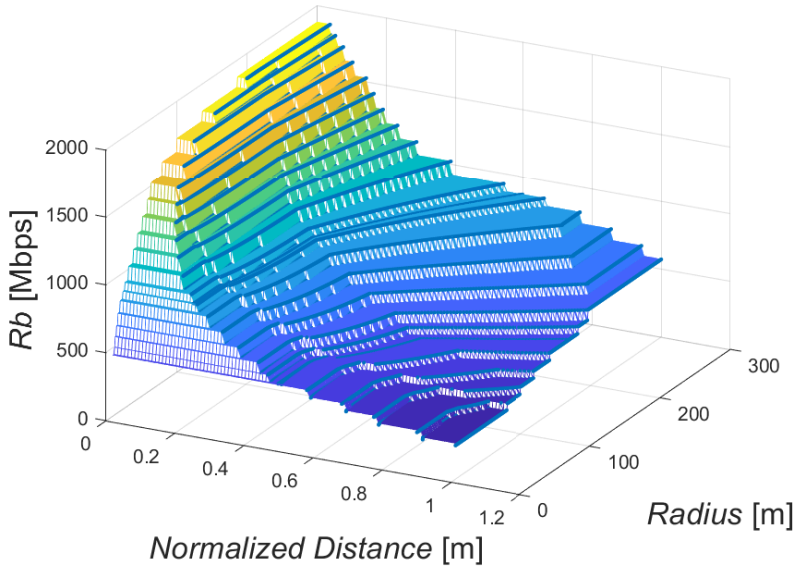

Figure 2.36: 3D View of the PHY throughput mapped into MCSs with Northeast Interferer at the 3.5 GHz band with $k = 3$

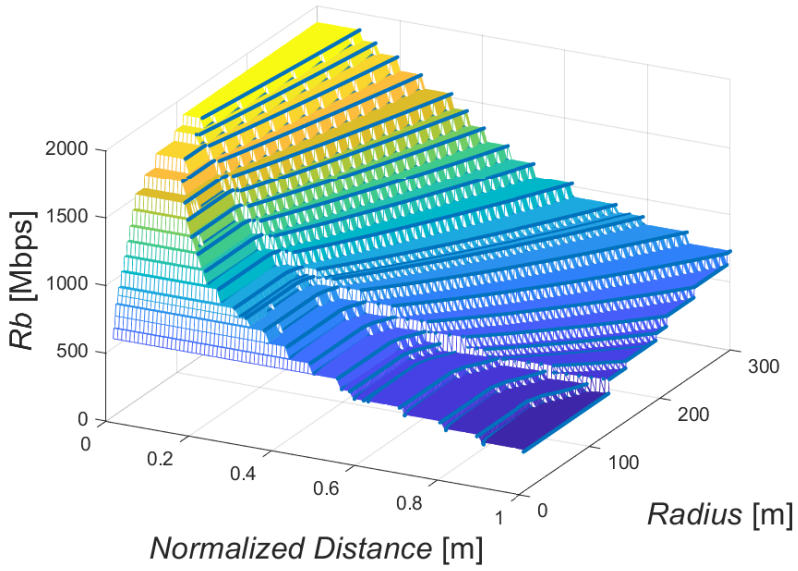

Figure 2.37: 3D View of the PHY throughput mapped into MCSs with No Interferer at the 5.62 GHz band with $k = 3$

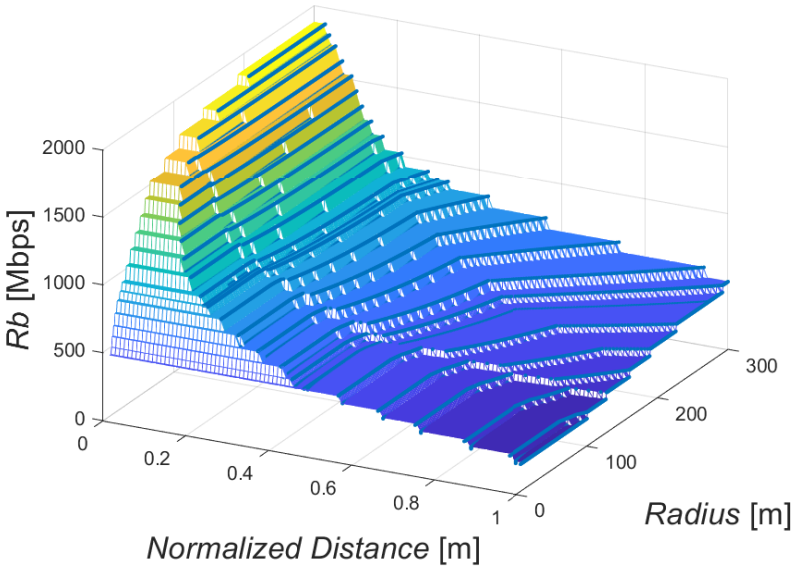

Figure 2.38: 3D View of the PHY throughput mapped into MCSs with Northeast Interferer at the 5.62 GHz band with $k = 3$

From the results shown in figure 2.33 one can see how the area covered by the available resources near the center of the cell is greatly improved when compared for the results in LTE, and it is also possible to see how the decrease in the system´s capacity accelerates as the user moves to distances greater than the breakpoint distance. For the 5.62 GHz frequency band the spread of resources across the cell´s radios happens more drastically, as shown in figures 2.37, 2.38, with the worst case happening for the NorthEast scenario, where the maximum achievable data rate occurs for shortest distances.

2.7 Analytical Formulation of the Average CNIR

The analytical formulation to compute the average CNIR, was proposed in [50]. It was first proposed for LTE-based networks, considering a typical OFDM channel and the mapping between minimum CNIR and MCSs following the technical specifications of 3GPP before Rel.8. Building upon the previous formulation, we also consider for the results presented in this section the 5.62 GHz frequency band as the mapping between CNIR and MCSs for 5G NR, assuming that the maximum modulation order is the same for both cases. The Matlab algorithm used to obtain the values presented computes the average power of the own cell and interferes and solve the integral that define the areas for the case scenarios. The complete mathematical formulation to compute the average CNIR is presented in appendix C.

Results for the average CNIR within LTE are shown for the 2.6 GHz, 3.5 GHz and 5,62 GHz are shown in figures 2.39a, 2.39b, and 2.39c, respectively. The analysis for the assumptions of

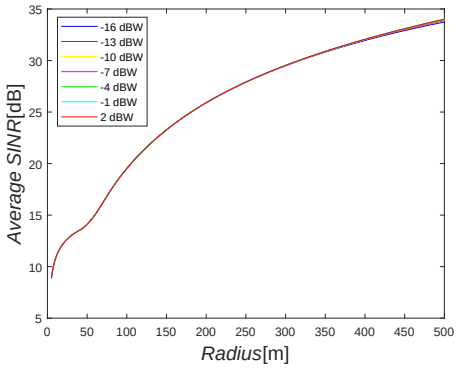

(a) 2.6 GHz

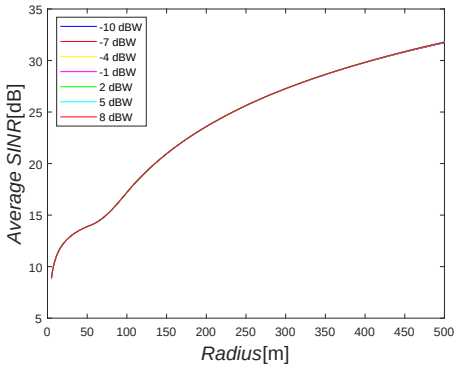

(b) 3.5 GHz

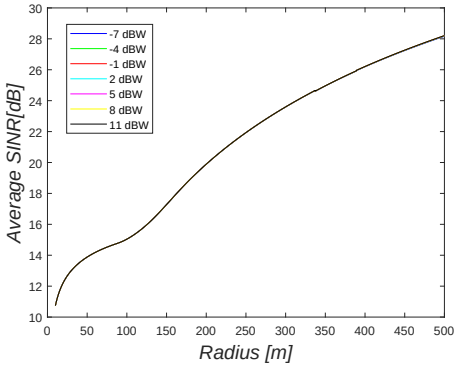

(c) 5.62 GHz

Figure 2.39: Average SINR different values for different transmitter powers

NR, by considering a bandwidth of 100 MHz, SCS of 60 kHz for the three frequency bands, with the same transmitter power assumed for LTE. The individual curves for the average CNIR are presented in figures 2.41a, 2.41b, and 2.41c. It is possible to see from the results obtained that the average CNIR do not dependent on the transmitter power.

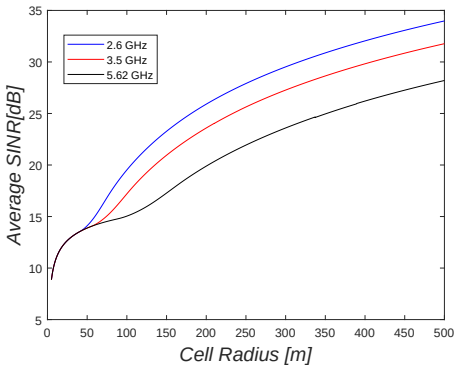

Figure 2.40: Comparison between Average SINR with different values for the transmitter power values for 2.6 GHz, 3.5 GHz and 5.62 GHz

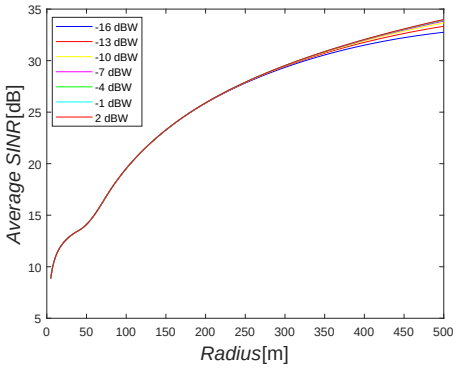

(a) 2.6 GHz

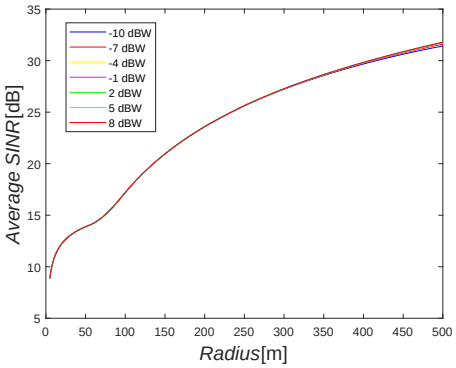

(b) 3.5 GHz

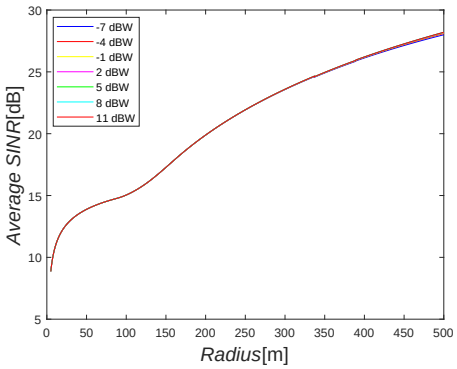

(c) 5.62 GHz

Figure 2.41: Average SINR different values for different transmitter powers with 100MHz bandwidth

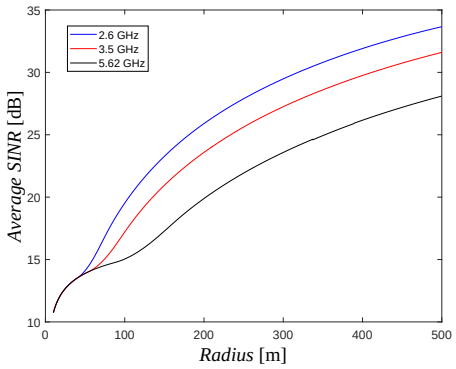

Figure 2.42: Comparison between Average SINR with different values for the transmitter power for the 2.6 GHz, 3.5 GHz and 5.62 GHz, and 100 MHz bandwidth

2.8 Analytical Formulation Supported Throughput

Another parameter of interest for evaluating system capacity in the cellular planning process is the supported throughput (R_{b_sup}) which is computed according to equation 2.34 [54], [55], where d is the distance in which there are MCSs transitions, R_b is the Physical throughput and R is the cell radius:

$$R_{b\_sup} = \sum_{i=1}^{n} \frac{R_{b_i}(d_i^2 - d_{i-1}^2)}{R^2} \quad (2.34)$$

The transition distances will be the radius of the coverage rings presented in figure 2.43 as an example.

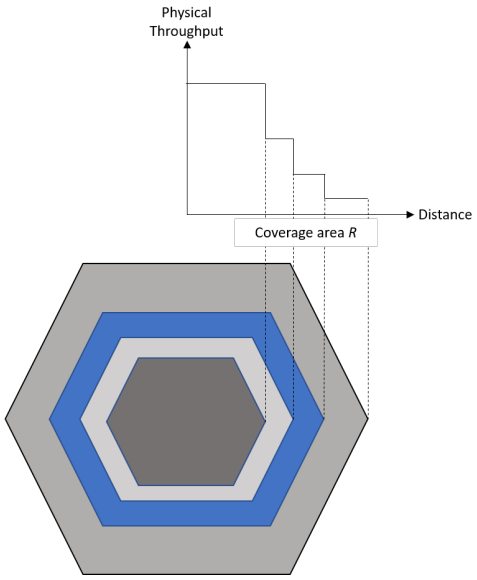

Figure 2.43: Areas of the coverage rings where a given value of PHY throughput for hexagonal has a transition

The supported throughput is computed for LTE and 5G NR, considering $k = 3$ and $k = 4$, with a coverage distance of 500 m for the case with no interferer and with interferer in different positions, simmilar to the analyzes performed in the previous sections. Results for LTE are shown in figure 2.44, 2.45 and for 5G NR inf figures 2.46 and 2.47.

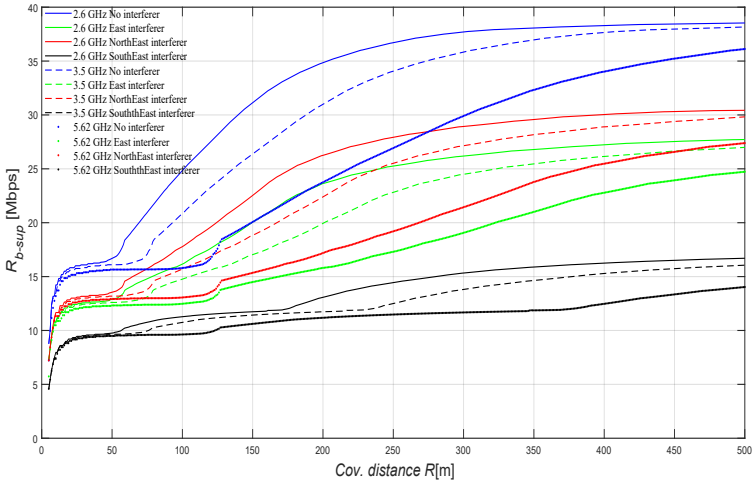

Figure 2.44: Comparison of the supported throughput for $k = 3$ in the pico cellular scenario, for different positions of the interferer from MO $\#2$ and for the case without interference with 20 MHz bandwidth

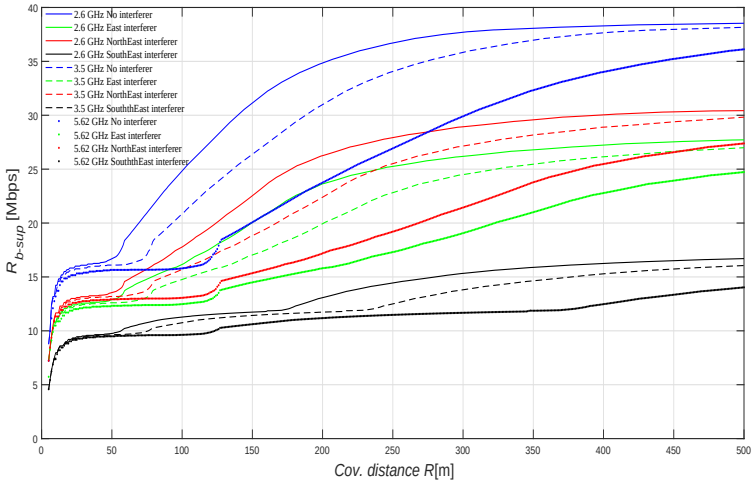

Figure 2.45: Comparison of the supported throughput for $k = 4$ in the pico cellular scenario, for different positions of the interferer from MO $\#2$ and for the case without interference with 20 MHz bandwidth

For both LTE and 5G NR, it is possible to see that the best results are achieved for the case with no interferer, for the 2.6 GHz frequency band, followed by 3.5 GHz and 5.62 GHz, for $k = 3$ and $k = 4$, mainly due to the fact that the breakpoint distance is smaller for 2.6 GHz.As one could expect, considering the analyzes performed in the previous sections, the values for the supported throughput are much higher for $5G$ NR, achieving values higher than 1000 Mbps for $k = 3$ and 1200 Mbps for $k = 4$. The worst case scenario occurs for the South East interferer, for

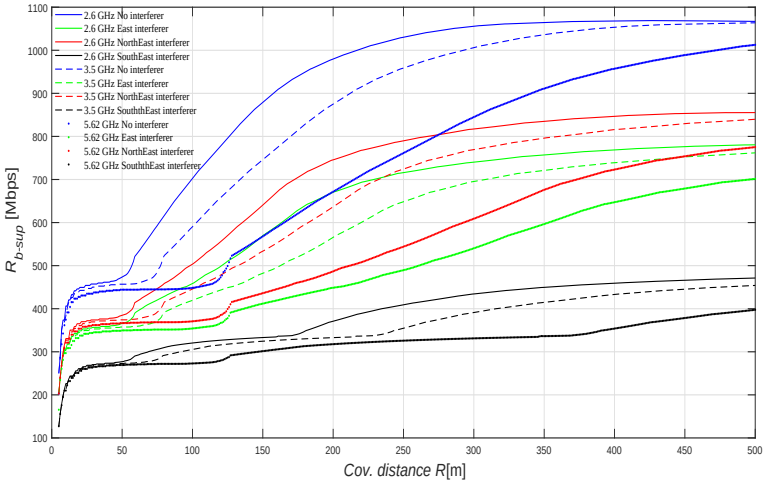

Figure 2.46: Comparison of the supported throughput for $k = 3$ in the pico cellular scenario, for different positions of the interferer from MO #2 and for the case without interference with 1000 MHz bandwidth

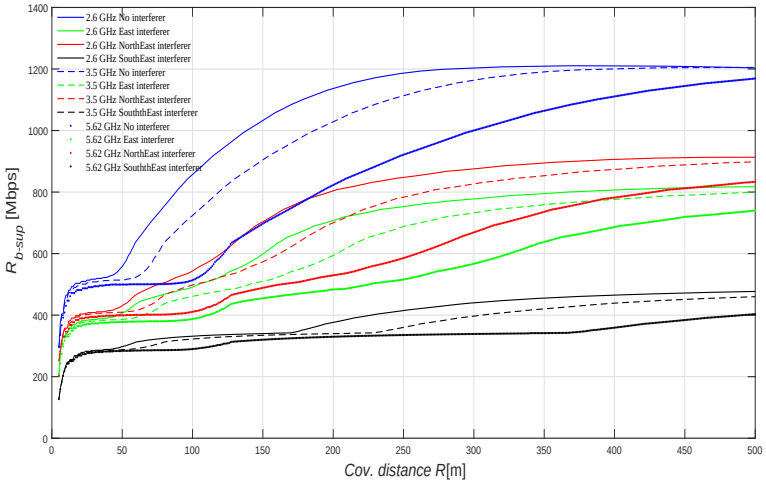

Figure 2.47: Comparison of the supported throughput for $k = 4$ in the pico cellular scenario, for different positions of the interferer from MO #2 and for the case without interference with 1000 MHz bandwidth

the frequency bands considered,while the performance in the sharing scenario became better for distances longer than circa 125 m.

2.9 Cost/Revenue Optimization

Cost revenue analysis and economic tradeoff are points of particular interest in the the planning and optimization of cellular systems. This analysis involves several parts such mobile operators, subscribers and equipment vendors. For mobile operators, the economic tradeoff analysis aims at achieving the maximum revenue taking into account the several types of expenses necessary to the deployment.

In this section one proposes a cost/revenue analysis based on the MO point of view, taking into account some of the core aspects for cellular planning and performing the analysis based on the achievable capacity of the network, following the results obtained in the previous sections of this chapter.According to the authors of [56] [57] and [58] one can classify the system's costs in two parts i.e., capital costs and operating costs. The capital costs are:

- Fixed expenses such as spectrum auctions, fees and licensing;
- The costs related to the number of transceivers per unit of area;
- Costs proportional to the number of BSs per unit of area.

The operating costs during the lifetime of the system can be summarized as follows:

- Costs proportional to the number of BSs per unit of area;
- Costs of the number of transceivers per unit of area.

For the analysis proposed in this work, one considers that the costs will be evaluated on an annual bases. First we define the cost per unit of area as follows:

$$C_{[€/km^2]} = C_{fi[€/km^2]} + C_b \cdot N_{hex/km^2} \quad (2.35)$$

In equation 2.35 C_{fi} represents the fixed terms of the costs and C_b is the cost per BS while N_{hex/km^2} is the number of hexagonal coverage zones per unit of area with its value given by:

$$N_{hex/km^2} = \frac{2}{3 \cdot \sqrt{3} \cdot R^2} \quad (2.36)$$

The cost per BS is:

$$C_b = \frac{C_{BS} + C_{bh} + C_{inst}}{N_{year}} + C_{M\&O} \quad (2.37)$$

In equation 2.37, N_{year} represents the project's lifetime, which is assumed to of 5 years for the purposes of this work. Moreover, C_{BS} is the cost of the BS, C_{inst} is the installation cost of the BS and $C_{M\&O}$ is the operation and maintenance cost.
C_b can be obtained by the assumptions presented in table 2.9 from [59], for a five-year project duration.

Table 2.9: Assumptions for base station costs

Parameters		Values[€]	
		UHF (2.6 and 3.5 GHz)	**SHF (5.62 GHz)**
Initial costs	**BS price,** C_{BS}	**2000**	**2000**
	Installation, C_{inst}	**200**	**200**
Annual costs	**Backhaul,** C_{Bh}	**2000**	**2000**
	Fixed, C_{fi}	**110**	**0**
	Op. and maint., $C_{M\&O}$	**250**	**250**

For a coverage area with a hexagonal shape, the revenue $(R_v)_{cov-zone}$ can be obtained considering the supported throughput per BS:

$$(R_v)_{cov-zone} = \frac{N_{hex[km^2]} R_{(b-sup)_{equiv}} \cdot T_{bh} \cdot R_{R_b[€/min]}}{R_{b-ch[kpbs]}} \quad (2.38)$$

where $R_{R_b[€/min]}$ is the revenue of a channel with data rate $R_{b[kbps]}$, $N_{hex[km^2]}$ is the number o hexagonal areas, $R_{b-ch[kpbs]}$ is the channel's data rate and T_{bh} represents the duration of busy hours per day. Considering the analytical formulation proposed in the last sections and the technical specifications of NR, results for CNIR and physical throughput are shown in figure , where the maximum considered coverage distance is d = 1000 m. The variation of the supported throughput is presented in figure 2.49.

With the above equations one can obtain the revenue per unit of area, by taken into account the revenue per cell and the number of cells per unit of area:

$$R_{V[€/km^2]} = N_{hex[km^2]} \cdot (R_v)_{cell} = N_{hex[km^2]} \cdot \frac{R_{b-sup[kbps]} \cdot T_{bh} \cdot R_{R_b[€/min]}}{R_{b-ch[kpbs]}} \quad (2.39)$$

Revenues are considered in an annual basis, where we considered six busy hours per day, 240 busy days per year [60], and the price of a 144 kbps "channel" per minute (corresponding to the price of ≈ 1 MB), considering $R_{144kbps[Euro/min]}$ =0.005, approximately 5€ per 1 GB. Figure 2.50 presents results for the revenue per cell per year, for R_b= 144 kbps, through variation of R for R_{max} = 1000 m. One can observe that the highest revenue per cell is only for 2.6 GHz band, overcame by 3.5 GHz bands at circa than 210 m and the over passed by 5.62 GHz at circa than 320 m.

Figure 2.51 shows the global cost per unit length per year, C_0, and the revenue per unit length per year. It is possible to observe that revenues are always higher than the costs. The profit, P_{ft}, is a metric that needs to be considered to improve the network, and is given by the difference

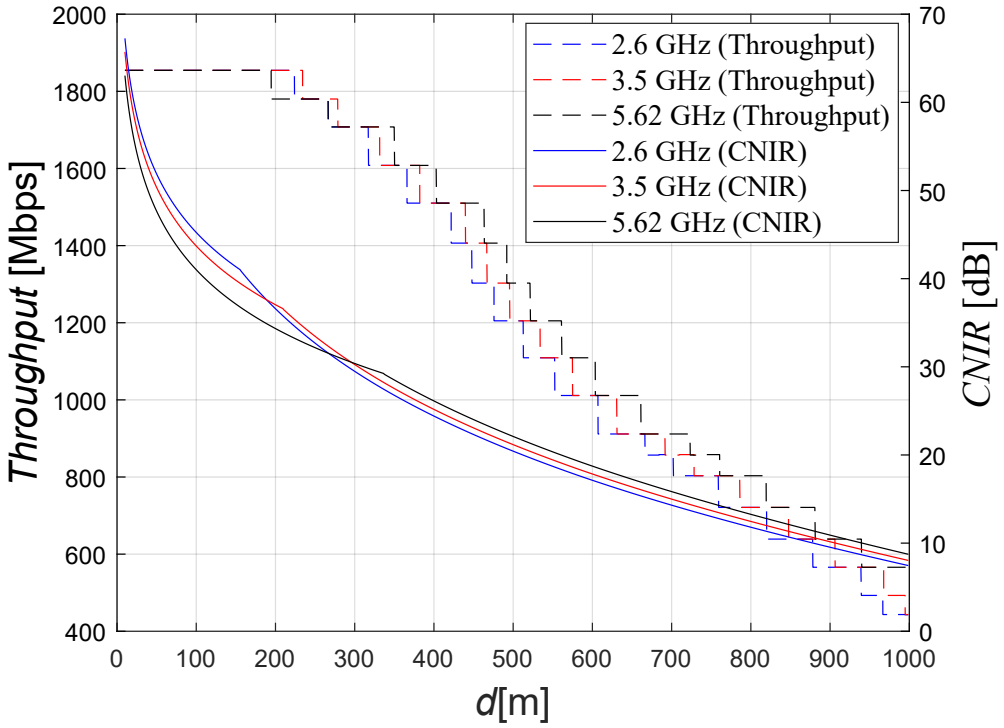

Figure 2.48: Variation of CNIR and Physical throughput for d_{max}=1000 m

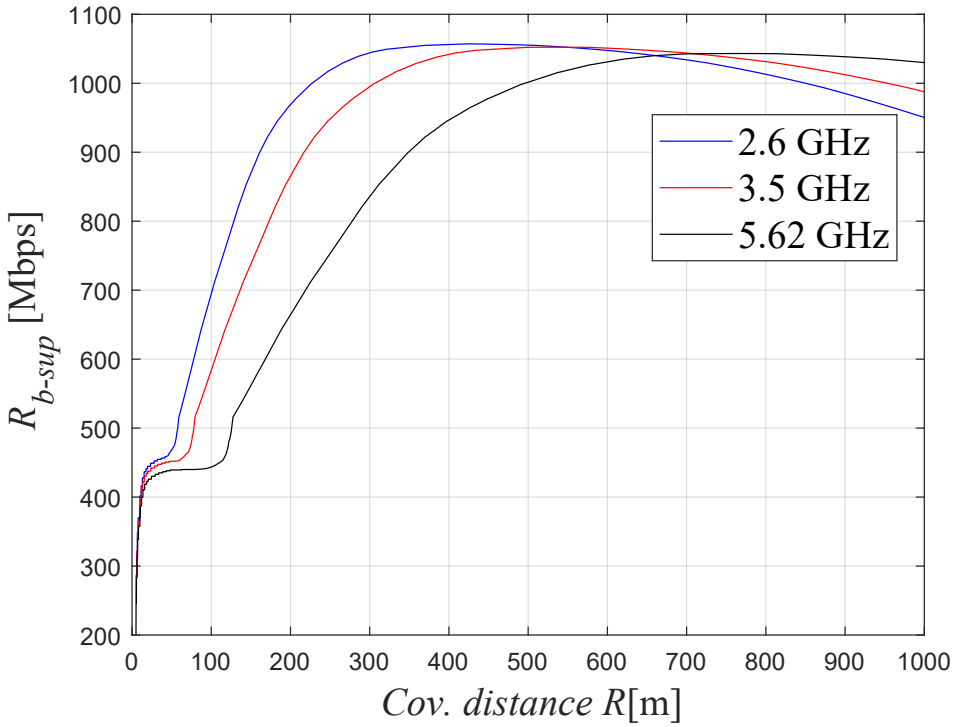

Figure 2.49: Variation of supported throughput for R_{max}=1000 m

between revenues and costs, in e/km^2.

The profit is given by:

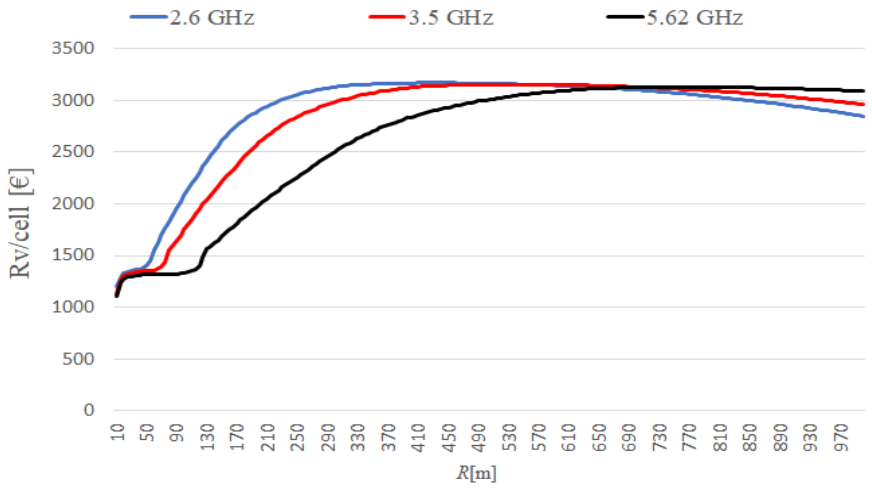

Figure 2.50: Revenue per cell for R_{max}=1000 m

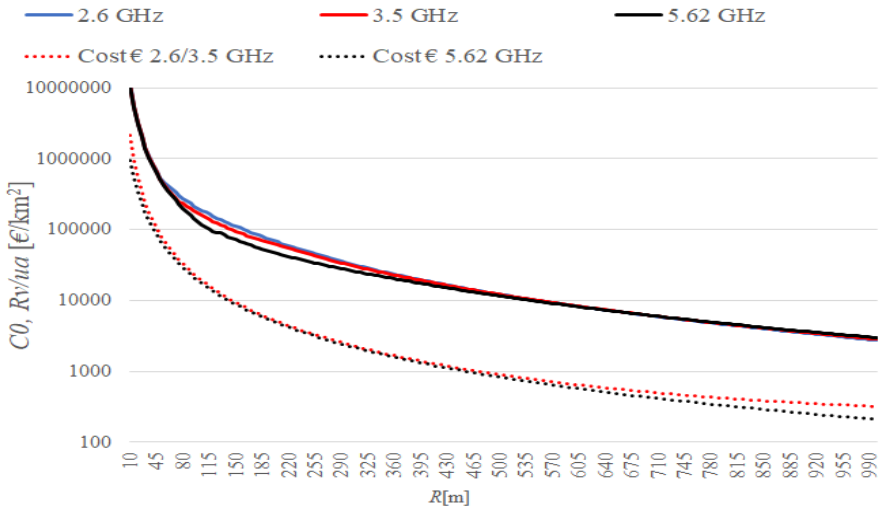

Figure 2.51: Network cost/revenue per unit are per year as a function of R, for R_{max}=1000 m

$$P_{[€/km^2]} = R_v - C \quad (2.40)$$

And the profit represented in percentage terms is given by:

$$P_{[\%]} = \frac{R_v - C}{C} \quad (2.41)$$

Figure 2.52 shows the profit in percentage, instead of the absolute profit, because this is a more relevant metric for operators and service providers [59]. If $R_{V[€/km^2]} - C_{0[€/km^2]}$ is positive, there will be positive profit. For the studied distances, all the frequency bands are profitable,

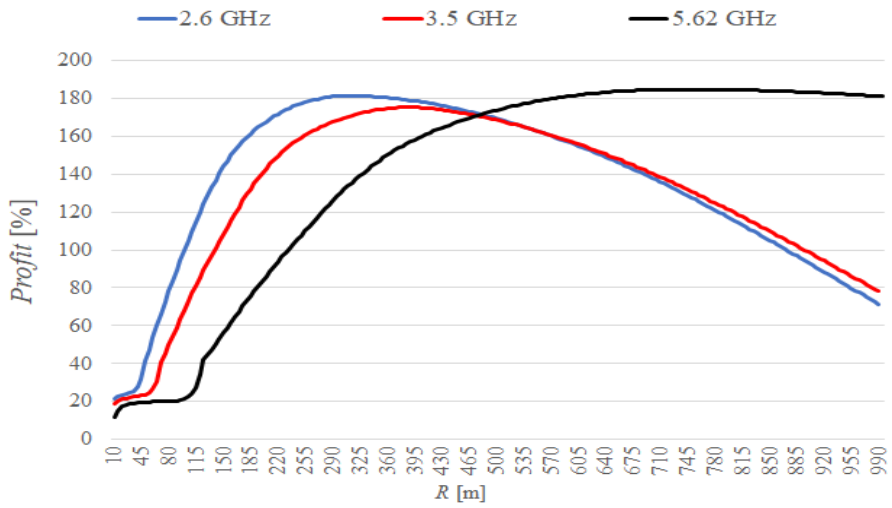

Figure 2.52: Profit per unit area per year as a function of R, R_{max}=1000 m

however, for distances higher than 1335 m the system is going to be unprofitable for the considered UHF bands, mainly due to fixed costs.

2.10 Summary and Conclusions

This chapter analyzes the use o Spectrum Sharing for UHF/SHF considering the assumptions of LTE/4G and 5G New Radio to perform the mapping between SINR and modulation code schemes and to obtain the physical throughput by considering the technical specifications of 3GPP for both 4G and 5G with an analytical formulation that considers a hexagonal topology and the use of the Umi LoS propagation model. The PHY and supported throughput have been analyzed by considering reuse patterns of 3 and 4 and a maximum bandwidth of 20 MHz for LTE/4G and 100 MHz for 5G.

The allocation of physical resources blocks for 5G New Radio depends not only on the bandwidth, as it is the case for LTE, but also on the Sub Carrier Spacing. As expected, the data rates for NR are considerable superior when compared to the results for LTE. For the analysis performed, one has considered the use of three frequency bands, i.e., 2.6 GHz, 3.5 GHz and 5.62 GHz. The last frequency band considered is part of the unlicensed spectrum, while the 3.5 GHz has been adopted in several parts of the world for use in the recently deployed 5G NR networks. In this sense, the proposed analysis gives a perspective regarding system capacity under different deployment scenarios.

Results indicate the higher values of Physical and supported throughput are achieved for the case of no interferer, with the 2.6 GHz frequency band performing better, specially for distances smaller than the break point distance. The worst case scenario for the supported throughput

happens with the presence of the East interferer, with the same behavior being observed for both, 5G and LTE assumptions.

We have also analytically compared the cost-capacity trade-off between the UHF and SHF bands for mobile cellular, while considering the technical specifications for 5G New Radio to perform the mapping between the carrier-to-noise-plus-interference and modulation code schemes to obtain the supported throughput for the considered frequency bands.We have studied the performance of the carrier-to-noise-plus-interference ratio with the coverage distance, figuring out the impact in the cellular planning optimization process. The equivalent supported throughput has been evaluated using reuse pattern k = 3.

For the UHF/SHF bands, the profit is very low for the shortest distances, and starts to increase at a distance equal to the ratio between the break-point distance and the co-channel reuse factor. It achieves maxima for values of R equal to circa than 310, 390 and 740 m, at 2.6, 3.5 and 5.62 GHz frequency bands, respectively.

As 5G New Radio will allow for communication with higher data rate when compared to previous LTE/LTE-A networks, bringing the possibility of reducing the general costs of the system while allowing for an increase on the number of mobile subscribers, resource planning and optimization are a core aspect for the success of this new technology.

Chapter 3

Cellular Planning and Optimization with Carrier Aggregation

3.1 LTE-Sim Packet Level Simulator

LTE-Sim is an open-source framework proposed to perform the verification of LTE-based systems and to simulate LTE networks [61]. It includes several aspects of LTE technical specifications, such as Evolved Packet System (EPS) and Evolved Universal Terrestrial Radio Access (E-UTRA), allowing for the use of single cell and multi-cell environments and handover procedures alongside traffic generators and scheduling procedures.

The ecosystem of LTE-Sim was built using the $C++$ programming language and the objected-oriented paradigm to ensure modularity, being composed of 90 classes. The protocol stack of LTE-Sim is shown in figure 3.1.

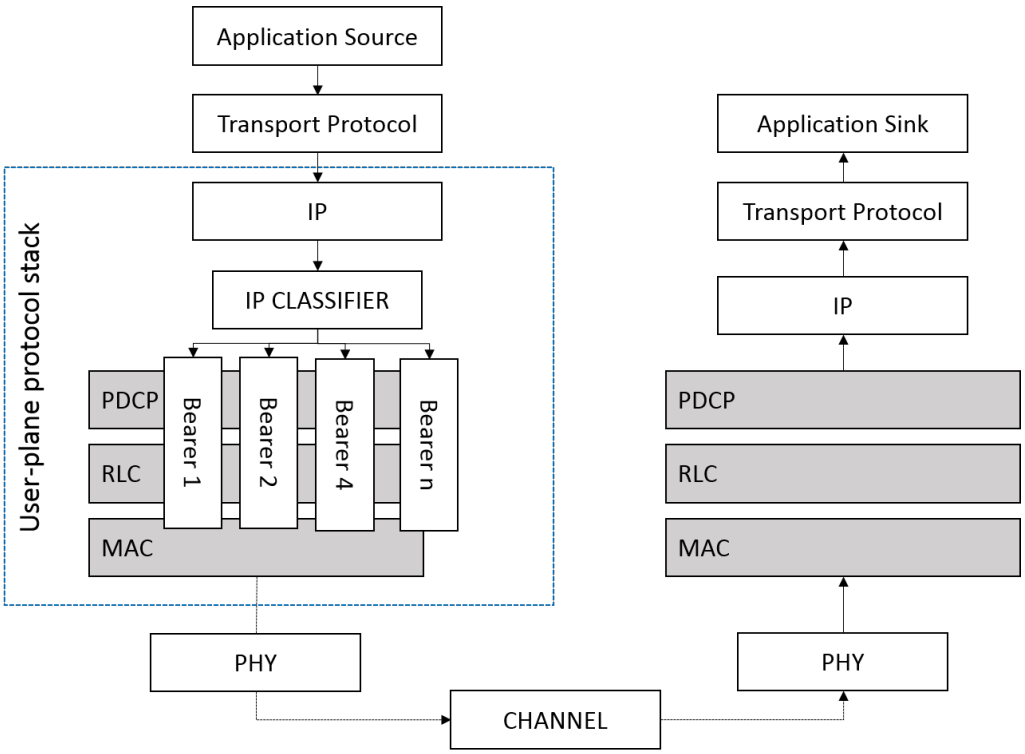

Figure 3.1: Protocol stack of LTE-Sim, adapted from [61]

The four main components of the project are:

- The simulator;

- Network Manager;
- Flows Manager;
- Frame Manager.

Radio resource allocation is made in the time-frequency domain with the time domain resources being allocated according to each TTI with duration of 1 ms. The frequency domain, on the other hand considers the division of the bandwidth into subchannels of 18 kHz. For every TTI, there are 14 OFDM symbols divided into 0.5 ms, with each consecutive TTI forming a LTE frame.
Regarding the application layer, the simulator offers four different traffic generators:

- Trace-based;
- Voice over IP (VoIP);
- Constant Bit Rate (CBR);
- Infinite Buffer.

The trace-based application uses trace files extracted from [62], that provides video traces created by the encoding of uncompressed video files [63] that allow the simulation of realistic video files transmissions.
VoIP applications operate by coding voice messages and sending them as data packets over IP-based networks and are common on telephony systems [64]. In LTE-Sim, these applications use flows based on G.729 which is a coder consisting of nano-rate that uses fixed-point arithmetic operations and works at 8 Kbits/s [65]. The simulator uses a Markov chain with the VoIP applications being divided into ON/OFF periods where the source sends packets of 20 bytes during the ON period and within intervals of 20 ms and keeps a 0 rate of transmission during the OFF period.
CBR refers to an encoding technique which allows for the use of applications that keep the bit rate the same throughout the transmission [66]. One of the dis-vantages of these types of applications is the lack of optimization in the relation quality versus storage. The simulator allows the configuration of packet size and packet time interval for this kind of applications.
The infinite Buffer generator works by creating applications that always have packets to be sent by the source.
At the level of channel structure, the simulator works with all the bandwidths for LTE-based systems i.e., 1.4, 3, 5, 10, 15, and 20 MHz, offering a bandwidth manager that allows for each device under a simulated scenario to know the bandwidth being used, by means of a PHY object

defined to each device. Furthermore, two types of frame structures are available i.e., FDD and TDD following the specifications for E-Ultra.

The FDD frame structure, referred to as frame structure type 1, is composed of 10 subframes available for DL and also 10 subframes for UL with transmissions at each 10 ms interval in the latter case [52], being applicable to full duplex and half duplex. Each radio frame is composed of 20 slots and each subframe comprises two consecutive slots, as represented in figure 3.6.

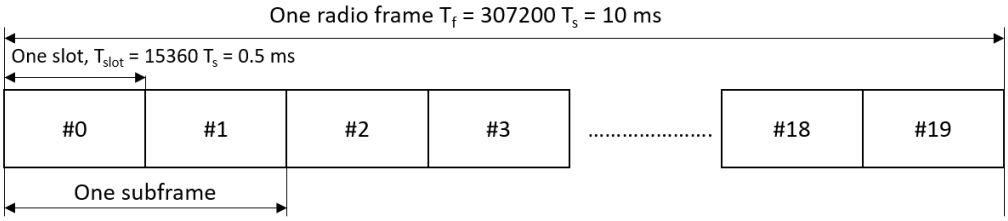

Figure 3.2: FDD Frame Structure, adapted from [52]

The TDD frame structure is represented in figure 3.3, where each radio frame is divided in two halves that in turn are composed of subframes corresponding to every TTI. For frame structure

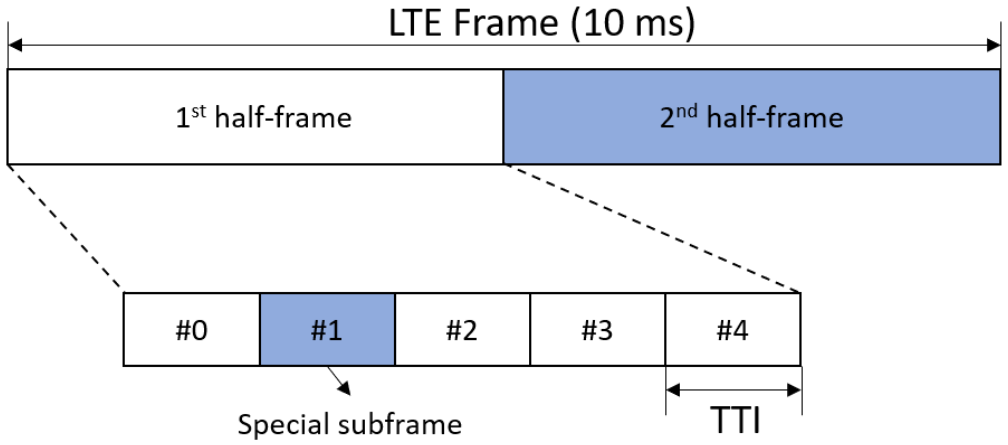

Figure 3.3: TDD Frame Structure, adapted from [52]

2, the possible configurations for UL-DL are listed in table 3.1, adapted from [52], where D stands for DL subframes that are reserved for DL transmissions, U for UL subframes reserved for UL transmissions, and S is a special type of subframe, that carries information for DL Pilot Time Slot (DwPTS), UL Pilot Time Slot (UpPTS), and Guard Period (GP).

The simulator computes the SINR for each subchannel according to equation 3.1, where F is the noise figure, N_0 is the noise spectral density, B is the bandwidth for a resource block, and I is the interference computed for the eNBs sharing the same frequency resources:

Table 3.1: Uplink-downlink configurations for frame structure 2

UL-DL configuration	DL-to-UL Switch-point periodicity	Subframe Number									
		0	1	2	3	4	5	6	7	8	9
0	5 ms	D	S	U	U	U	D	S	U	U	U
1	5 ms	D	S	U	U	D	D	S	U	U	D
2	5 ms	D	S	U	D	D	D	S	U	D	D
3	10 ms	D	S	U	U	U	D	D	D	D	D
4	10 ms	D	S	U	U	D	D	D	D	D	D
5	10 ms	D	S	U	D	D	D	D	D	D	D
6	5 ms	D	S	U	U	U	D	S	U	U	D

$$SINR_{i,j} = \frac{P_{RX,i,j}}{(FN_0B) + I} \quad (3.1)$$

For the transmit power $P_{RX,i,j}$, in this study one considers a normalized transmit power computed to ensure the delivery of SINR for all cell radius, for the 800 MHz and 2.6 GHz frequency bands.

Regarding mobility, LTE-Sim offers two implementations, i.e., random direction and random walk. In the random direction mobility model, an entity chooses a random direction in which to travel and moves towards the pre-defined border following that direction. When the entity achieves the border, it pauses its movement and chooses a new direction to follow [67]. For the random walk model, an entity chooses randomly a direction and a speed and moves from its current location to a new location using the variables assigned. For the results presented in the following sections, the random direction mobility model is used to perform the movements of the UEs.

3.2 Carrier Aggregation in 3GPP

Carrier Aggregation is one of the key technologies addressed by 3GGP and it is proposed to deal with the spectrum fragmentation offering flexibility to adapt new technological solutions to a variety of spectrum scenarios [68]. Basically CA aims at increasing transmission bandwidth what results in direct benefit to the achievable data rate [69]. LTE and LTE-Advanced allow for the deployment of CA with carriers at contiguous Radio Frequency (RF) bands or at different bands and each aggregated carrier is called a Carrier Component (CC).

Figure 3.4 presents the possible applications of CA in LTE and LTE-A. Release 10 of LTA-A allows for a maximum of two carriers for CA for devices of classes 6 and 7 while class 8 devices have the possibility of up to 5 carrier, what allows for 100 MHz band. Also, for Rel.10 the number of DL CCs is always grater than or equals to the number of UL carriers [68].

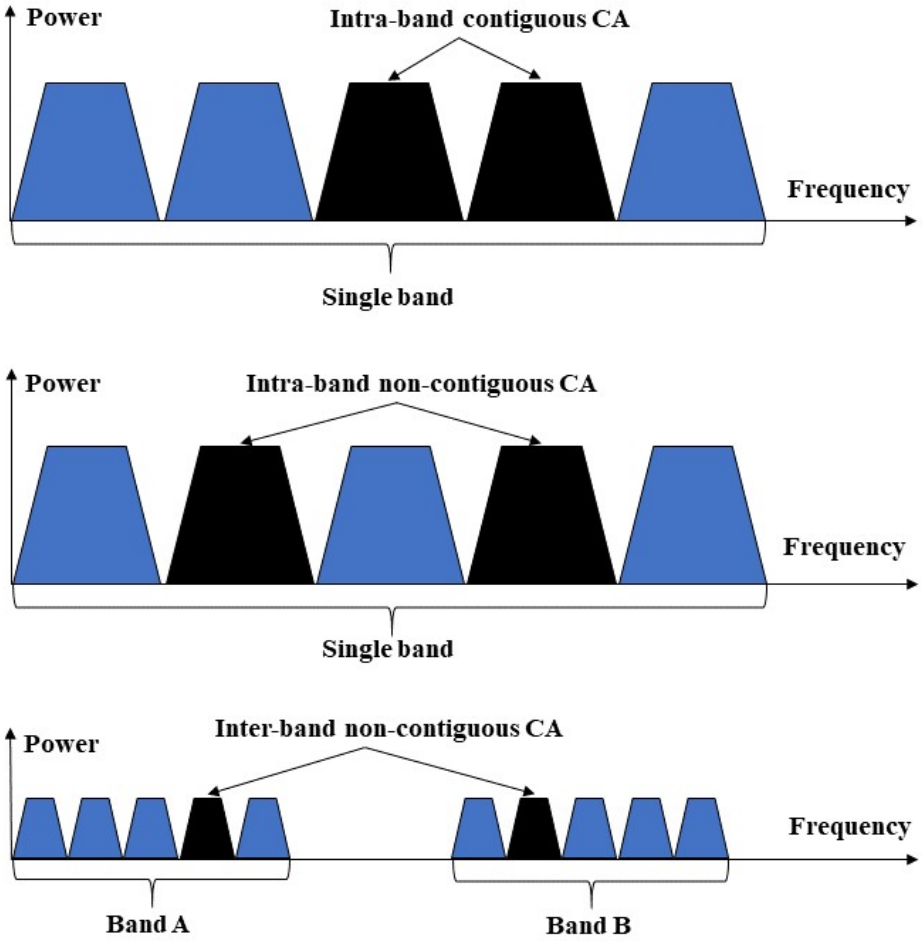

Figure 3.4: CA allocation examples in LTE/LTE-A, adapted from [56]

3.3 Carrier Aggregation with LTE-Sim

For the analysis proposed in this work, one considers the ITU radio propagation model for Macro-cell propagation scenarios in urban and suburban areas proposed in [70] and described by equation 3.2.

$$PL = 40(1 - 4 \times 10^{-3})log_{10}(R_{km}) - 18log(D_{hb}) + 21log10(f) + 80dB \quad (3.2)$$

where R is the distance between UE and eNB in kilometers, D_{hb} is the height of the BS which is assumed to be 15 m, f is the carrier frequency in MHz. Following the definitions from equation 3.2, the path loss model for the 800 MHz frequency band is give by equation 3.3, while 3.4 shows the pathloss model for the 2.6 GHz frequency band. Furthermore, for the study the will be presented in the next sections, this work assumes a bandwidth of 5 MHz and omnidirectional antenna gain of 14 dBi.

$$L_{800MHz} = 119.8 + 37.6log_{10}(R_{km}) \quad (3.3)$$

$$L_{2.6GHz} = 130.5 + 37.6log_{10}(R_k m) \quad (3.4)$$

The first scenario described in this chapter is represented in figure 3.6. Here, one considers the existence of two collocated CCs hexagonal coverage zones operating at frequency band 7 (2.6 GHz) and frequency band 20 (800 MHz), while also considering the existence of the first tier of interferes, as illustrated in figure 3.6. The allocation of UEs at each CC is decided in every TTI, fallowing the the metrics of three packet schedulers, namely, the Enhance Multi Band Scheduler (EMBS), General Multi Band Scheduler and Basic Multi-Band Scheduler (BMBS), that will be described in further details in the following sections.

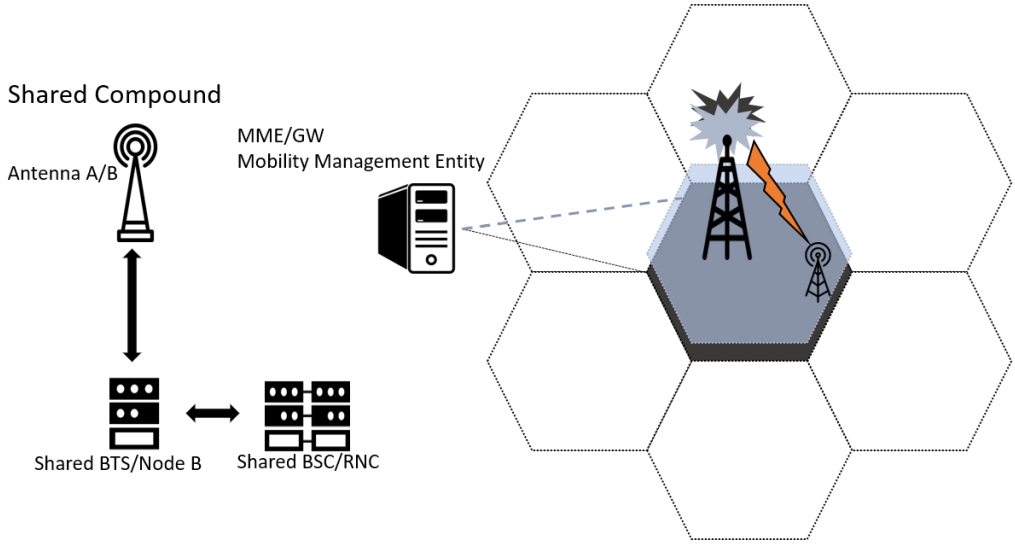

Figure 3.5: Inter band carrier aggregation deployment scenario, adapted from [56]

Next, a second scenario is considered, where the aggregation is performed with the introduction of SCs. The idea is this scenario is to have SCs with a maximum radius of 200 positioned near the center coordinates of the Macrocell. The aggregation in this case will be performed between Macrocell and SCs, and the decision about in which band to allocate UEs at every TTI is performed by the three schedulers i.e., EMBS, GMBS, and BMBS. For the cases where UEs are outside the coverage zone of the SCs, decision are performed by the Modified Largest Weighted Delay First (M-LWDF), where users are allocated to one single frequency band. For this second case scenario, one also considers the existence of a second tier of interferes.

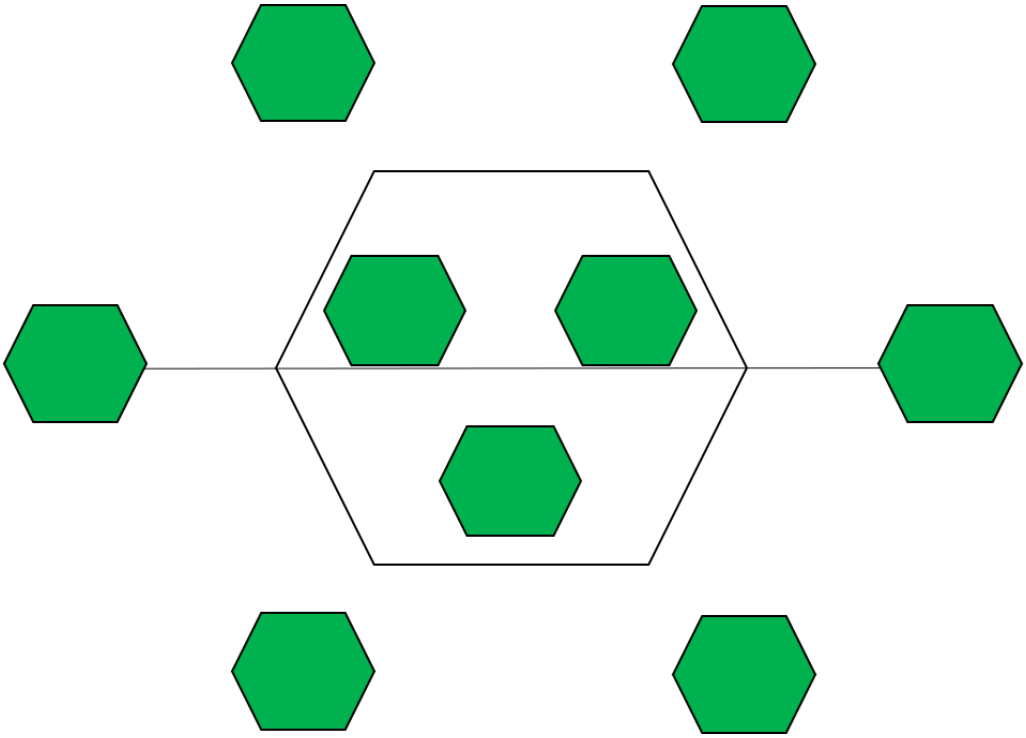

Figure 3.6: Inter band carrier aggregation deployment scenario with Small Cells

3.3.1 General Multi-band Scheduler

The proposed General Multi-band Scheduler as well as the following scheduler described in this section were proposed in [71], [56] and [72] as a way to offer CA as resource to improving network capacity adding an extra dimension of scheduling at the TTI level. The authors proposed the scheduling solution by using Integer Programing (IGP) establishing a Profit Function (PF) which considers the ratio between the requested application rate and the available rate on the DL channel, as described in equation 3.5:

$$(PF) = \sum_{b=1}^{m} \sum_{u=1}^{n} W_{\mathrm{B,U}} \cdot X_{\mathrm{B,U}} \quad (3.5)$$

where $X_{\mathrm{B,U}}$ indicates whether the UE is allocated in band u or not. Also, in equation 3.5, $W_{\mathrm{B,U}}$ is a normalized metric whose values is given by:

$$W_{\mathrm{B,U}} = \frac{[1 - BER(CQI_{\mathrm{B,U}})] \cdot R(CQI_{\mathrm{B,U}})}{S_{\mathrm{RATE}}} \quad (3.6)$$

where $BER(CQI_{\mathrm{B,U}})$ is the Bit Error Rate (BER), in taken from the previous DL transmission, $R(CQI_{\mathrm{B,U}})$ is the throughput as function of the MCS and S_{RATE} is the bit rate of the video encoding service.

For the purposes of the proposed work, one considers that each UE in the network can only transmit and receive over a single frequency band at a time. This constraint is specified by equation 3.7:

$$(ACt)\sum_{b=1}^{m} X_{\mathtt{B,U}} \leq 1, X_{\mathtt{B,U}} \in \{0,1\}\,\forall u \in \{0,...,n\} \quad \textbf{(3.7)}$$

Furthermore, a constraint is established to control the number of UEs allocated at each band at each given time. The constraint considers the maximum normalized load that a band can handle, as shown in equation 3.8:

$$(BC)\sum_{b=1}^{n} \frac{S_{rate}\cdot(1+R_{Tx}\cdot BER(CQI_{b,u}))}{RCQI_{b,u}}\cdot X_{\mathtt{B,U}} \leq L_b^{MAX}\forall u \in \{0,...,n\} \quad \textbf{(3.8)}$$

where S_{rate} is the throughput of the requested service, which is normalized by the maximum throughput that the network can offer, $RCQI_{b,u}$. After the process of maximization is performed, a allocation matrix, $X = [x_{b,u}]$ is created to help allocating RBs to the UEs.

After the allocation matrix is created, the Modified Largest Weighted Delay First (M-LWDF) DL packet scheduler is used to compute metrics to the assigned CC. This algorithm is designed to support multiple data users while considering different QoS parameters [73], by computing a metric $W_{i,j,b}$ described by equation 3.9, where $D_{HOL,i}$ is the $i-th$ flow head of line packet delay, $\bar{R}_i$ is the flow average transmission rate, given by equation 3.10 and $r_{i,j}$ is the instantaneous available rate for each sub channel in each flow:

$$W_{i,j,b} = \alpha_i D_{HOL,i} \times \frac{r_{i,j}}{R_{i,j}} \quad \textbf{(3.9)}$$

$$\bar{R}_i(k) = 0.8\bar{R}_i(k-1) + 0.2\bar{R}_i(k) \quad \textbf{(3.10)}$$

In equation 3.10, $R_i(k)$ is the throughput achieved in each flow and $R_i(k-1)$ is the throughput for the previous TTI. Furthermore, in equation 3.9, the parameter α_i is used to ensure precedence to users with strongest requirements in terms of acceptable loss rate in cases of flows with equal HOL. The variable α_i is computed according to equation 3.11, where δ_i is the probability that the delay will exceed the established threshold τ_i:

$$\alpha_i = \frac{log(\delta_i)}{\tau_i} \quad (3.11)$$

3.3.2 Enhanced Multi-band Scheduler

The Enhanced Multi-Band Scheduler (EMBS) uses a scheduling metric to perform decisions about the allocation of each RB in each CC, according to equation 3.12:

$$W_{i,j,b} = D_{HOL,i} \cdot \frac{R(CQI_{i,j,b})^2}{\bar{R} \cdot S_{rate}} \quad (3.12)$$

where $R(CQI_{i,j,b})$ is the throughput for in the $i-th$ flow for band b and $j-th$ sub channel as a function of MCS, $D_{HOL,i}$, $\bar{R}$, and S_{rate} stands for the same parameters as in the GMBS.

3.3.3 Basic Multi-band Scheduler

The Basic Multi-Band Scheduler (BMBS) algorithm is also studied in the context of this work. This algorithm works by allocating UEs to a preselected frequency band, until a threshold, L_b^{MAX}, is reached. Once the threshold is reached, the remaining UEs are allocated to the next frequency band. Equation 3.13 describes the allocation process for this scheduler:

$$x_{bu} = \begin{cases} 1, & \text{if } L_b \leq L_b^{MAX} \\ 0, & \text{if } L_b > L_b^{MAX} \end{cases} \quad (3.13)$$

The GMBS is more complex when compared to EMBS and BMBS but it only allows for UEs to be allocated at one CC at time, while EMBS uses a metric that allows for the allocation of user in more than one CC. Also, the use of IGP makes the computation process in GMBS more demanding, what reduces its performance when the number of UEs is higher.

3.4 Simulations Results

With the proposed CA schedulers implemented upon the LTE-Sim stack, it was possible to evaluate the performance by computing the average Packet Loss Ratio, Throughput and delay. In this section we analyze the results considering first the following scenarios:

- Two separated LTE systems operating at 2.6 GHz and 800 MHz;

- One LTE scenario with the aggregation between both bands being managed by the CRRM scheduler;
- One LTE scenario with the aggregation between both bands being managed by the GMBS scheduler;
- One LTE scenario with the aggregation between both bands being managed by the EMBS scheduler;

To perform the simulations described in this section, one first considers a cell radius of $1km$, with the number of UEs from 8 to 80. The simulations are executed a total of 50 times and the results for the measured parameters are the average of the total number of simulations. The simulations were performed with transmissions based o video traces of 128 kbps video bitrate, considering a maximum a maximum delay of 0.1 s, with flows durations of 40 s assuming that the UE distributed are moving with a speed of 3 kmph.

3.4.1 Packet Loss Ratio for Scenario 1

Figure 3.7 shows the average values of cell PLR, where the yellow line highlights the points corresponding to a PLR 2%. As one would expect, GMBS and EMBS schedulers perform better, with EMBS presenting a lower value of average PLR in most of the cases, when compared to the remaining schedulers.

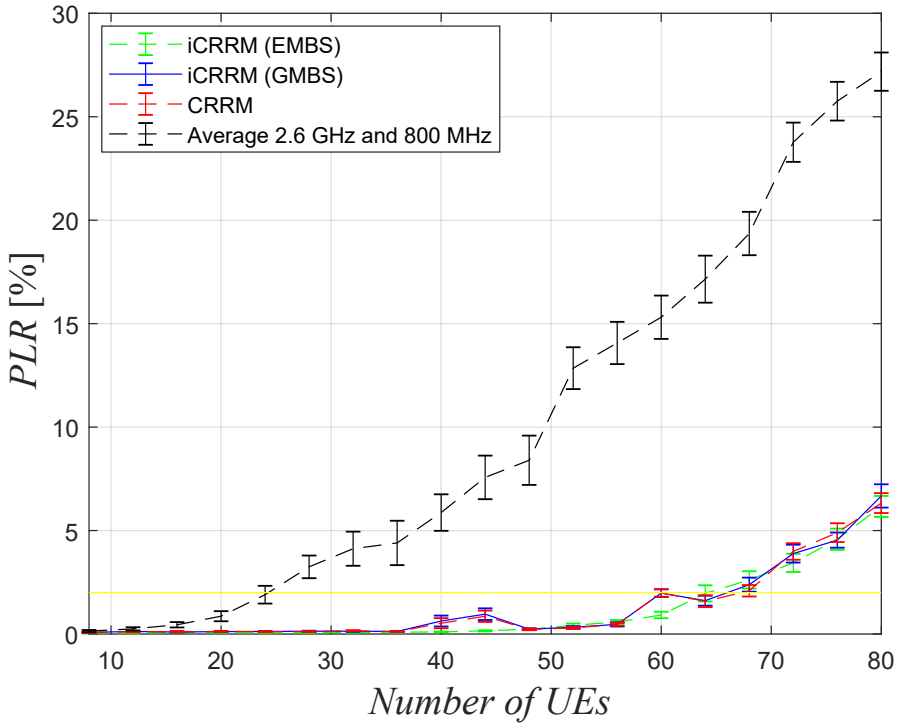

Figure 3.7: Average cell PLR as a function of UEs for R=1000 m

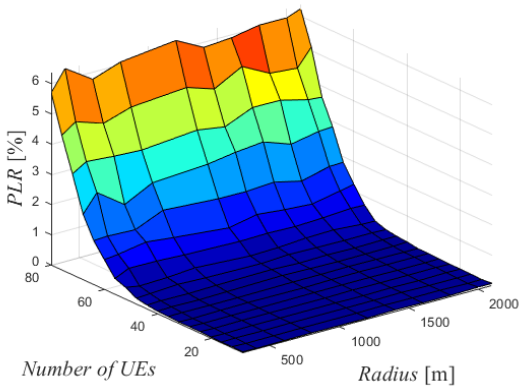

(a) Average cell PLR for EMBS

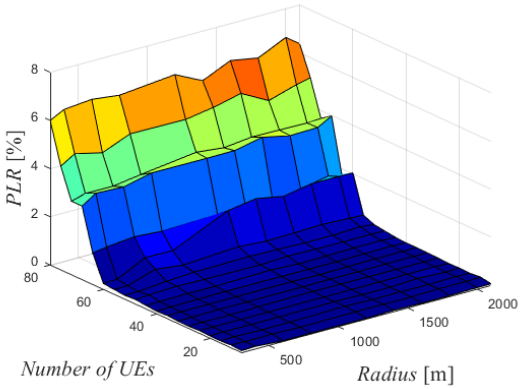

(b) Average cell PLR for GMBS

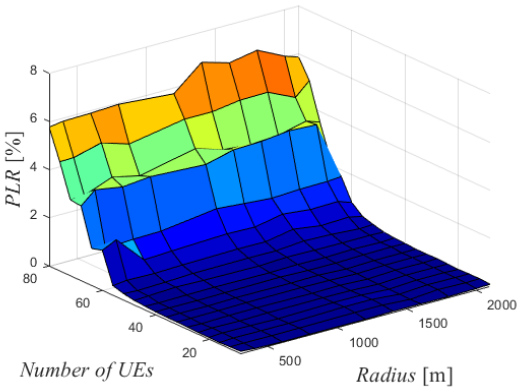

(c) Average cell PLR for BMBS

Figure 3.8: 3D view of the average cell PLR for the three schedulers

In order to evaluate the system´s capacity, this study also computed the performance of the proposed schedulers for different cell radii. Results for PLR are shown in figure 3.8 in which the values were obtained by considering cell radius from 300 m up to 2100 m and the number of UEs from 8 to 80.

Results in figure 3.8 show that the values of PLR achieved by EMBS are lower when compared to GMSB and BMBS, especially as the cell radius is increased, with the difference being more perceptible for cases with the number of UEs higher than 60. It should be pointed out that, even though GMBS produces acceptable values of PLR for most cases, the use IGP considerably increases the computational cost of the scheduling process.

3.4.2 Delay for Scenario 1

The average delay is evaluated considering the previous parameters. Figure 3.9 shows the values of delay in seconds for the total of 80. It is possible to see that, while CRRM and GMBS show values of delay that are relatively close, EMBS shows lower values, specially on the range after

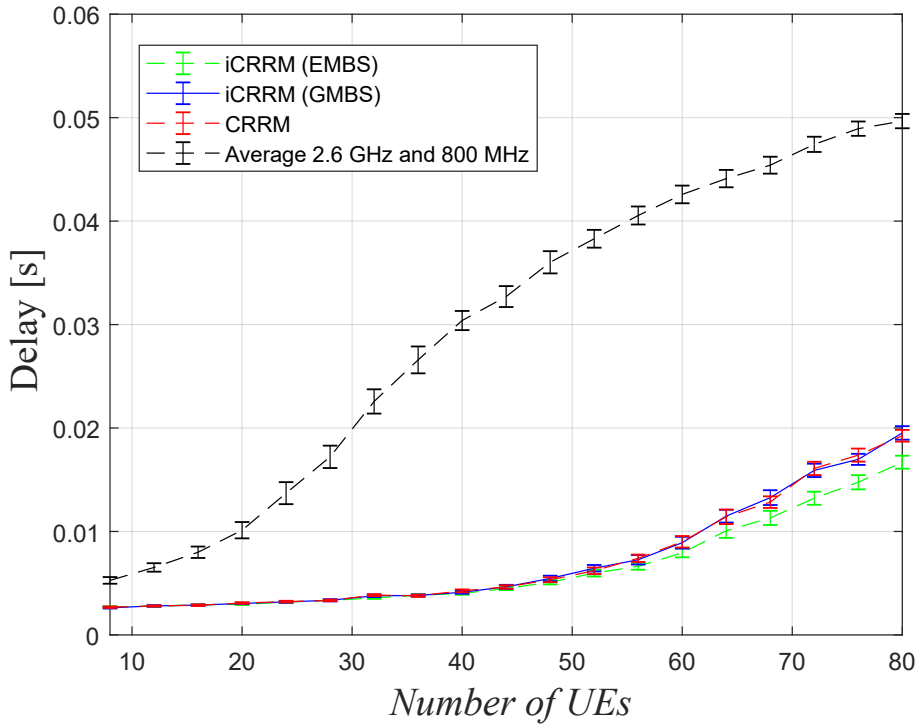

Figure 3.9: Average cell delay as a function of UEs for R=1000 m

50 UEs.

Results for the average cell delay are also shown in figure 3.10 where different cell radii are used for simulation, as described on the previous subsection.

As expected from the previous results, the values of delay for EMBS are less concentrated around the maximum point. Another important point to be observed in results for delay and in the previous results is that the values achieved by EMBS follow a much more stable progression when compered to GMBS and BMBS. This last fact can be explained, for BMBS if one considers how computational performance is a strong requirement, due to the use IGP and of a much less straightforward decision process. For BMBS, the decision process becomes less efficient as the number of UEs allocated in each CC increases over time.

3.4.3 Goodput for Scenario 1

Figure 3.11 presents the supported goodput for a radius of 1000 m. Even though in this case the difference of performance among the scheduler seems less apparent, figure 3.11 shows that as the number of UEs increases, EMBS tends to perform better when compared to CRRM and GMBS.

A 3D view of the the average cell goodput for different cell radius and number of UEs is also presented in in figure 3.12.

In order to further evaluate the system´s capacity one also considers the maximum goodput

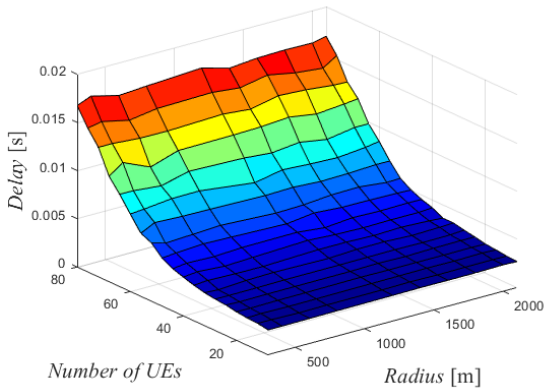

(a) Average cell delay for EMBS

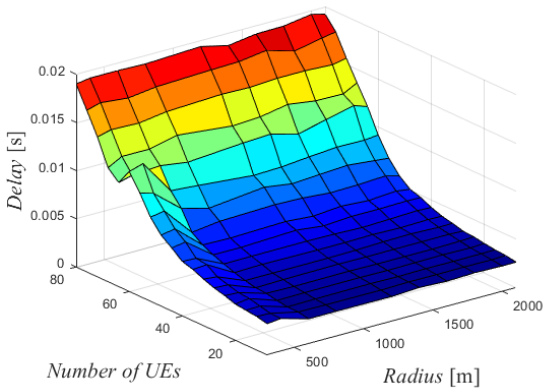

(b) Average cell delay for GMBS

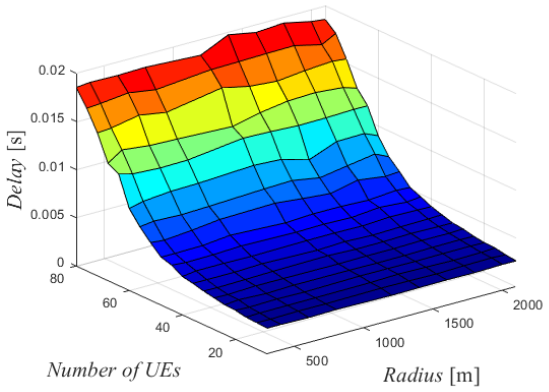

(c) Average cell delay for BMBS

Figure 3.10: 3D view of the average cell delay for the three schedulers

achieved with each scheduler, considering a PLR threshold of 2%. Results for this analysis are presented in figure 3.13, where it is possible to see that the performance of the three schedulers are very close for most cases considered, with the EMBS performing better for cell radius higher than 1800 m.

One also analyzes the system´s capacity in terms of the spatial distribution for the SINR experienced during transmissions as well as the distributions of MCSs. The results have been obtained for a total of 80 active UEs for a cell radius of 300 m, performing the simulations for a total a 50 times and averaging the results obtained. The spatial distribution of the SINR is shown in figures 3.14 and 3.15 while the distribution of MCSs is presented in figures 3.16 and 3.17, for both frequency bands.

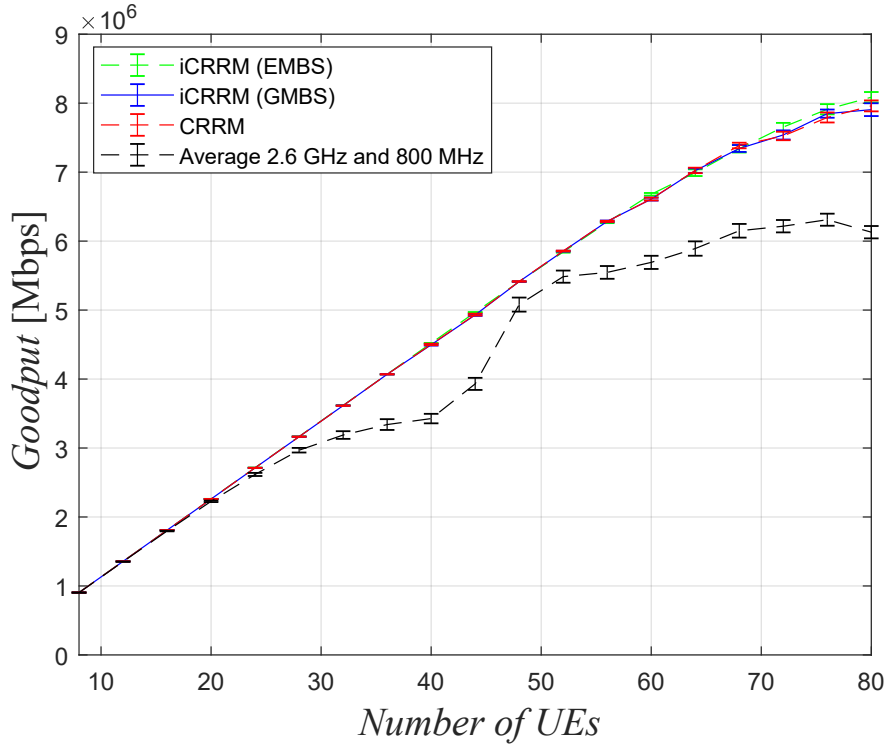

Figure 3.11: Average cell supported goodput as a function of UEs for R=1000 m

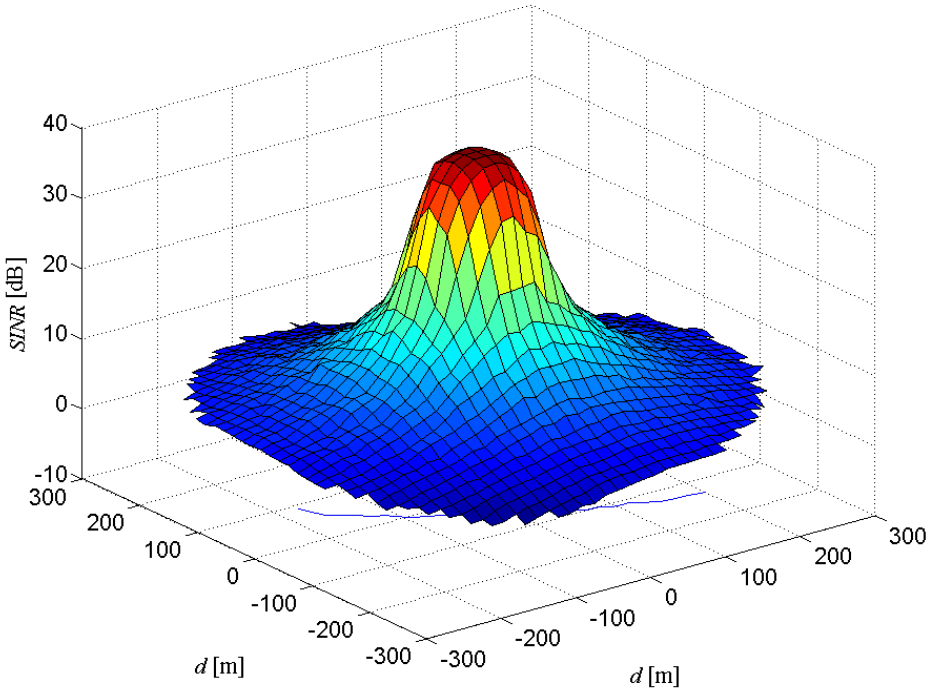

Figure 3.15: 3D representation of the cell SINR for the 800 MHz carrier

In figures 3.14 and 3.15, the highest values of SINR are achieved at the center of the cell´s coordinates and it is possible to see that, for the 800 MHz frequency band, the concentration

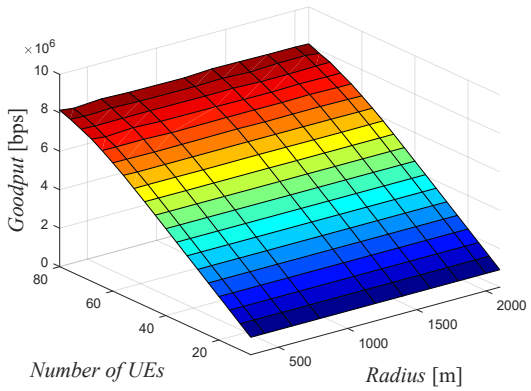

(a) Average cell goodput for EMBS

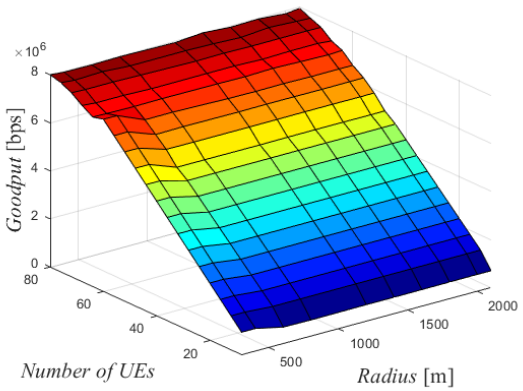

(b) Average cell goodput for GMBS

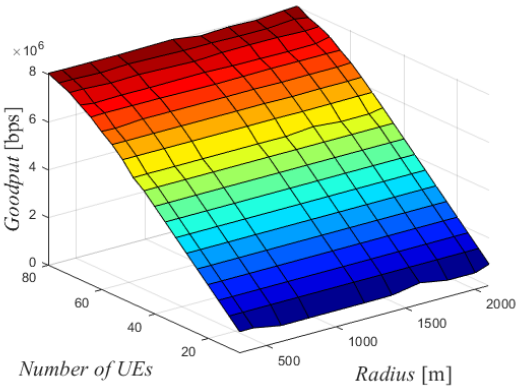

(c) Average cell goodput for BMBS

Figure 3.12: 3D view of the average cell goodput for the three schedulers

of resources around the center of the cell is slightly lower than for the the 2.6 GHz frequency band, with the same effect being observed for the results in figures 3.16 and 3.17. Values for the SINR go from 1 to 4 dB at the edge of the cell and reach values next to 40 dB at the center of the cell.

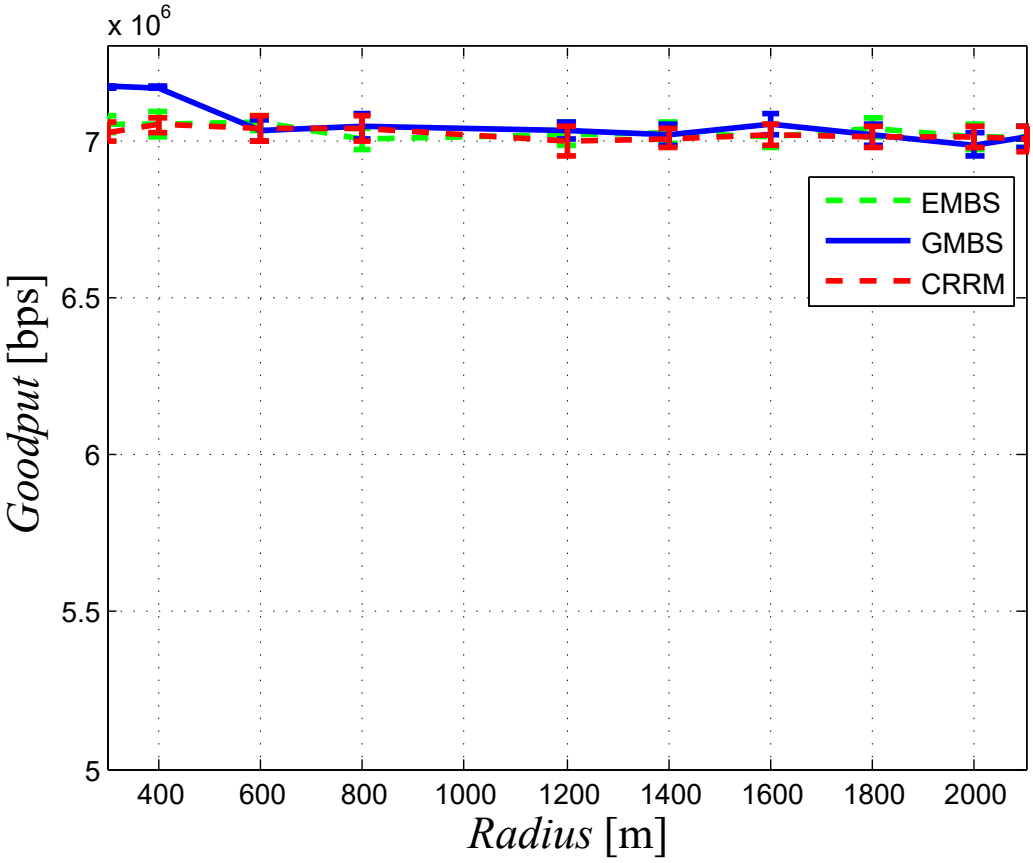

Figure 3.13: Average cell goodput for a threshold of 2% PLR

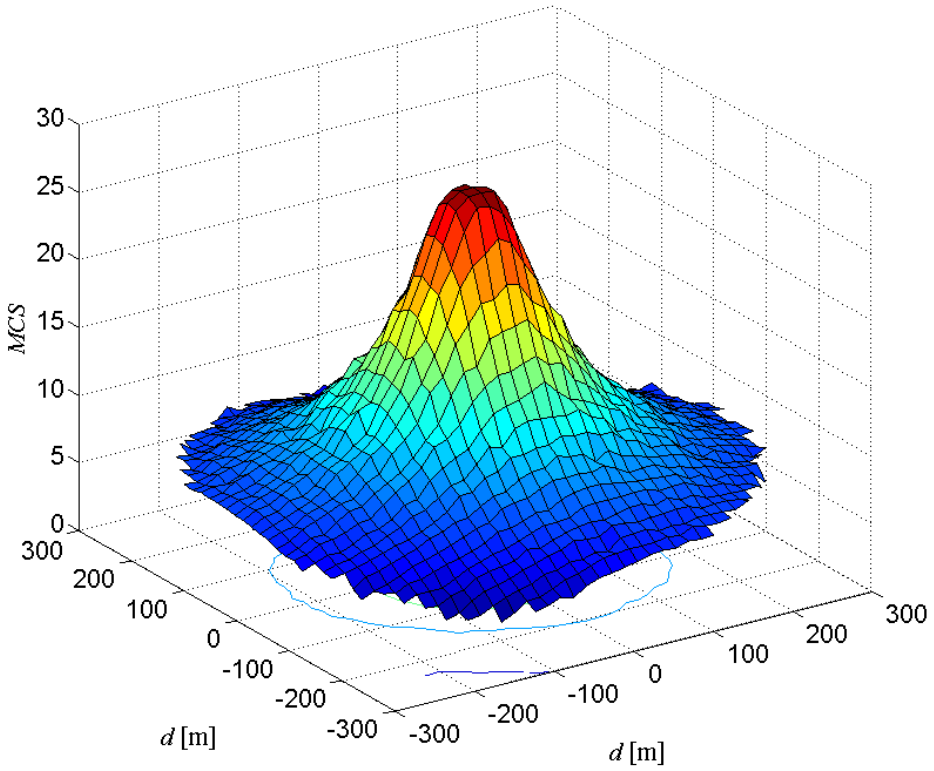

Figure 3.16: 3D representation of cell MCS for the 2.6 GHz carrier

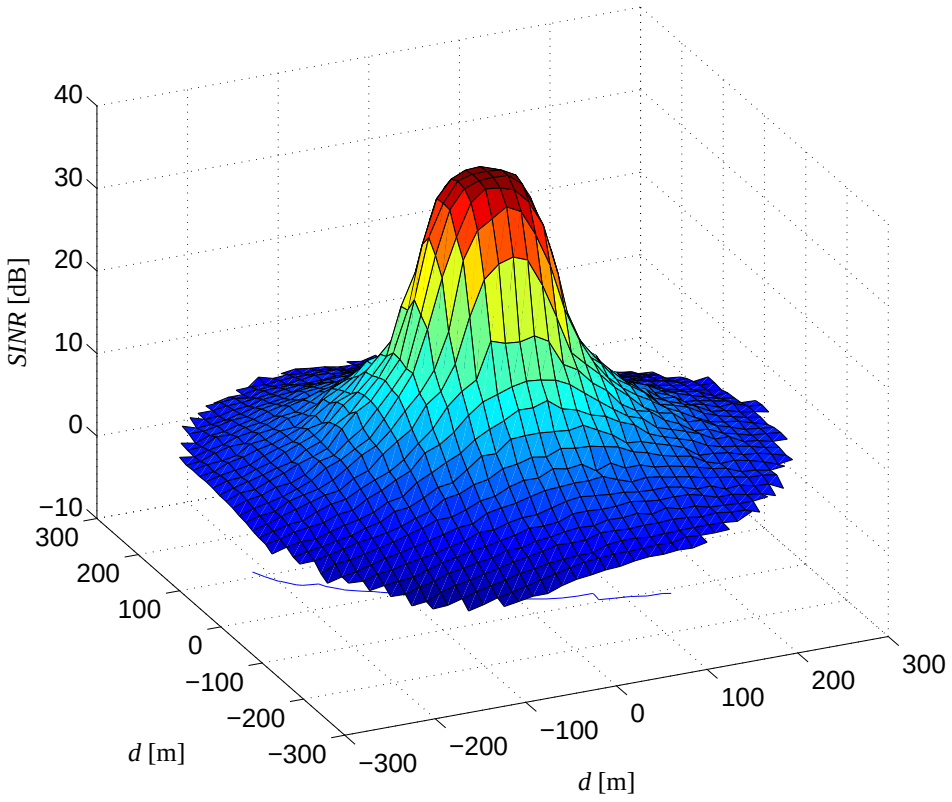

Figure 3.14: 3D representation of the cell SINR for the 2.6 GHz carrier

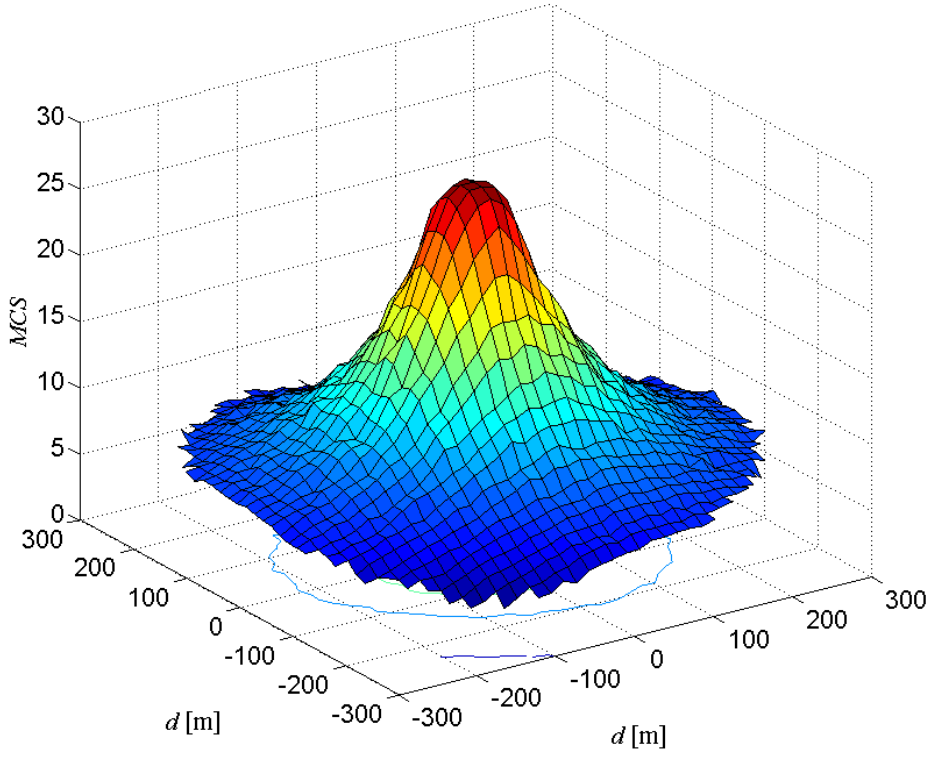

Figure 3.17: 3D representation of cell MCS for the 800 MHz carrier

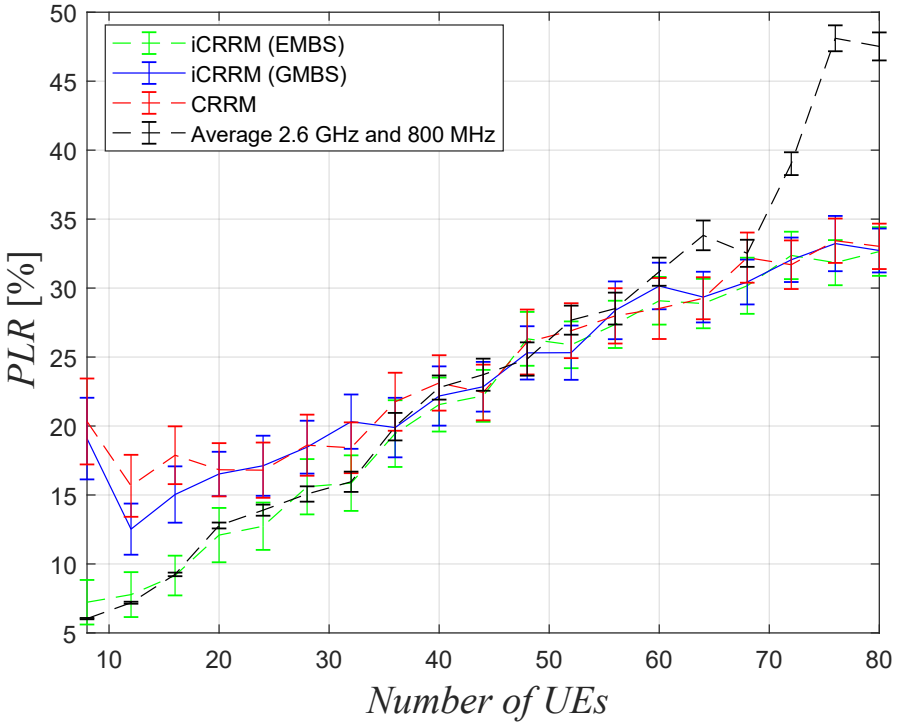

Figure 3.18: Average cell PLR as a function of UEs for R=1000 m

3.4.4 Packet Loss Ratio for Scenario 2

Results for PLR in the scenario with SCs deployment are shown in figure 3.18, where PLR is evaluated for the total number of cells. Results show that, for number of UEs smaller than 50, the performance of the three considered schedulers shows higher values of PLR. This fact is manly due to the fact that, as user are moving through the are of the Macrocell, the percentage of UEs allocated to the SCs in this case is less expressive, when compared to the total of UEs allocated to Macrocell throughout the duration of the simulatio.

As the number of UEs progresses to higher values, the values for PLR in the scenario without CA surpasses the values obtained for the case where CA is employed, what shows the potential of the employment of CA to offload the Macrocell.

3.4.5 Delay for Scenario 2

Results for the delay in the second scenario are shown in figure 3.19. It is possible to notice how results for delay are vary similar for the 3 schedulers considered, while the results for the scenario without CA increases for higher number of UEs, achieving its maximum at the total of 80 users. It also important to notice how the increase in delay for EMBS, GMBS and BMBS becomes less accentuated for higher number of UEs, as a consequence of the increase in the total number of UEs allocated to the 3 SCs in this scenario.

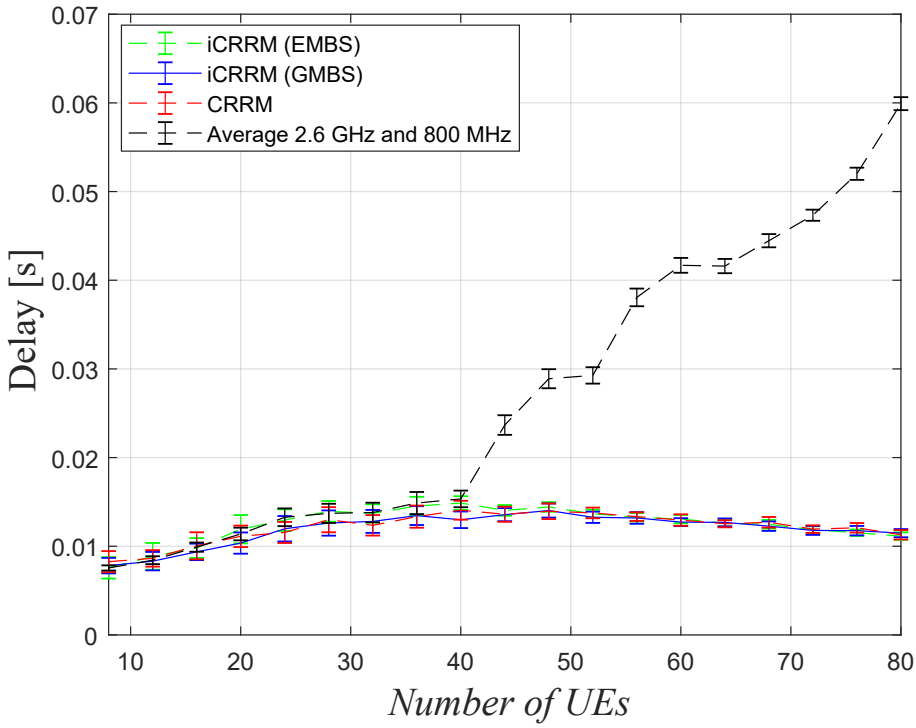

Figure 3.19: Average cell delay as a function of UEs for R=1000 m

3.4.6 Goodput for Scenario 2

For the goodput achieved in the scenario with SCs, results are shown in figure 3.20. Following the tendency for the results obtained for PLR, when the number of UEs in the simulation is smaller than 50, the results for the case without CA are slightly better when compared to the case were is employed, being surpassed is the number of UEs increases. For a total of 80 UEs, the maximum value of goodput achieved in the scenario without CA is of 4.23 Mbps while for the case when CA is employed, this value achieves 5.65 Mbps.

Regarding the performance of the three schedulers in this scenario, EMBS performs better for all the cases with number of UEs smaller than 30. From this point, the performance of the 3 scheduler becomes more similar, even though the behavior of EMBS shows to be more uniform through the simulations.

3.5 Conclusions

In this chapter Carrier Aggregations has been explored within the context of LTE, via the use of a iCRRM entity that performs inter-band CA via the scheduling of two Carrier Components, i.e., band 7 and band 20. The main motivation behind this work is to have a framework that is able to deliver services to mobile subscriber ensuring satisfactory levels of Quality of Service, reducing

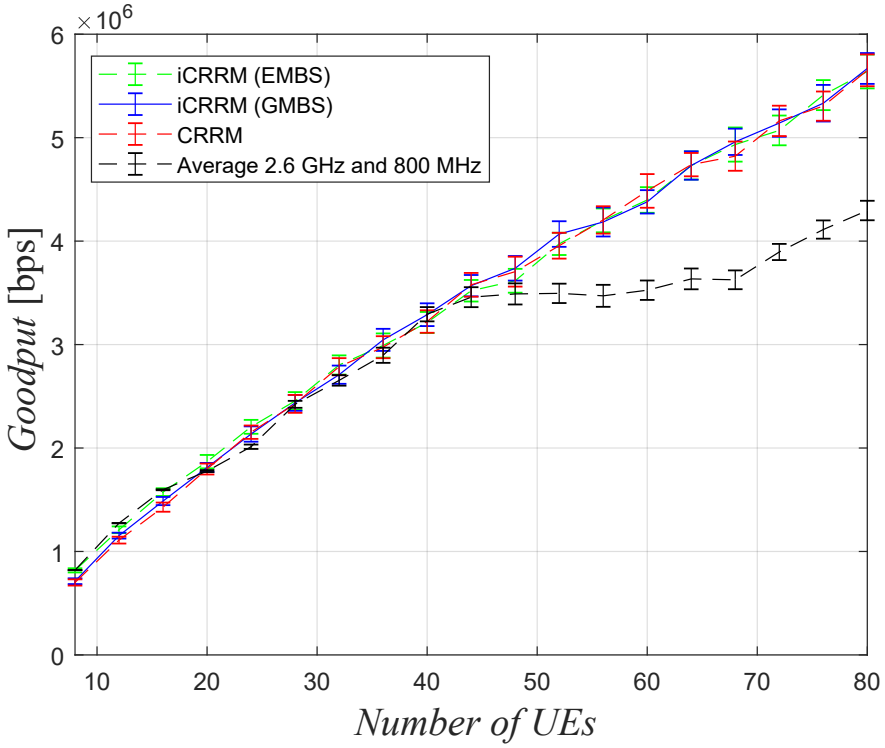

Figure 3.20: Average cell goodput as a function of UEs for R=1000 m

the levels of Packet Loss Ratio and thus increasing the throughput achieved in communication. For the simulations presented in this chapter the LTE-Sim packet level simulator was used, where the three proposed schedulers were tested for applications based on traces of videos of 128 kbps.

To evaluate the system´s capacity, scenarios were considered where the different cell radius and number of User Equipments were used in simulations obtained data to evaluate the performance of the system. First, a scenario has been considered where the cell´s radius was 1000 and the number of UEs changed from 8 to 80. In this first case, the three proposed schedulers were tested and their performance have been compared to results obtained for a scenario without CA, for the same cell radius and number of UEs. The analysis for the first case scenario demonstrate that the use of CA reduces the levels of PLR considerable, with the case of no CA achieving 27% of PLR against a maximum of 7% achieved by GMBS.

In a second analysis the cell´s radius was evaluated for values between 300 and 2100 m, with the number of UEs going from 8 to 80. Again the use of CA proved to be capable of surpassing for the cell´s radii and number of UEs. Values obtained in this second case scenario were also used to estimate the system´s capacity by considering a threshold of 2% for PLR. Under these assumptions, one is able to obtain a values of 7.5 Mbps for a cell radius of 300 m and of 7 Mbps for 2100 m of cell radius, with the PLR threshold being exceeded at a total of 67 UEs, for latter case for cell the cell radius.

One also proposes the use of CA in scenario where 3 SCs placed near the center of the Macrocell offer an extra Carrier Component for user to be allocated in. One explores this scenario for a Macrocell radius of 1000 m, a SC radius of 200 m, with the number of users considered between 8 and 80. Our results show that, when the number UEs is lower, the effect of CA is less perceptible, mainly due to the fact that user are moving through the are of the Macrocell, not being allocated to the SC during all the time of the simulation. As the number of UE increases, the effects of having one extra CC for scheduling become more perceptible, especially as for number of UEs higher the 40.

Chapter 4

Conclusions and Future Research

4.1 Conclusions

The exponential growth experienced by the number of mobile subscribers in heterogeneous mobile networks in the last decades has created a demand for research in solutions enhance the utilization of the available spectrum to be be used by Mobile Operators. In this context, Carrier Aggregation and Spectrum Sharing are presented as ways to ensure a more dynamic use of the available spectrum while ensuring the delivery of Quality of Service to users. Furthermore, mobile networks are now entering on the 5G New Radio phase, where much higher values of data rate are expected to be delivered to users, in both Up link and Down Link directions. This new technology is exploring the use of new frequency bands, such as 3.5 GHz and millimeter wave bands and it is expected to make massive use of solutions such as Small Cells deployment and Multiple Input Multiple Output based networks.

Taken the challenges presented into consideration, this work explored the concepts of Carrier Aggregation and Spectrum Sharing, making use of the LTE-Sim packet level simulator and analytical formulations previously developed by researches from the Instituto de Telecomunicações-Covilhã, offering contributions to CONQUEST (CMU/ECE/030/2017) and ORCIP (CENTRO-01-0145-FEDER-022-141).

In Chapter two, a hexagonal topology is used alongside the Umi LoS dual slope propagation model and analytical formulation to compute the physical throughput, supported throughput and average CNIR. One first uses the assumptions contained in the technical specifications of the Third Generation Partnership Project for LTE, considering the 2.6, 3.5 and 5.62 GHz frequency bands and performing the mapping between Modulation Code Schemes and minimum CNIR what allows one to obtain the values for the metrics under consideration.Results are obtained considering different positions for the interferer in the cellular topology and it is possible to see that values for the physical and support throughput are higher for the 2.56 GHz frequency band, fallowed by 3.5, and 5.62 GHz. It also possible to see that the values for the average CNIR are independent from the transmitter power value, as expressed in the analytical formulation.

Next, Chapter 2 uses the same analytical formulation, but this time under the technical specifications for 5G New Radio brought by Rel.15 of 3GPP. For this part of the work, one considers maximum modulation order 6. Results are computed by considering a bandwidth of 100 MHz

with sub-carrier spacing of 60 kHz. The results obtained show how 5G New Radio technology is capable of delivering higher data rates for the case previously considered.Results obtained for this analysis are used to perform a cost/revenue study, considering results obtained for the supported throughput for a cell radius up to 1000 m. Even though the analysis performed does not consider the use of MIMO, our results show how to optimize the economic tradeoff of a 5G based network considering the assumption of the Umi Los dual slope propagation model and hexagonal topology.

The third Chapter of this work explored Carrier Aggregation within the context of LTE, by means of the LTE-Sim packet level simulator. The work developed builds upon the research conducted at the Instituto de Telecomunicações, considering a hexagonal topology where the aggregation is performed between the macro-cells, operating at the 2.6 GHz and 800 MHz. The computations are performed and analyzed using three different schedulers, designed to decide in every TTI in which band user should be allocated, in order to ensure the quality of the communication. Our results demonstrated how Carrier Aggregation is able to ensure lower values of Packet Loss Ratio when compared to a scenario where the aggregation is not performed, thus providing higher values of goodput in the downlink direction.

4.2 Future activities

One of the main features explored in this work is the implementation of Carrier Aggregation performed with the LTE-Sim packet level simulator. This concept explored Carrier Aggregation within a hexagonal topology for two different frequency bands. The work performed demonstrated the advantages of applying Carrier Aggregation to obtain lower values of packet loss ratio and higher data rates, considering the framework of LTE. Even though the non standalone phase of 5G New Radio considers the coexistence with previous LTE networks, it is of importance to consider the possibilities of NR regarding higher bandwidths, different forms of modulation and higher modulation orders.

In this sense, for future activities regarding this research, one possibility is to implement the features brought by Rel.15 of 3GGP and of 5G NR to evaluate the work performed within this new paradigm. Several changes have to be considered in order to be able to perform the adaptation of a simulator from one technology to the other. As it has been shown in Chapter 2,while it is possible to map all the possibilities for the mapping between Modulation Code Schemes and Transport Block Sizes in LTE, 5G New Radio adopts a different approach, where values from variables configured by higher layers, as well as the sub-carrier spacing considered in every TTI. The adoption of new values of sub-carrier spacing also implies a change in the channel´s

capacity, frame structure, and also in the way the that resource blocks are allocated according to the bandwidth.

One will also investigate different scenarios for aggregation with SCs within the framework of LTE-Sim, in order to better understand the behavior of the system when SCs are considered. Different cell positioning and radius will be evaluated as well the performance of different multiband schedulers to investigate the system performance. Of especial concern are the levels of Packet Loss Ratio obtained in the second scenario presented in chapter 3.

Regarding practical experimentation, the exploration of LTE-Unlicensed brings possibilities for the validation of analytical results, while ensuring that the test performed will not interfere with the licensed frequency bands. Instituto de Telecomunicações has been performing the implementation of a LTE-based network built upon the OpenLTE/srsLTE protocol stack using USRP B210 devices to work as EnodeB and User Equipment. The stack can be adjusted to work with higher frequency bands belonging to LTE-U, such as 5.62 GHz, that has been explored for the analytical results presented in Chapter 2. Future steps of the research will make use of OpenLTE/srsLTE to perform practical validation of the Umi LoS propagation model, by following the approach suggested in [74].

References

[1] M. G. Kibria, G. P. Villardi, K. Nguyen, K. Ishizu, and F. Kojima, “Heterogeneous networks in shared spectrum access communications,” *IEEE Journal on Selected Areas in Communications*, vol. 35, no. 1, pp. 145–158, Jan 2017. 1

[2] X. Lin, J. G. Andrews, and A. Ghosh, “Modeling, analysis and design for carrier aggregation in heterogeneous cellular networks,” *IEEE Transactions on Communications*, vol. 61, no. 9, pp. 4002–4015, September 2013. 1

[3] P. Sharma, “Evolution of mobile wireless communication networks-1G to 5G as well as future prospective of next generation communication network,” 2013. 2

[4] M. Ratana Bhalla and A. Vardhan Bhalla, “Generations of mobile wireless technology: A survey,” *International Journal of Computer Applications*, vol. 5, 08 2010. 2

[5] G. Neonakis Aggelou and R. Tafazolli, “On the relaying capability of next-generation gsm cellular networks,” *IEEE Personal Communications*, vol. 8, no. 1, pp. 40–47, Feb 2001. 2

[6] UMTS, “UMTS / 3G history and future milestones,” http://www.umtsworld.com/umts/history.htm, accessed: 2019-10-03. 2

[7] A. R. Mishra, *Fundamentals of Cellular Network Planning and Optimisation: 2G/2.5G/3G... Evolution to 4G*. USA: John Wiley & Sons, Inc., 2004. 2

[8] A. Samukic, “UMTS universal mobile telecommunications system: development of standards for the third generation,” *IEEE Transactions on Vehicular Technology*, vol. 47, no. 4, pp. 1099–1104, Nov 1998. 2

[9] Jun Wang, R. Sinnarajah, Tao Chen, Yongbin Wei, and E. Tiedemann, “Broadcast and multicast services in cdma2000,” *IEEE Communications Magazine*, vol. 42, no. 2, pp. 76–82, Feb 2004. 2

[10] 3GPP, “Interoperability and compatibility of 5G specifications,” https://www.3gpp.org/news-events/3gpp-news/1994-copatibility, accessed: 2019-20-04. 3

[11] S. McCaskill, “South korea gets world’s first 5G network,” https://www.techradar.com/news/south-korea-gets-worlds-first-5g-network, accessed: 2019-20-04. 3

[12] G. Koroneos, “Customers in chicago and minneapolis are first in the world to get 5g-enabled smartphones connected to a 5G network,” https://www.verizon.com/about/news/

customers-chicago-and-minneapolis-are-first-world-get-5g-enabled-smartphones-connected-5g, accessed: 2019-20-04. 3

[13] V. Cortés, "Uruguay launches latin america's first 5G network, el salvador trails behind," https://www.contxto.com/en/news/uruguay-launches-latin-americas-first-5g-network-el-salvador-trails-behind/, accessed: 2019-20-04. 3

[14] 3GPP, "About 3gpp," http://www.3gpp.org/about-3gpp, accessed: 2018-11-25. 3

[15] R. W. World, "5G NR frame structure, 5G frame as per NR standard," http://www.rfwireless-world.com/5G/5G-NR-Frame-Structure.html, accessed: 2019-20-04. 3

[16] CableFree, "Overview of LTE 3GPP releases," https://www.cablefree.net/wirelesstechnology/4glte/overview-of-lte-3gpp-releases/, accessed: 2019-02-17. 4

[17] M. Iwamura, K. Etemad, M. Fong, R. Nory, and R. Love, "Carrier aggregation framework in 3GPP LTE-advanced [wimax/lte update]," *IEEE Communications Magazine*, vol. 48, no. 8, pp. 60–67, August 2010. 4

[18] S. Ye, S. H. Wong, and C. Worrall, "Enhanced physical downlink control channel in LTE advanced Release 11," *IEEE Communications Magazine*, vol. 51, no. 2, pp. 82–89, February 2013. 4

[19] Rajiv, "What is 5G NR (new radio) and how it works," https://www.rfpage.com/what-is-5g-nr-new-radio-and-how-it-works, accessed: 2018-11-25. 5, 40

[20] N. Instruments, "3GPP Release 15 overview," https://spectrum.ieee.org/telecom/wireless/3gpp-release-15-overview, accessed: 2019-02-17. 5

[21] A. Damnjanovic, J. Montojo, Y. Wei, T. Ji, T. Luo, M. Vajapeyam, T. Yoo, O. Song, and D. Malladi, "A survey on 3gpp heterogeneous networks," *IEEE Wireless Communications*, vol. 18, no. 3, pp. 10–21, June 2011. 5

[22] C. Hoymann, W. Chen, J. Montojo, A. Golitschek, C. Koutsimanis, and X. Shen, "Relaying operation in 3GPP LTE: challenges and solutions," *IEEE Communications Magazine*, vol. 50, no. 2, pp. 156–162, February 2012. 5

[23] O. Galinina, A. Pyattaev, S. Andreev, M. Dohler, and Y. Koucheryavy, "5g multi-rat lte-wifi ultra-dense small cells: Performance dynamics, architecture, and trends," *IEEE Journal on Selected Areas in Communications*, vol. 33, no. 6, pp. 1224–1240, June 2015. 5

[24] D. Lopez-Perez, X. Chu, and . Guvenc, “On the expanded region of picocells in heterogeneous networks,” *IEEE Journal of Selected Topics in Signal Processing*, vol. 6, no. 3, pp. 281–294, June 2012. 6

[25] J. G. Andrews, H. Claussen, M. Dohler, S. Rangan, and M. C. Reed, “Femtocells: Past, present, and future,” *IEEE Journal on Selected Areas in Communications*, vol. 30, no. 3, pp. 497–508, April 2012. 6

[26] Y. . E. Wang, X. Lin, A. Adhikary, A. Grovlen, Y. Sui, Y. Blankenship, J. Bergman, and H. S. Razaghi, “A primer on 3GPP Narrowband Internet of Things,” *IEEE Communications Magazine*, vol. 55, no. 3, pp. 117–123, March 2017. 6, 7

[27] Y. D. Beyene, R. Jantti, K. Ruttik, and S. Iraji, “On the performance of narrow-band internet of things (nb-iot),” in *2017 IEEE Wireless Communications and Networking Conference (WCNC)*, March 2017, pp. 1–6. 6

[28] D. Astely, E. Dahlman, A. Furuskär, Y. Jading, M. Lindström, and S. Parkvall, “Lte: the evolution of mobile broadband,” *IEEE Communications Magazine*, vol. 47, no. 4, pp. 44–51, April 2009. 11

[29] A. Hoglund, X. Lin, O. Liberg, A. Behravan, E. A. Yavuz, M. Van Der Zee, Y. Sui, T. Tirronen, A. Ratilainen, and D. Eriksson, “Overview of 3GPP release 14 enhanced NB-IoT,” *IEEE Network*, vol. 31, no. 6, pp. 16–22, November 2017. 11

[30] H. Kwon, J. Jeon, A. Bhorkar, Q. Ye, H. Harada, Y. Jiang, L. Liu, S. Nagata, B. L. Ng, T. Novlan, J. Oh, and W. Yi, “Licensed-assisted access to unlicensed spectrum in LTE release 13,” *IEEE Communications Magazine*, vol. 55, no. 2, pp. 201–207, February 2017. 11

[31] X. Lin, V. Yajnanarayana, S. D. Muruganathan, S. Gao, H. Asplund, H. Maattanen, M. Bergstrom, S. Euler, and Y. . E. Wang, “The sky is not the limit: Lte for unmanned aerial vehicles,” *IEEE Communications Magazine*, vol. 56, no. 4, pp. 204–210, April 2018. 11

[32] *3GPP TS 36.213 version 13.0.0 Release 13, LTE, Evolved Universal Terrestrial Radio Access (E-ULTRA), Physical Layer Procedures for Data*, 3rd Generation Partnership Project, May 2016, technical Specification Group Radio Access Network. 11

[33] *3GPP TS 36.211 version 13.2.0 Release 13, LTE, Evolved Universal Terrestrial Radio Access (E-ULTRA), Physical Channels and Modulation*, 3rd Generation Partnership Project, May 2016, technical Specification Group Radio Access Network. 12, 13

[34] *3GPP TR 21.915, Release 15 Description, Summary of Rel-15 Work Items (Release 15)*, 3rd Generation Partnership Project, Nov. 2017, technical Specification Group Services and System Aspects. 13

[35] *3GPP TS 28.501 version 15.2.0, 5G, System Architecture for the 5G System*, 3rd Generation Partnership Project, Jun. 2018, technical Specification Group Radio Access Network. 13

[36] and, W. Chen, , and J. Smee, "5g ultra-reliable and low-latency systems design," in *2017 European Conference on Networks and Communications (EuCNC)*, June 2017, pp. 1–5. 14, 15

[37] *3GPP TS 138.214 version 15.3.0 Release 15, 5G, NR, Physical Layer Procedures for Data*, 3rd Generation Partnership Project, Oct. 2018, technical Specification Group Radio Access Network. 14, 41, 107

[38] R. W. World, "5G NR frame structure, 5G frame as per NR standard," http://www.rfwireless-world.com/5G/5G-NR-Frame-Structure.html, accessed: 2019-20-04. 16

[39] S. Lien, S. Shieh, Y. Huang, B. Su, Y. Hsu, and H. Wei, "5g new radio: Waveform, frame structure, multiple access, and initial access," *IEEE Communications Magazine*, vol. 55, no. 6, pp. 64–71, June 2017. 17

[40] *3GPP TS 38.101-1 version 1.0.0, NR, User Equipment (UE), Radio Transmission and Receptions, Part 1: Range 1 Standalone (Release 15)*, 3rd Generation Partnership Project, Dec. 2017, technical Specification Group Radio Access Network. 17, 18, 40

[41] B. H. Fleury and P. E. Leuthold, "Radiowave propagation in mobile communications: an overview of european research," *IEEE Communications Magazine*, vol. 34, no. 2, pp. 70–81, Feb 1996. 17

[42] A. F. Molisch, D. Cassioli, C. Chong, S. Emami, A. Fort, B. Kannan, J. Karedal, J. Kunisch, H. G. Schantz, K. Siwiak, and M. Z. Win, "A comprehensive standardized model for ultrawideband propagation channels," *IEEE Transactions on Antennas and Propagation*, vol. 54, no. 11, pp. 3151–3166, Nov 2006. 17

[43] X. Chu, D. Lopez-Perez, I. Dd, and F. Gunnarsson, *Heterogeneous Cellular Networks Theory, Simulation and Deployment*, 1st ed. Cambridge, UK: Cambridge University Press, 07 2013. 17

[44] K. Low, "Comparison of urban propagation models with cw-measurements," in *[1992 Proceedings] Vehicular Technology Society 42nd VTS Conference - Frontiers of Technology*, May 1992, pp. 936–942 vol.2. 19

[45] M. Lott and I. Forkel, “A multi-wall-and-floor model for indoor radio propagation,” in *IEEE VTS 53rd Vehicular Technology Conference, Spring 2001. Proceedings (Cat. No.01CH37202)*, vol. 1, May 2001, pp. 464–468 vol.1. 19

[46] Y. Lostanlen and Y. Corre, “Indoor coverage maps over large urban areas: An enhanced ray-tracing method,” vol. 626, 10 2006. 19

[47] Guidelines for evaluation of radio interface technologies for imt-advanced, report itu-r m.2135-1,. [Online]. Available: https://www.itu.int/dms_pub/itu-r/opb/rep/R-REP-M.2135-1-2009-PDF-E.pdf 19

[48] N. Ul Hasan, W. Ejaz, N. Ejaz, H. S. Kim, A. Anpalagan, and M. Jo, “Network selection and channel allocation for spectrum sharing in 5g heterogeneous networks,” *IEEE Access*, vol. 4, pp. 980–992, 2016. 20

[49] K. Zhu, E. Hossain, and D. Niyato, “Pricing, spectrum sharing, and service selection in two-tier small cell networks: A hierarchical dynamic game approach,” *IEEE Transactions on Mobile Computing*, vol. 13, no. 8, pp. 1843–1856, Aug 2014. 20

[50] B. C. da Silva, “Optimization of small cells deployment and frequency assignment using spectrum sharing,” Master’s thesis, Departamento de Engenharia Electromecânica - Universidade da Beira Interior, Covilhã, Portugal, 8 2018. 26, 28, 33, 48

[51] rserodio, “Sistema celular,” https://www.geogebra.org/m/Jfbvr67w, accessed: 2019-20-04. 27

[52] *3GPP TS 36.211 version 13.0.0 Release 13, Evolved Universal Terrestrial Radio Access (E-UTRA), Physical channels and modulation*, 3rd Generation Partnership Project, Jun. 2016, technical Specification Group Radio Access Network. 33, 63

[53] *3GPP TS 36.213 version 13.0.0 Release 13, Evolved Universal Terrestrial Radio Access (E-UTRA), Physical layer procedures*, 3rd Generation Partnership Project, May 2016, technical Specification Group Radio Access Network. 33

[54] F. J. Velez, D. Robalo, and J. A. Flores, “Lte radio and network planning: Basic coverage and interference constraints,” in *2015 7th IEEE Latin-American Conference on Communications (LATINCOM)*, Nov 2015, pp. 1–6. 51

[55] F. J. Velez, A. H. Aghvami, and O. Holland, “Basic limits for fixed worldwide interoperability for microwave access optimisation based in economic aspects,” *IET Communications*, vol. 4, no. 9, pp. 1116–1129, June 2010. 51

[56] D. L. S. Robalo, “Planning and dynamic spectrum management in heterogeneous mobile networks with qoe optimization,” Ph.D. dissertation, Departamento de Engenharia Electromecânica - Universidade da Beira Interior, Covilhã, Portugal, 8 2014. 54, 65, 66, 67

[57] D. P. Reed, “The cost structure of personal communication services,” *IEEE Communications Magazine*, vol. 31, no. 4, pp. 102–108, April 1993. 54

[58] J. Sarnecki, C. Vinodrai, A. Javed, P. O’Kelly, and K. Dick, “Microcell design principles,” *IEEE Communications Magazine*, vol. 31, no. 4, pp. 76–82, April 1993. 54

[59] F. J. Velez, O. Cabral, F. Merca, and V. Vassiliou, “Service characterization for cost/benefit optimization of enhanced umts,” *Telecommunication Systems*, vol. 50, no. 1, pp. 31–45, Apr 2012. [Online]. Available: https://doi.org/10.1007/s11235-010-9383-2 54, 57

[60] R. Prasad and F. J. Velez, Eds., *WiMAX Networks: Techno-economic Vision and Challenges*. Dordrecht, The Netherlands: Springer, 2010. 55

[61] G. Piro, L. A. Grieco, G. Boggia, F. Capozzi, and P. Camarda, “Simulating lte cellular systems: An open-source framework,” *IEEE Transactions on Vehicular Technology*, vol. 60, no. 2, pp. 498–513, Feb 2011. 61

[62] V. T. Library, “Mirrors,” http://trace.eas.asu.edu, accessed: 2019-10-03. 62

[63] P. Seeling and M. Reisslein, “Video transport evaluation with h.264 video traces,” *IEEE Communications Surveys Tutorials*, vol. 14, no. 4, pp. 1142–1165, Fourth 2012. 62

[64] P. C. K. Hung and M. V. Martin, “Security issues in voip applications,” in *2006 Canadian Conference on Electrical and Computer Engineering*, May 2006, pp. 2361–2364. 62

[65] ITU-T, “G.729 : Coding of speech at 8 kbit/s using conjugate-structure algebraic-code-excited linear prediction (cs-acelp),” https://www.itu.int/rec/T-REC-G.729-201206-I/en, accessed: 2019-10-03. 62

[66] Y. Ghiassi-Farrokhfal and J. Liebeherr, “Output characterization of constant bit rate traffic in fifo networks,” *IEEE Communications Letters*, vol. 13, no. 8, pp. 618–620, August 2009. 62

[67] T. Camp, J. Boleng, and V. Davies, “A survey of mobility models for ad hoc network research,” *Wireless Communications and Mobile Computing*, vol. 2, 08 2002. 64

[68] C. S. Park, L. Sundström, A. Wallén, and A. Khayrallah, “Carrier aggregation for LTE-advanced: design challenges of terminals,” *IEEE Communications Magazine*, vol. 51, no. 12, pp. 76–84, December 2013. 64

[69] J. T. J. Penttinen, *The LTE/SAE Deployment Handbook*. Wiley, 2012. 64

[70] *3GPP TR 25.942 version 9.0.0, Radio Frequency (RF) system scenarios (Release 9)*, 3rd Generation Partnership Project, Dec. 2009, technical Specification Group Radio Access Network. 65

[71] O. Cabral, F. Meucci, A. Mihovska, F. J. Velez, N. R. Prasad, and R. Prasad, "Integrated common radio resource management with spectrum aggregation over non-contiguous frequency bands," *Wireless Personal Communications*, vol. 59, no. 3, pp. 499–523, Aug 2011. [Online]. Available: https://doi.org/10.1007/s11277-011-0242-6 67

[72] D. Robalo, F. J. Velez, R. R. Paulo, and G. Piro, "Extending the lte-sim simulator with multi-band scheduling algorithms for carrier aggregation in lte-advanced scenarios," in *2015 IEEE 81st Vehicular Technology Conference (VTC Spring)*, May 2015, pp. 1–6. 67

[73] R. Basukala, H. A. M. Ramli, and K. Sandrasegaran, "Performance analysis of exp/pf and m-lwdf in downlink 3gpp lte system," in *2009 First Asian Himalayas International Conference on Internet*, Nov 2009, pp. 1–5. 68

[74] D. Robalo, J. R. Oliveira, F. J. Velez, O. Holland, and A. H. Aghvami, "Dynamic configuration and optimization of wimax networks with relay power saving modes: Measurement-based scenario in a hilly region," *Wireless Personal Communications*, vol. 85, no. 3, pp. 937–958, Dec 2015. [Online]. Available: https://doi.org/10.1007/s11277-015-2818-z 85, 128

[75] X. Xiong, W. Xiang, K. Zheng, H. Shen, and X. Wei, "An open source sdr-based noma system for 5G networks," *IEEE Wireless Communications*, vol. 22, no. 6, pp. 24–32, December 2015. 123

[76] T. Limberg, M. Winter, M. Bimberg, R. Klemm, E. Matus, M. B. S. Tavares, G. Fettweis, H. Ahlendorf, and P. Robelly, "A fully programmable 40 gops sdr single chip baseband for LTE/WiMAX terminals," in *ESSCIRC 2008 - 34th European Solid-State Circuits Conference*, Sep. 2008, pp. 466–469. 123

[77] F. Clermidy, C. Bernard, R. Lemaire, J. Martin, I. Miro-Panades, Y. Thonnart, P. Vivet, and N. Wehn, "Magali: A network-on-chip based multi-core system-on-chip for mimo 4G sdr," in *2010 IEEE International Conference on Integrated Circuit Design and Technology*, June 2010, pp. 74–77. 123

[78] S. Haas, T. Seifert, B. Nöthen, S. Scholze, S. Höppner, A. Dixius, E. P. Adeva, T. Augustin, F. Pauls, S. Moriam, M. Hasler, E. Fischer, Y. Chen, E. Matúš, G. Ellguth, S. Hartmann, S. Schiefer, L. Cederström, D. Walter, S. Henker, S. Hänzsche, J. Uhlig, H. Eisenreich,

S. Weithoffer, N. Wehn, R. Schüffny, C. Mayr, and G. Fettweis, “A heterogeneous sdr mpsoc in 28 nm cmos for low-latency wireless applications,” in *Proceedings of the 54th Annual Design Automation Conference 2017*, ser. DAC ’17. New York, NY, USA: ACM, 2017, pp. 47:1–47:6. [Online]. Available: http://doi.acm.org/10.1145/3061639.3062188 123

[79] F. K. Jondral, “Software-defined radio: Basics and evolution to cognitive radio,” *EURASIP J. Wirel. Commun. Netw.*, vol. 2005, no. 3, pp. 275–283, Aug. 2005. [Online]. Available: http://dx.doi.org/10.1155/WCN.2005.275 123

[80] N. Nikaein, M. K. Marina, S. Manickam, A. Dawson, R. Knopp, and C. Bonnet, “Openairinterface: A flexible platform for 5G research,” *SIGCOMM Comput. Commun. Rev.*, vol. 44, no. 5, pp. 33–38, Oct. 2014. [Online]. Available: http://doi.acm.org/10.1145/2677046.2677053 123

[81] Q. Zheng, H. Du, J. Li, W. Zhang, and Q. Li, “Open-LTE: An open LTE simulator for mobile video streaming,” in *2014 IEEE International Conference on Multimedia and Expo Workshops (ICMEW)*, July 2014, pp. 1–2. 123

[82] S. R. Systems, “About us,” https://https://www.softwareradiosystems.com/about-us/, accessed: 2019-10-03. 123

[83] I. Gomez-Miguelez, A. Garcia-Saavedra, P. D. Sutton, P. Serrano, C. Cano, and D. J. Leith, “srslte: An open-source platform for LTE evolution and experimentation,” *CoRR*, vol. abs/1602.04629, 2016. [Online]. Available: http://arxiv.org/abs/1602.04629 123

[84] mcc-mnc country networks, “Mobile country codes (mcc) and mobile network codes (mnc),” http://mcc-mnc.com, accessed: 2019-10-03. 126

[85] X. Li and Y. Wang, “Security enhanced authentication and key agreement protocol for LTE/SAE network,” in *2011 7th International Conference on Wireless Communications, Networking and Mobile Computing*, Sep. 2011, pp. 1–4. 126

Appendix A

Further Results for 5G New Radio and LTE

The numerology of 5G New Radio allows for the combinations of different values of subcarrier spacing and bandwidth, what results in different number of physical resource blocks to be allocated in every TTI. In this sense, expending the scope of the results presented in Chapter 2, this sections presents some further results for the physical throughput in NR and LTE. First, one considers different bandwidth values, and subcarrier spacing, to highlight the differences in the system´s capacity when compared to the previous results, for NR. Next,further results for the $3D$ visualization of the mapping between MCS and physical throughput are presented, covering the cases not represented in Chapter 2.

A.1 Further Results for physical throughput in 5G New Radio

In Chapter 2 analytical results for 5G New Radio were presented considering a subcarrier spacing of 60 kHz and a bandwidth of 100MHz. This combination of subcarrier spacing and bandwidth allows for the allocations of 273 PRBs, which is the maximum value achievable in 5G NR, according to the specifications of 3GPP Rel.15. Nonetheless, it is important to evaluate the system´s capacity under different configurations i.e., lower bandwidth values, especially with one takes into consideration the fact that the non-standalone phase of 5G New Radio will be characterized by the coexistence with existing LTE infrastructure.

In this sense, tables A.1 and A.2 show results for 30 and 40MHz bandwidth with a sub-carrier spacing of 30kHz, while table A.3 presents results for 100MHz with the same sub-carrier spacing. It is possible to see from the results presented how different sub-carrier spacings and bandwidth alters the maximum values obtained for the physical throughput. Specifically, for the 100MHz case, values are much lower when compared to the results from Chapter 2.

Table A.1: NR UL maximum Throughput for a bandwidth of 30 MHz and subcarrier spacing of 30 kHz

MCS	Code Rate	Modulation Order	Throughput (Mpbs)
0	120	2	226
1	193	2	364
2	308	2	580
3	449	2	846
4	602	2	113
5	378	4	142
6	434	4	164
7	490	4	185
8	553	4	208
9	616	4	232
10	658	4	248
11	466	6	263
12	517	6	292
13	567	6	320
14	616	6	348
15	666	6	376
16	719	6	406
17	772	6	436
18	822	6	465
19	873	6	493
20	682.5	8	514
21	711	8	536
22	754	8	568
23	797	8	601
24	841	8	634
25	885	8	667
26	916.5	8	691
27	948	8	714

A.2 3D view of the Mapping between MCS and Physical Throughput for Different Interferer Positioning

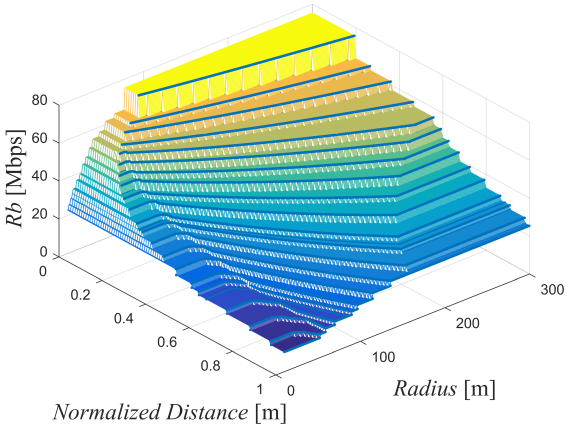

Figure A.1: 3D View of the PHY throughput mapped into MCSs with No Interferer at the 2.6 GHz band with $k = 4$

Table A.2: NR UL maximum Throughput for a bandwidth of 40 MHz and sucarrier spacing of 30 kHz

MCS	Code Rate	Modulation Order	Throughput (Mpbs)
0	120	2	31
1	193	2	49
2	308	2	79
3	449	2	115
4	602	2	154
5	378	4	194
6	434	4	222
7	490	4	251
8	553	4	283
9	616	4	315
10	658	4	337
11	466	6	358
12	517	6	397
13	567	6	435
14	616	6	473
15	666	6	511
16	719	6	552
17	772	6	593
18	822	6	631
19	873	6	670
20	682.5	8	699
21	711	8	728
22	754	8	772
23	797	8	816
24	841	8	861
25	885	8	906
26	916.5	8	938
27	948	8	971

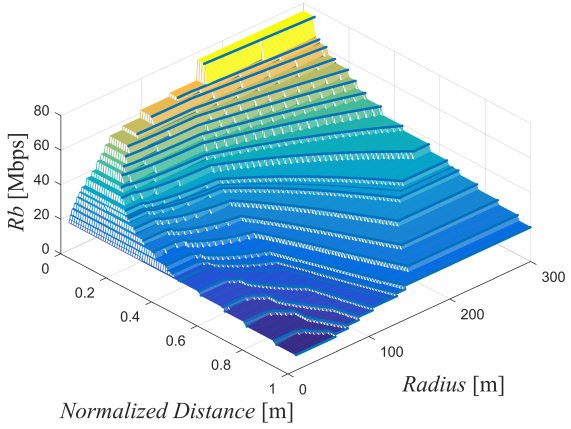

Figure A.2: 3D View of the PHY throughput mapped into MCSs with Northeast Interferer at the 2.6 GHz band with $k = 4$

Table A.3: NR UL maximum Throughput for a bandwidth of 100 MHz and sucarrier spacing of 30 kHz

MCS	Code Rate	Modulation Order	Throughput (Mpbs)
0	120	2	79.12
1	193	2	127.24
2	308	2	203.06
3	449	2	296.02
4	602	2	396.90
5	378	4	498.43
6	434	4	572.27
7	490	4	646.11
8	553	4	729.18
9	616	4	812.25
10	658	4	867.63
11	466	6	921.69
12	517	6	1022.57
13	567	6	1121.46
14	616	6	1218.38
15	666	6	1317.27
16	719	6	1422.10
17	772	6	1526.93
18	822	6	1625.82
19	873	6	1726.69
20	682.5	8	1799.88
21	711	8	1875.03
22	754	8	1988.43
23	797	8	2101.83
24	841	8	2217.87
25	885	8	2333.90
26	916.5	8	2416.98
27	948	8	2500.05

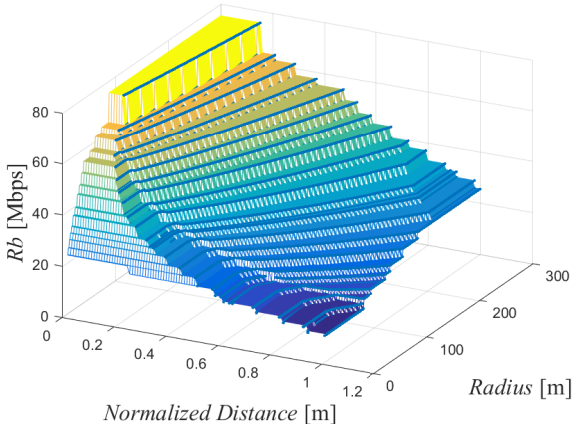

Figure A.3: 3D View of the PHY throughput mapped into MCSs with No Interferer at the 3.5 GHz band with $k = 4$

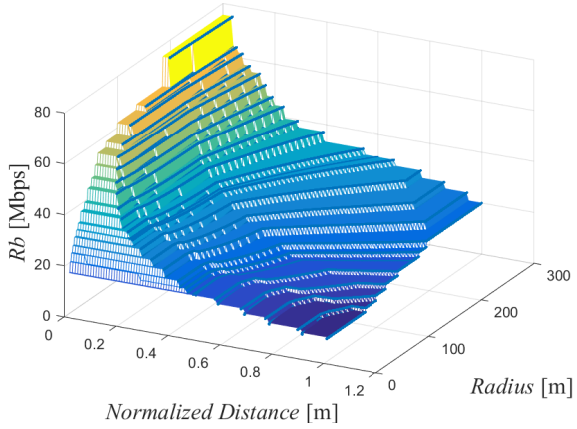

Figure A.4: 3D View of the PHY throughput mapped into MCSs with Northeast Interferer at the 3.5 GHz band with $k = 4$

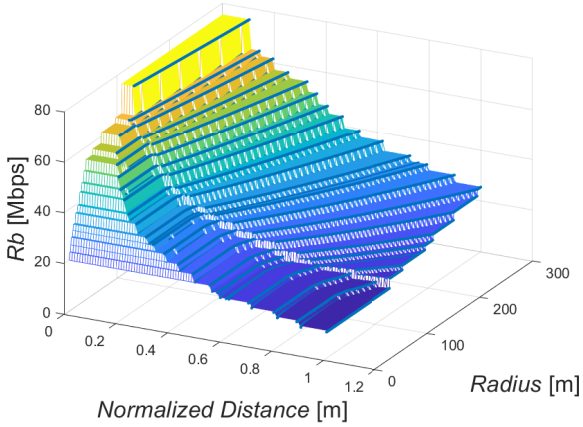

Figure A.5: 3D View of the PHY throughput mapped into MCSs with No Interferer at the 5.62 GHz band with $k = 4$

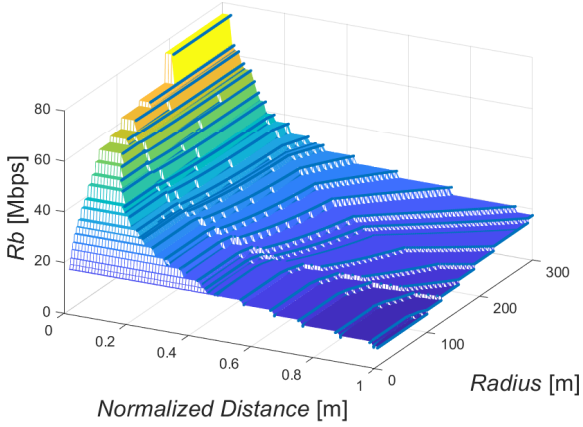

Figure A.6: 3D View of the PHY throughput mapped into MCSs with Northeast Interferer at the 5.62 GHz band with $k = 4$

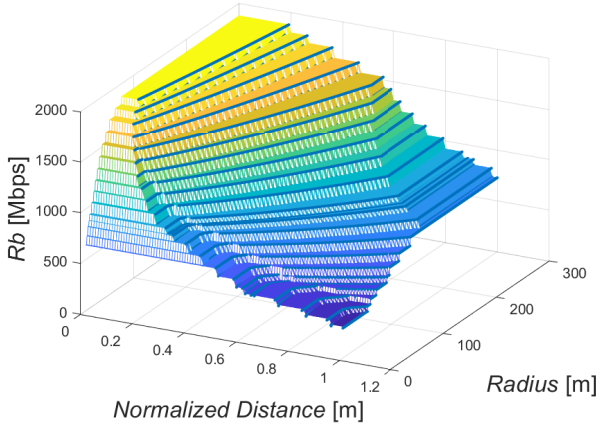

Figure A.7: 3D View of the PHY throughput mapped into MCSs with No Interferer at the 2.6 GHz band with $k = 4$

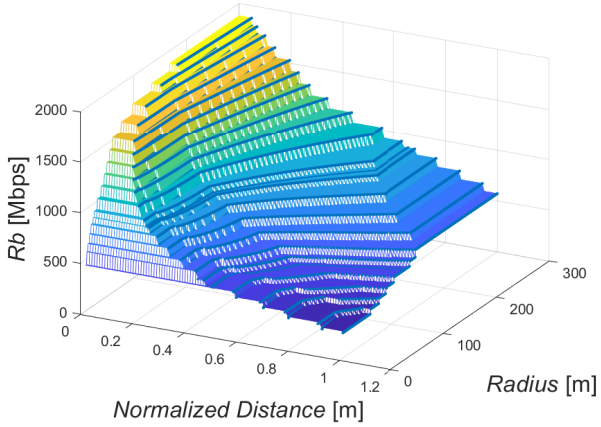

Figure A.8: 3D View of the PHY throughput mapped into MCSs with Northeast Interferer at the 2.6 GHz band $k = 4$

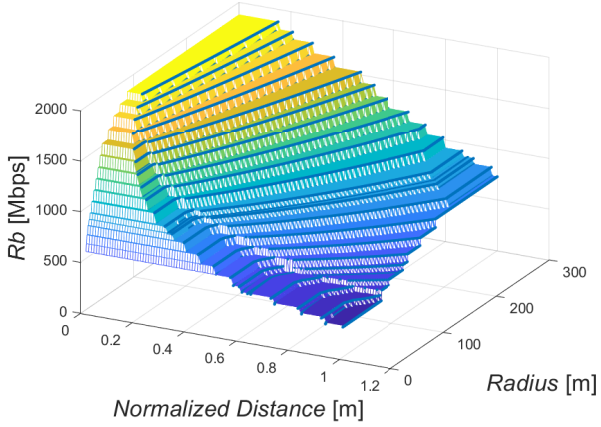

Figure A.9: 3D View of the PHY throughput mapped into MCSs with No Interferer at the 3.5 GHz band with $k = 4$

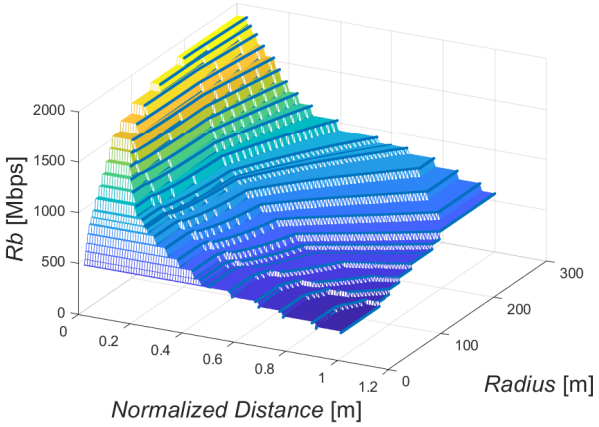

Figure A.10: 3D View of the PHY throughput mapped into MCSs with Northeast Interferer at the 3.5 GHz band with $k = 4$

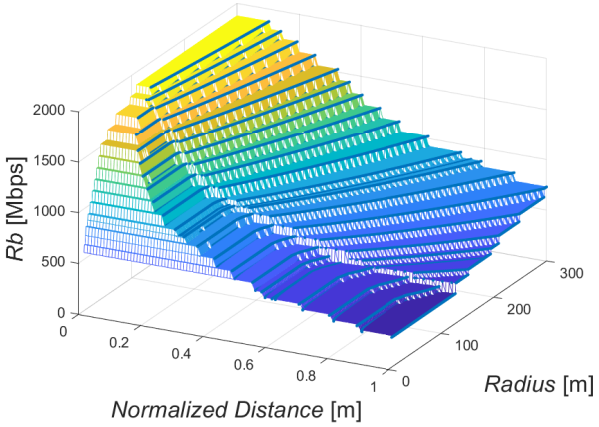

Figure A.11: 3D View of the PHY throughput mapped into MCSs with No Interferer at the 5.62 GHz band with $k = 4$

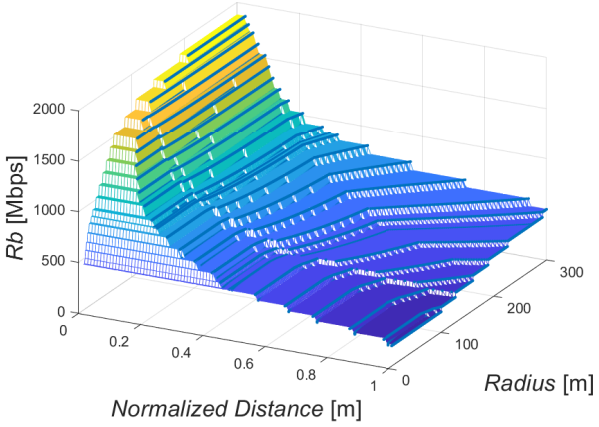

Figure A.12: 3D View of the PHY throughput mapped into MCSs with Northeast Interferer at the 5.62 GHz band with $k = 4$

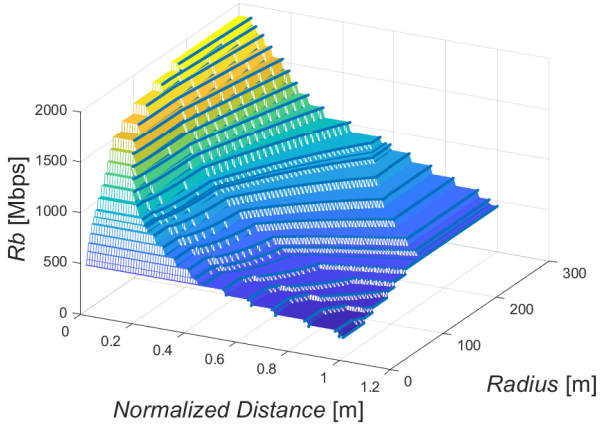

Figure A.13: 3D View of the PHY throughput mapped into MCSs with East Interferer at the 2.6 GHz band with $k = 3$, bandwidth of 100 MHz and SCS 60 kHz

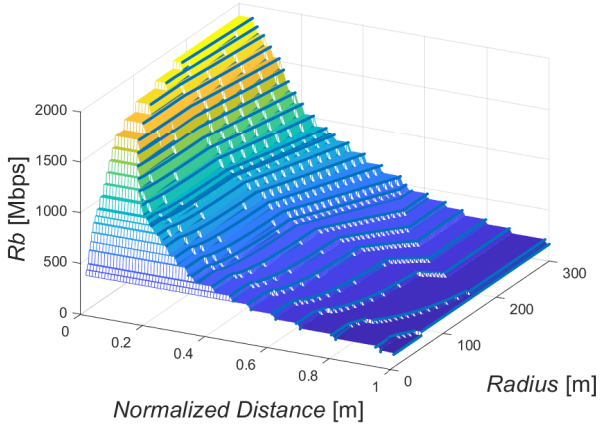

Figure A.14: 3D View of the PHY throughput mapped into MCSs with South East Interferer at the 2.6 GHz band with $k = 3$, bandwidth of 100 MHz and SCS 60 kHz

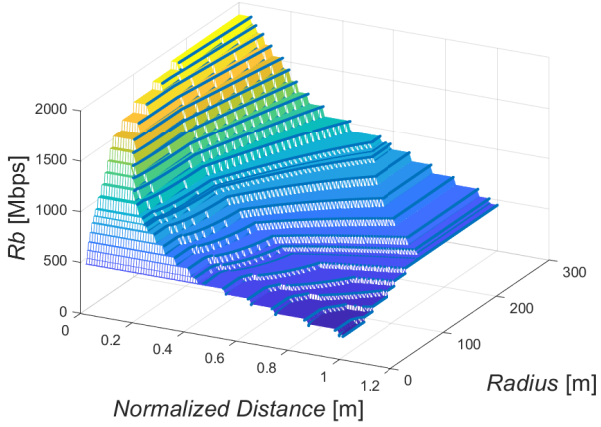

Figure A.15: 3D View of the PHY throughput mapped into MCSs with East Interferer at the 2.6 GHz band with $k = 4$, bandwidth of 100 MHz and SCS 60 kHz

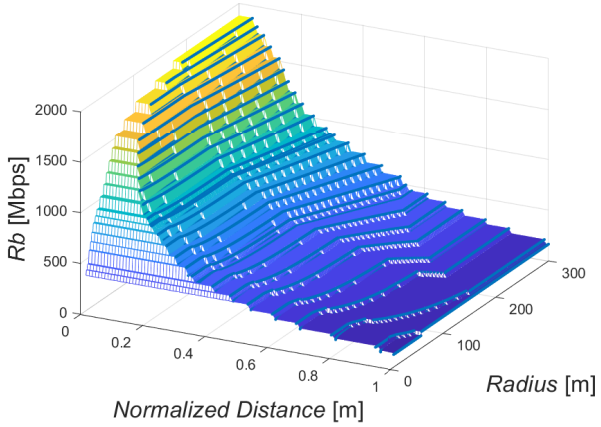

Figure A.16: 3D View of the PHY throughput mapped into MCSs with South East Interferer at the 2.6 GHz band $k = 4$, bandwidth of 100 MHz and SCS 60 kHz

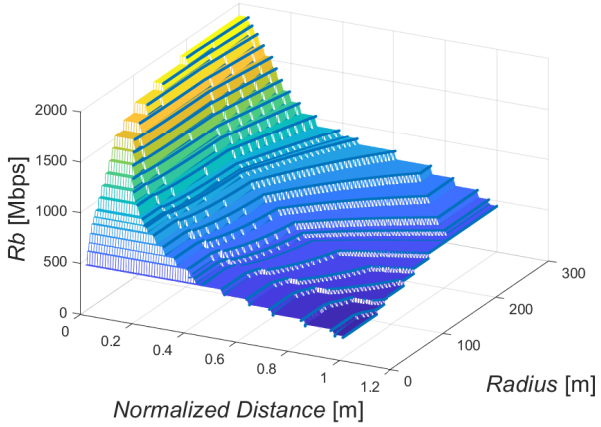

Figure A.17: 3D View of the PHY throughput mapped into MCSs with East Interferer at the 3.5 GHz band with $k = 3$, bandwidth of 100 MHz and SCS 60 kHz

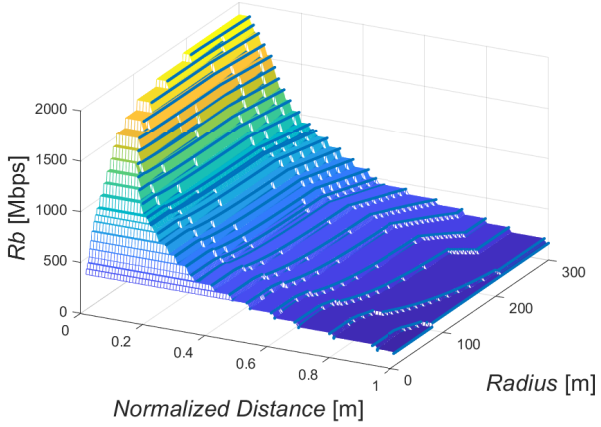

Figure A.18: 3D View of the PHY throughput mapped into MCSs with South East Interferer at the 3.5 GHz band with $k = 3$, bandwidth of 100 MHz and SCS 60 kHz

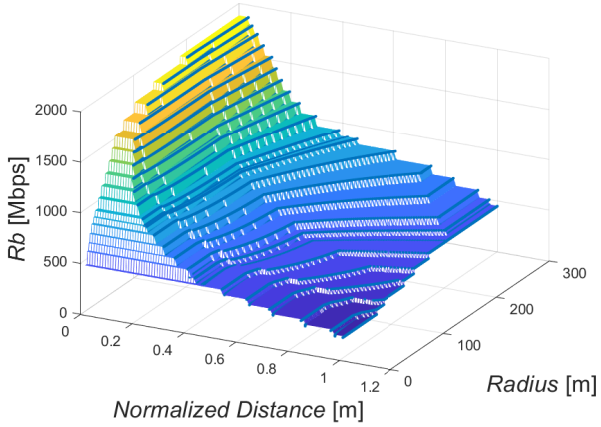

Figure A.19: 3D View of the PHY throughput mapped into MCSs with East Interferer at the 3.5 GHz band with $k = 4$, bandwidth of 100 MHz and SCS 60 kHz

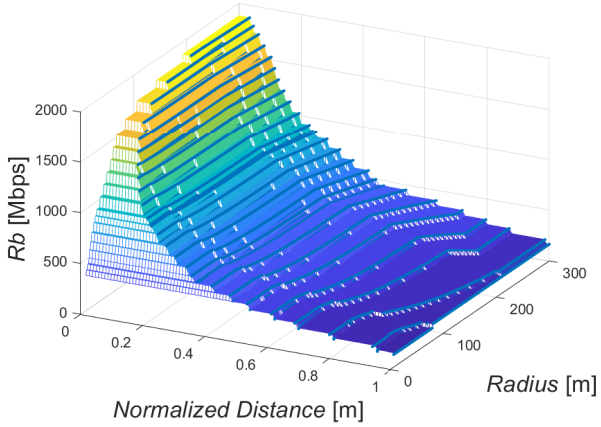

Figure A.20: 3D View of the PHY throughput mapped into MCSs with South East Interferer at the 3.5 GHz band with $k = 4$, bandwidth of 100 MHz and SCS 60 kHz

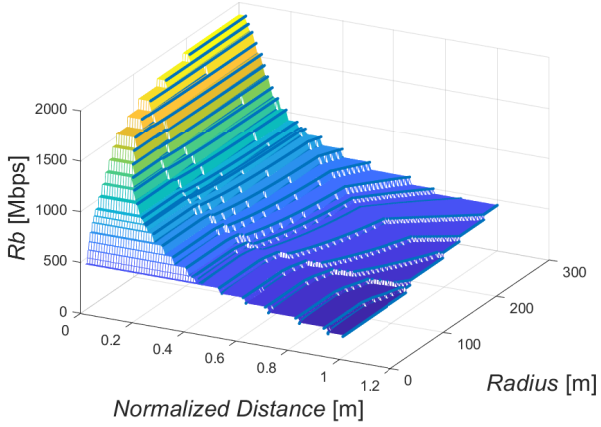

Figure A.21: 3D View of the PHY throughput mapped into MCSs with East Interferer at the 5.62 GHz band with $k = 3$, bandwidth of 100 MHz and SCS 60 kHz

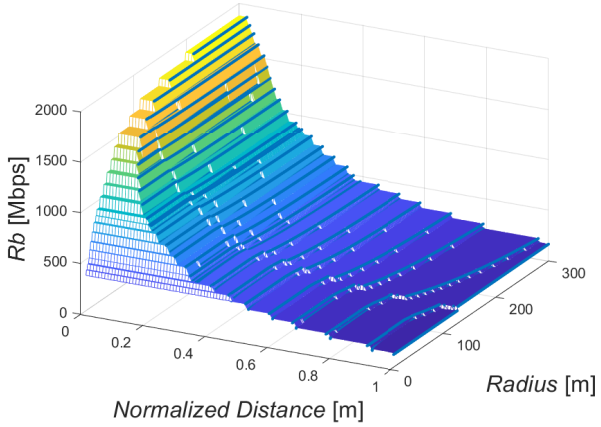

Figure A.22: 3D View of the PHY throughput mapped into MCSs with South East Interferer at the 5.62 GHz band with $k = 3$, bandwidth of 100 MHz and SCS 60 kHz

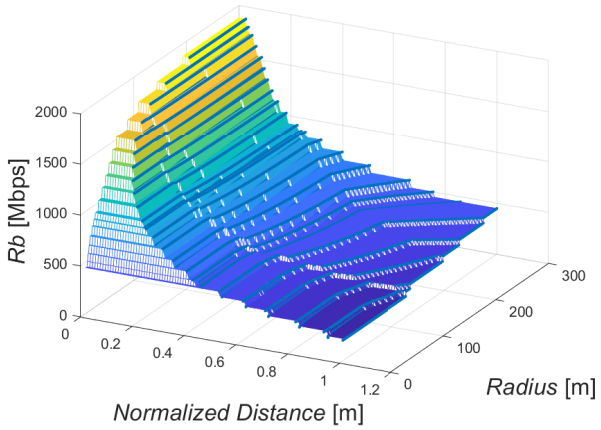

Figure A.23: 3D View of the PHY throughput mapped into MCSs with East Interferer at the 5.62 GHz band with $k = 4$, bandwidth of 100 MHz and SCS 60 kHz

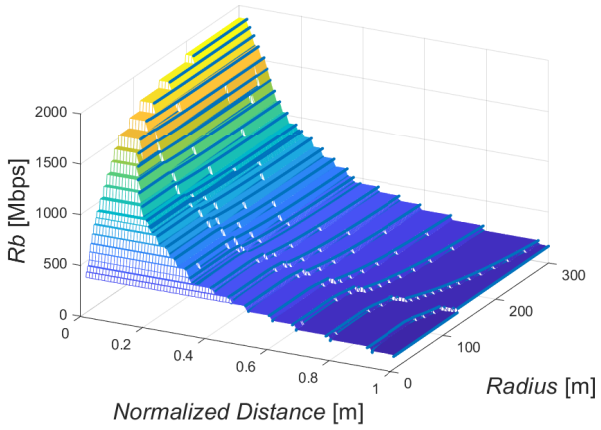

Figure A.24: 3D View of the PHY throughput mapped into MCSs with South East Interferer at the 5.62 GHz band with $k = 4$, bandwidth of 100 MHz and SCS 60 kHz

Appendix B

Matlab code for 5G New Radio

One of the key differences between the specifications of LTE and 5G NR is the way the two technologies deal with the determination of transport block sizes. While LTE uses a mapping between allocated resource blocks and and modulation code schemes to determine which TBS to use, 5G new radio adopts a different approach, where variables such as the number of CP-OFDM symbols and the number of layers used play a role in the decision process.

In this sense, Chapter 2 presented a road map for determining the TBS values for NR and in this section one shows a brief Matlab code that summarizes the process.The code starts with the determination of variables to be used in the computation process. The use should consult the technical specification of of Rel.15 series 36 to choose the desired configuration. First it is necessary to specify the number of scheduled OFDM symbols in a slot, the number of sub-carriers in the frequency domain, the number of allocated PRB in the scheduled duration, the overhead configured by higher layers, modulation order, number of layer considered in each transmission, the total number of allocated resource blocks for each user, the channel bandwidth, the respective code rate and, the sub-carrier spacing configure for the CP-OFDM.

Next, the values for MCSs, modulation order, code rates, and TBS index are inserted in the code, fallowing the values extracted from [37].It is possible to have modulation code schemes for modulation orders up to 6 and up to 8, and the code performs the computation of TBSs for both cases. Next, considering the size of the two different MCS tables, the code start a for cycle to first compute the number of information required for each case, according to the cases described in Chapter 2. The number of allocated resource blocks is then chosen according to the combination of sub-carrier spacing and bandwidth.

The number of information required is the computed taken into consideration the desired code rate and the modulation order. In case the number obtained is lower than 3824, the TBS choice will be made fallowing the values contained in the matrix tbs_table.For the remaining cases, the code fallows through a $else$ instruction to compute the TBS value according to equations 2.30 and 2.33.

```
clear all
clc
n_sh_symbol=12; %number of scheduled OFDM symbols in a slot(14 or 12)
n_rb_sc=12;     %number of subcarriers in the frequency domain in a physical resource block
```

```
n_prb_drms=0;   %is the number of REs for DM-RS per PRB in the scheduled duration including
%                the overhead of the DM-RS CDM groups indicated
n_prb_oh=6;     %the overhead configured by higher layer parameter Xoh-PDSCH (0,6,12 or 18)
q_m=6;          %modulation order
v=4;            %number o layers
n_prb=0;        %total number of allocated PRBs for the UE
r=948;          %code rate
bd=50;          %desired bandwidth (MHz)
sc=30;          %cp-ofdm spacing (kHz)
n_re_line=0;
n_re_line_b=0;
n_info_line=0;
n_info=0;               %Intermediate number of information bits
j=1;                    %single carrier component
f_j=1;                  %least scaling
T_duration = 0;          %avarege ofdm symbol duration
u=1;                     %NR numerology(0, 1, 2, 3 for sc = 15, 30, 60, 120, 240)
oh = 0.14;                  %overhead (0.14 and 0.08 for DL and UL in FR1)

%initialize tables with MCS, code rates and espectral efficiency
tbs_table_1=[24 32 40 48 56 64 72 80 88 96 104 112 120 128 136 144 152 160 168 176 184 192 208 224 ...
    240 256 272 288 304 320 336 352 368 384 408 432 456 480 504 528 552 576 608 640 672 704 736 768 ...
    808 848 888 928 984 1032 1064 1128 1160 1192 1224 1256 1288 1320 1352 1416 1480 1544 1608 1672 ...
    1736 1800 1864 1928 2024 2088 2152 2216 2280 2408 2472 2536 2600 2664 2728 2792 2856 2976 3104 ...
    3240 3368 3496 3624 3752 3824];

mcs_table_1=[0 1 2 3 4 5 6 7 8 9 10 11 12 13 14 15 16 17 18 19 20 21 22 23 24 25 26 27 28];
mcs_table_2=[0 1 2 3 4 5 6 7 8 9 10 11 12 13 14 15 16 17 18 19 20 21 22 23 24 25 26 27];

modulation_order_1=[2 2 2 2 2 2 2 2 2 2 4 4 4 4 4 4 4 6 6 6 6 6 6 6 6 6 6 6 6];
coderate_1=[120 157 193 251 308 379 449 526 602 679 340 378 434 490 553 616 658 438 466 517 ...
    567 616 666 719 772 822 873 910 948];

spectralefficieny_1=[0.234400000000000 0.306600000000000 0.377000000000000 0.490200000000000...
    0.601600000000000 0.740200000000000 0.877000000000000 1.02730000000000 1.17580000000000...
    1.32620000000000 1.32810000000000  1.47660000000000 1.69530000000000 1.91410000000000 ...
    2.16020000000000 2.40630000000000 2.57030000000000 2.56640000000000 2.73050000000000...
    3.02930000000000 3.32230000000000 3.60940000000000 3.90230000000000 4.21290000000000 ...
    4.52340000000000 4.81640000000000 5.11520000000000 5.33200000000000 5.55470000000000];

modulation_order_2=[2 2 2 2 2 4 4 4 4 4 4 6 6 6 6 6 6 6 6 6 8 8 8 8 8 8 8 8];
coderate_2=[120 193 308 449 602 378 434 490 553 616 658 466 517 567 616 666 719 772 822 873 ...
```

```
    682.500000000000 711 754 797 841 885 916.500000000000 948];

spectralefficieny_2=[0.234400000000000 0.377000000000000 0.601600000000000 0.877000000000000 ...
    1.17580000000000 1.47660000000000 1.69530000000000 1.91410000000000 2.16020000000000 ...
    2.40630000000000 2.57030000000000 2.73050000000000 3.02930000000000 3.32230000000000 ...
    3.60940000000000 3.90230000000000 4.21290000000000 4.52340000000000 4.81640000000000 ...
    5.11520000000000 5.33200000000000 5.55470000000000 5.89060000000000 6.22660000000000 ...
    6.57030000000000 6.91410000000000 7.16020000000000 7.40630000000000];

scs_table = [NaN 5 10 15 20 25 30 40 50 60 70 80 90 100;15 25 52 79 106 133 160 216 270 NaN...
    NaN NaN NaN NaN;30 11 24 38 51 65 78 106 133 162 NaN 217 245 273;60 NaN 11 18 24 31 ...
    38 51 65 79 NaN 107 121 135];

%TBS for each modulation code scheme, with fixed bandwidth and scs;
for i=1:29

    n_re_line=(n_rb_sc*n_sh_symbol)-n_prb_drms-n_prb_oh;

    if n_re_line<=9
        n_re_line_b=6;
    end
    if n_re_line>9 && n_re_line<=15
        n_re_line_b=12;
    end
    if n_re_line>15 && n_re_line<=30
        n_re_line_b=18;
    end
    if n_re_line>30 && n_re_line<=57
        n_re_line_b=42;
    end
    if n_re_line>57 && n_re_line<=90
        n_re_line_b=72;
    end
    if n_re_line>90 && n_re_line<=126
        n_re_line_b=108;
    end
    if n_re_line>126 && n_re_line<=150
        n_re_line_b=144;
    end
    if n_re_line>150
        n_re_line_b=156;
    end
```

```
if sc==15
    aux=2;
end
if sc==30
    aux=3;
end
if sc==60
    aux=4;
end

for k=1:14
    if(scs_table(1,k)==bd)
        n_prb=scs_table(aux,k);
        break;
    end
end
%n_prb=40;
n_re=n_re_line_b*n_prb;
n_info=n_re*(coderate_1(i)/1024)*modulation_order_1(i)*v;

if n_info<=3824
    n=max(3, (log2(n_info)-6));
    n_info_line=max(24,((2^n)*(n_info/2^n)));
    for j=1:93
        if tbs_table_1(j)>n_info_line
            tbs_choice(i)=tbs_table_1(j-1);
            break;
        end
    end
else

    n=log2(n_info-24)-5;
    n_info_line=(2^n)*(round((n_info-24)/(2^n)));

    if (coderate_1(i)/1024)<=0.25
        c=((n_info_line+24)/3816);
        tbs_choice(i)=round(8*c*((n_info_line+24)/(8*c))-24);
    else
        if n_info_line>8424
            c=((n_info_line+24)/8424);
            tbs_choice(i)=8*c*((n_info_line+24)/(8*c))-24;
```

```
            else
                tbs_choice(i)=round(8*((n_info_line+24)/8)-24);
            end
        end
    end
end
```

Appendix C

Analytical Formulation for the Average CNIR

For the analytical formulation of the average CNIR, the analysis starts by considering the UE at a given position described by the pair of Cartesian coordinates (x, y). One thus define the CNIR fallowing equation C.1, where P_{OW} is the power received from the BS under consideration, α is is the orthogonality level for the codes from P_{OW}, P_{Noise} is the noise power, and P_{tx} is the BS transmitter power.

$$CNIR(P_{tx}, x, y) = \frac{P_{OW}(P_{tx}, x, y)}{(1-\alpha)P_{OW}(P_{tx}, x, y) + P_{nh}(P_{tx}) + P_{Noise}} \quad \text{(C.1)}$$

For the Umi LoS propagation model, the power received from the own cell, considering the break point distance, are given by equation C.2.

$$\begin{aligned} &P_{OW}(P_{Tx}, x, y) = P_{Tx}G_{Tx}G_{Rx}10^{(\frac{-36.2995+22\log_{10}(\sqrt{x^2+y^2})}{10})}, \\ &When R \leq d_{BP} \\ &P_{OW}(P_{Tx}, x, y) = P_{Tx}G_{Tx}G_{Rx}10^{(\frac{-8.62995-18\log_{10}(h_{BS})-18\log_{10}(h_{UE})+22\log_{10}(\sqrt{x^2+y^2})}{10})}, \\ &When R > d_{BP} \end{aligned} \quad \text{(C.2)}$$

Where G_{Tx} is the transmitter antenna gain, G_{Rx} is the receiver antenna gain, R is the cell radius, P_{Tx} is the transmitter power, and P_{nh} is the interfering power received from the first ring o cells, give by equation C.3, where I_i. is equal for every interferer.

$$P_{nh}(P_{Tx}, x, y) = \sum_{i=1}^{6} I_i(P_{Tx}, x, y) \quad \text{(C.3)}$$

Considering the received power, it is possible to define two areas, given by equations C.4 and C.5, extracted from the hexagonal unit with apothem to the Fraunhofer distance for the P_{OW}.

$$A_{own} = \frac{3\sqrt{3}R^2 - r^2}{2} \quad \text{(C.4)}$$

$$A_{nh} = \frac{3\sqrt{3}R^2}{2} \quad \text{(C.5)}$$

Where r is the Fraunhofer distance.

For the average received power of the own cell, 12 triangules are dfined to represent the are of the whole cell, resulting in equations C.6 and C.7.

When we have PL1, then:

$$12\frac{pegegr10^{-2.8}(integrals)}{f^2 A_{own}} \quad \text{(C.6)}$$

if we have PL2, then:

$$12\frac{pegegr10^{-0.3957825248}(integrals)}{f^{0.2} A_{own}} \quad \text{(C.7)}$$

The own cell power case will be divided in three scenarios, represented in figures C.1 and C.2, while the interferers case will be divided in five scenarios, each one with a representation of the areas and cells represented in figures C.3, C.4, C.5, C.6, and C.7.

For all the Own Power scenarios, it was considered C.8 and C

$$Pathloss1 = \frac{1}{\sqrt{x^2 + y^2}^{2.2}} \quad \text{(C.8)}$$

$$Pathloss2 = \frac{1}{\sqrt{x^2 + y^2}^{4}} \quad \text{(C.9)}$$

The scenarios are characterized as fallows:

1. First Scenario

The first scenario occurs when the cell´s radius is smaller than the break point distance, represented in figure C.1. For this case, the integrals are give by equations C.10 and C.11.

$$\int_r^{\frac{3R}{4}} \int_0^{\frac{\sqrt{3x}}{3}} Pathloss1 dy dx \quad \text{(C.10)}$$

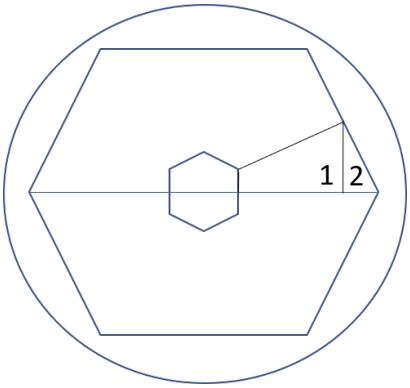

Figure C.1: Division of the Own cell for the first scenario

$$\int_{\frac{3R}{4}}^{R}\int_{0}^{\sqrt{3}(R-x)} Pathloss1dydx \quad \text{(C.11)}$$

2. Second Scenario

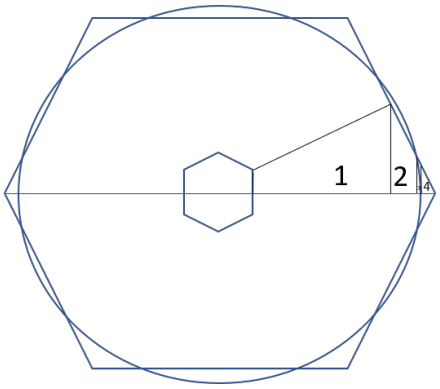

Figure C.2: Division of the Own cell for the second scenario

In the second scenario, represente in figure C.2 the cell´s radius will be between the breakpoint distance and $\frac{\sqrt{3}}{2}$, being described by the following equations:

$$\int_{r}^{\frac{3R}{4}}\int_{0}^{\frac{\sqrt{3x}}{3}} Pathloss1dydx \quad \text{(C.12)}$$

$$\int_{\frac{3R}{4}}^{6R+\frac{\sqrt{16d_{BP}^2-12R^2}}{8}}\int_{0}^{\sqrt{3}(R-x)} Pathloss1dydx \quad \text{(C.13)}$$

$$\int_{6R+\frac{\sqrt{16d_{BP}^2-12R^2}}{8}}^{d_{BP}} \int_0^{\sqrt{d_{BP}^2-x^2}} Pathloss1 dydx \quad \text{(C.14)}$$

$$\int_{6R+\frac{\sqrt{16d_{BP}^2-12R^2}}{8}}^{d_{BP}} \int_{\sqrt{d_{BP}^2-x^2}}^{\sqrt{3}(R-x)} Pathloss2 dydx \quad \text{(C.15)}$$

$$\int_{d_{BP}}^{R} \int_0^{\sqrt{3}(R-x)} Pathloss2 dydx \quad \text{(C.16)}$$

3. Third Scenario

For the third scenario, radius is higher than $\frac{\sqrt{3}}{2}$ of the breakpoint distance. The integrals for this case scenario are:

$$\int_r^{\frac{\sqrt{3}d_{BP}}{2}} \int_0^{\frac{\sqrt{3}x}{3}} Pathloss1 dydx \quad \text{(C.17)}$$

$$\int_{\frac{\sqrt{3}d_{BP}}{2}}^{d_{BP}} \int_0^{\sqrt{d_{BP}^2-x^2}} Pathloss1 dydx \quad \text{(C.18)}$$

$$\int_{\frac{\sqrt{3}d_{BP}}{2}}^{d_{BP}} \int_{\sqrt{d_{BP}^2-x^2}}^{\frac{\sqrt{3}x}{3}} Pathloss2 dydx \quad \text{(C.19)}$$

$$\int_{d_{BP}}^{\frac{3R}{4}} \int_0^{\frac{\sqrt{3}x}{3}} Pathloss2 dydx \quad \text{(C.20)}$$

$$\int_{\frac{3R}{4}}^{R} \int_0^{\sqrt{3}(R-x)} Pathloss2 dydx \quad \text{(C.21)}$$

For the interferes scenarios, the pathlosses are described by equations C.22 for pathloss 1 and equation C.23, for pathloss 2.

$$Pathloss1 = \frac{1}{\sqrt{(3R-x)^2+y^2}^{2.2}} \quad \text{(C.22)}$$

$$Pathloss2 = \frac{1}{\sqrt{(3R-x)^2+y^2}^{4}} \quad \text{(C.23)}$$

One can identity five scenarios for this case.

1. First Scenario

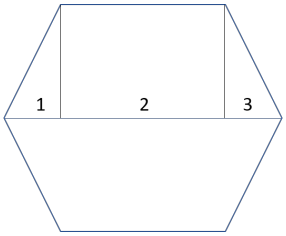

Figure C.3: Division of the cell to calculate integrals

For the first scenario in the interferers case, the cell´s radius is outside the circle, and so one only considers the second pathloss case, where the radius is higher than 78 meters. Under these considerations, the integrals for this scenario are:

$$\int_{-R}^{\frac{-R}{2}} \int_{0}^{\sqrt{3}(R+x)} Pathloss2 dy dx \quad \text{(C.24)}$$

$$\int_{\frac{-R}{2}}^{\frac{R}{2}} \int_{0}^{\frac{\sqrt{3}R}{2}} Pathloss2 dy dx \quad \text{(C.25)}$$

$$\int_{\frac{R}{2}}^{R} \int_{0}^{\sqrt{3}(R-x)} Pathloss2 dy dx \quad \text{(C.26)}$$

2. Second Scenario

The second case scenario for the interferers is represented in figure C.4. Here, the radius of the cell is between $\frac{156 d_{BP}}{59}$ and $\frac{d_{BP}}{2}$, what gives the following integrals.

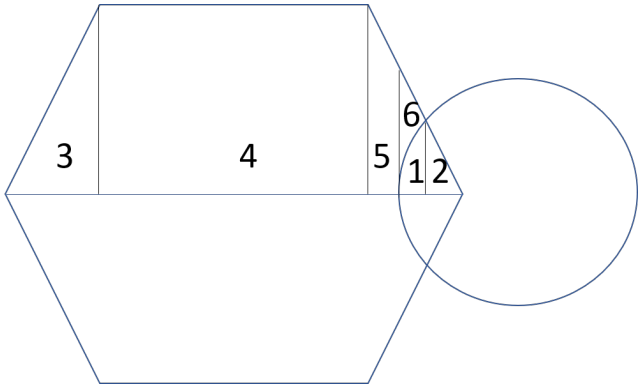

Figure C.4: Division of the cell

$$\int_{3R-d_{BP}}^{12R-\frac{\sqrt{16d_{BP}^2-48R^2}}{8}} \int_{0}^{\sqrt{d_{BP}^2-(3R-x)^2}} Pathloss1 dydx \quad \text{(C.27)}$$

$$\int_{12R}^{R} \int_{\frac{\sqrt{16d_{BP}^2-48R^2}}{8}}^{\sqrt{3}(R-x)} Pathloss1 dydx \quad \text{(C.28)}$$

$$\int_{-R}^{\frac{-R}{2}} \int_{0}^{\sqrt{3}(x+R)} Pathloss2 dydx \quad \text{(C.29)}$$

$$\int_{\frac{-R}{2}}^{\frac{R}{2}} \int_{0}^{\frac{\sqrt{3}R}{2}} Pathloss2 dydx \quad \text{(C.30)}$$

$$\int_{\frac{R}{2}}^{3R-d_{BP}} \int_{0}^{\sqrt{3}(R-x)} Pathloss2 dydx \quad \text{(C.31)}$$

$$\int_{3R-d_{BP}}^{12R-\frac{\sqrt{16d_{BP}^2-48R^2}}{8}} \int_{\sqrt{d_{BP}^2-(3R-x)^2}}^{\sqrt{3}(R-x)} Pathloss2 dydx \quad \text{(C.32)}$$

3. Third Scenario

For scenario 3, shown in figure C.5, the cells radius is comprehended between $\frac{156d_{BP}}{43}$ and $\frac{156d_{BP}}{59}$.

The equations for this part are:

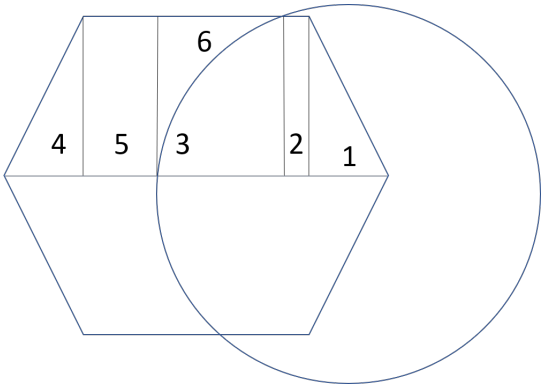

Figure C.5: Division of the cell

$$\int_{\frac{R}{2}}^{R}\int_{0}^{\sqrt{3}(R-x)} Pathloss1 dydx \quad \text{(C.33)}$$

$$\int_{3R-\frac{\sqrt{4d_{BP}^2-3R^2}}{2}}^{\frac{R}{2}}\int_{0}^{\frac{\sqrt{3}R}{2}} Pathloss1 dydx \quad \text{(C.34)}$$

$$\int_{3R-d_{BP}}^{3R-\frac{\sqrt{4d_{BP}^2-3R^2}}{2}}\int_{0}^{\sqrt{d_{BP}^2-(3R-x)^2}} Pathloss1 dydx \quad \text{(C.35)}$$

$$\int_{\frac{-R}{2}}^{-R}\int_{0}^{\sqrt{3}(x+R)} Pathloss2 dydx \quad \text{(C.36)}$$

$$\int_{\frac{-R}{2}}^{3R-d_{BP}}\int_{0}^{\frac{\sqrt{3}R}{2}} Pathloss2 dydx \quad \text{(C.37)}$$

$$\int_{3R-d_{BP}}^{3R-\frac{\sqrt{4d_{BP}^2-3R^2}}{2}}\int_{\sqrt{d_{BP}^2-(3R-x)^2}}^{\frac{\sqrt{3}R}{2}} Pathloss2 dydx \quad \text{(C.38)}$$

4. Forth Scenario

Scenario 4 is characterized by a cells radius between $\frac{d_{BP}}{4}$ and $\frac{156d_{BP}}{43}$. This scenario is mathematically described by equations C.39, C.40, C.41, C.42, C.43, and C.44.

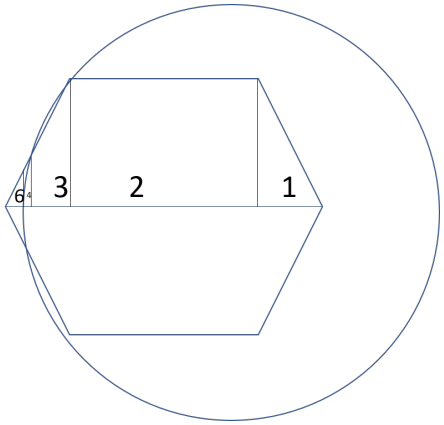

Figure C.6: Division of the cell

$$\int_{\frac{R}{2}}^{R}\int_{0}^{\sqrt{3}(R-x)} Pathloss1dydx \quad \text{(C.39)}$$

$$\int_{\frac{-R}{2}}^{\frac{R}{2}}\int_{0}^{\frac{\sqrt{3}R}{2}} Pathloss1dydx \quad \text{(C.40)}$$

$$\int_{\frac{-\sqrt{d_{BP}^2-12R^2}}{2}}^{\frac{-R}{2}}\int_{0}^{\sqrt{3}(x+R)} Pathloss1dydx \quad \text{(C.41)}$$

$$\int_{3R-d_{BP}}^{\frac{-\sqrt{d_{BP}^2-12R^2}}{2}}\int_{0}^{\sqrt{d_{BP}^2-(3R-x)^2}} Pathloss1dydx \quad \text{(C.42)}$$

$$\int_{3R-d_{BP}}^{\frac{-\sqrt{d_{BP}^2-12R^2}}{2}}\int_{\sqrt{d_{BP}^2-(3R-x)^2}}^{\sqrt{3}(x+R)} Pathloss2dydx \quad \text{(C.43)}$$

$$\int_{-R}^{3R-d_{BP}}\int_{0}^{\sqrt{3}(x+R)} Pathloss2dydx \quad \text{(C.44)}$$

5. Fifth Scenario

Finally, scenario 5 occurs when the cell´s radius is smaller than $\frac{d_{BP}}{4}$.

For the this fifth case, the integrals are:

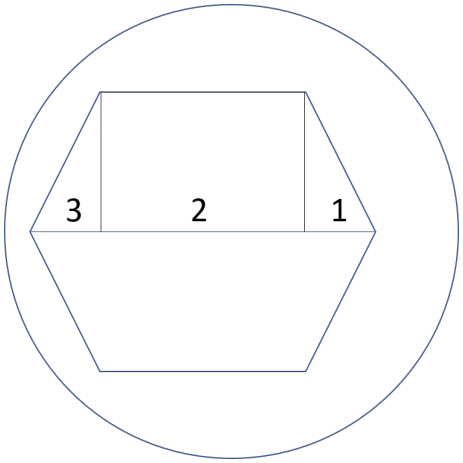

Figure C.7: Division of the cell

$$\int_{\frac{R}{2}}^{R}\int_{0}^{\sqrt{3}(R-x)} Pathloss1dydx \quad \text{(C.45)}$$

$$\int_{\frac{-R}{2}}^{\frac{R}{2}}\int_{0}^{\frac{\sqrt{3}R}{2}} Pathloss1dydx \quad \text{(C.46)}$$

$$\int_{-R}^{\frac{-R}{2}}\int_{0}^{\sqrt{3}(x+R)} Pathloss1dydx \quad \text{(C.47)}$$

Appendix D

4G Network with OpenLTE and srsLTE

The recent dynamic of development of mobile communications has lad to the development of a series o researches and [75] [76] [77] [78] addressing algorithm implementations for the experimental verification LTE-based networks and the development of solutions oriented towards 5 NR. In this context, testbeds play a paramount role when it comes to experimental verification, product development and scientific research. The development of increasingly more affordable software defined radio (SDR) [79] systems has allowed the development of solutions that integrate hardware and software solutions

Several open source protocol stacks have been proposed over the year to offer solutions regarding experimentation and development of LTE-based networks. One notable example is the OpenAirInterface (OAI) [80] that offers a complete implementation of 3GPP standards offering a PC hosted software that implements the Evolved Universal Terrestrial Network (E-ULTRA) and Evolved Packet Core (EPC), offering the possibility of using SDR driven devices such as the Universal Software Radio Peripheral (USRP) that will be explored in more detail in the next sections.

Another solution that offers a 3GPP open framework is the Open-LTE, [81] which offers support to the Ettus USRP $B2x0$ and is strongly based on the concept of modularity, meaning that the process of code development is considerably facilitated, making it easy to researchers to modify its structure and develop new features.On the other hand, openLTE does not provide a UE module, what reduces the possibilities when it comes to practical experimentation.

SrsLTE is developed by the Software Radio Systems company [82] and it aims at improving the capabilities of openLTE by offering also a UE module what bring the possibility of deploying complete LTE-based networks for experimentation. As it is the case with openLTE, srsLTE supports a variety of SDR systems, including Ettus USRP $B2x0$, which has been used for the experiments described in this chapter, and it also provides an extra module called srsGUI, that can be used to perform graphical of signals in both time and frequency domain.

D.1 srsLTE General Description

srsLTE is an open source library for the PHY layer of LTE and it is accompanied of a complete software radio LTE EU (srsUE) [83], providing interfaces for the Universal Hardware Driver (UHD)

that allow for the use of USRP devices. The modules are written in ANSI C and it possible to interact over GNU Radio to make use of resources such as spectrum analyzer.The library is organized in modules with the objective of creating a structure where each part can be changed and replaced without altering or having to modify the rest of the structure. It also offers a series of features such as Matlab library generation, synchronization procedures and cell search, and support for bandwidth of 1.4, 3, 5 10 and 20 MHz. Figure D.1 shows the general structure of the library.

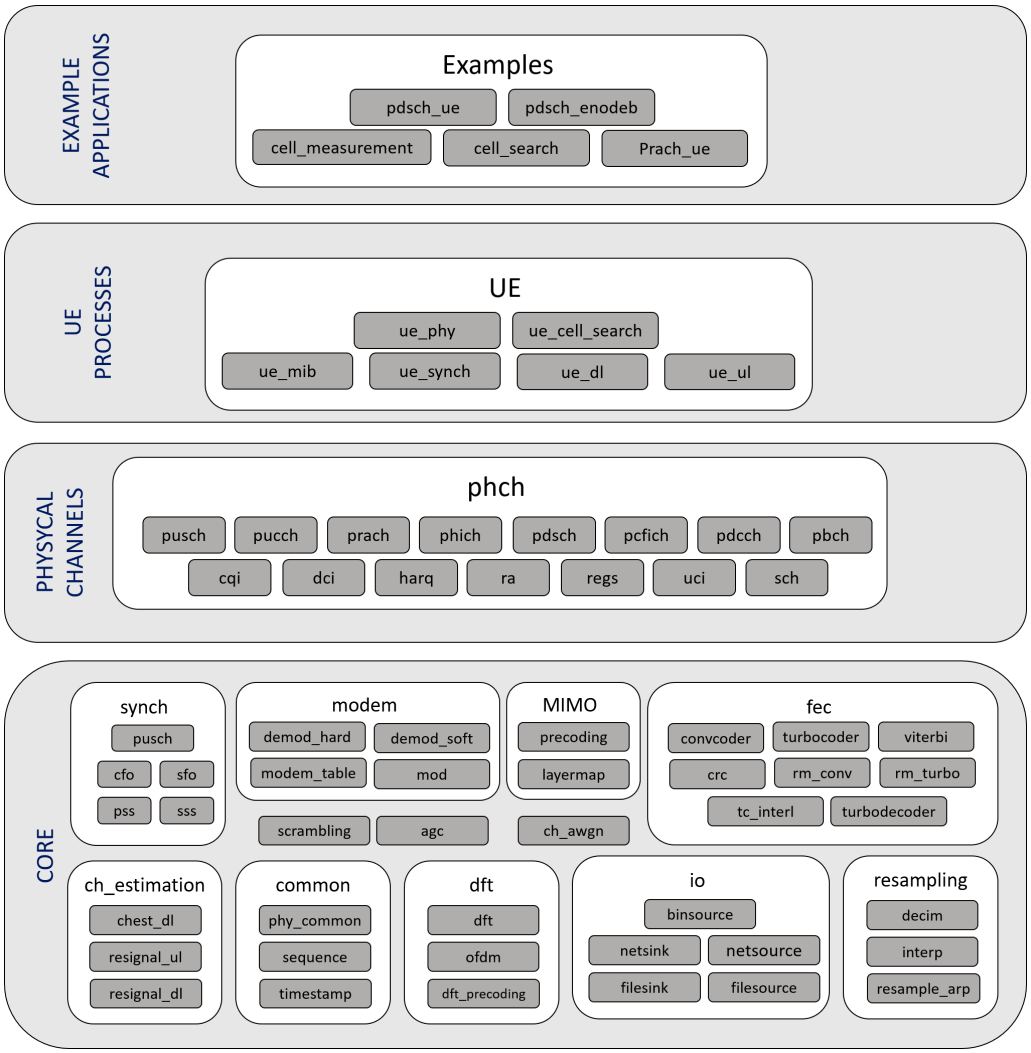

Figure D.1: srsLTE labrary structure

The modules that comprise the srsLTE structure are:

- Core: Inside the core modules one can find the main building blocks responsible for the physical layer of the library, such as OFDM and SC-FDMA processing, demodulators and modulators, channel estimation and so on.
- UE Processes: In this module it is possible to find the code for the physical channel in terms of uplink and downlink functions.

- Physical Channels: Uplink and downlink channel are coded inside this module, with one module for each channel. Each of this modules converts bits into samples and vice-versa, making use of code from the core module.

- Applications: This module implements a series of examples that allow for the use of the library using UE coding, such as receiver application and PDSCH transmitter.

Table D.1: LTE Frequency Bands in srsLTE

Band	Name	Downlink Earfcn - Low	Downlink Earfcn - Low
1	2110	0	18000
2	1930	600	18600
3	1805	1200	19200
4	2110	1950	19950
5	869	2400	20400
6	875	2650	20650
7	2620	2750	20750
8	925	3450	21450
9	1844.9	3800	21800
10	2110	4150	22150
11	1475.9	4750	22750
12	729	5010	23010
13	746	5180	23180
14	758	5280	23280
17	734	5730	23730
18	860	5850	23850
19	875	6000	24000
20	791	6150	24150
21	1495.9	6450	24450
22	3500	6600	24600
23	2180	7500	25500
24	1525	7700	25700
25	1930	8040	26040
26	859	8690	26690
27	852	9040	27040
28	758	9210	27210
29	717	9660	0
30	2350	9770	27660
31	462.5	9870	27760
32	1452	9920	0
64	0	10359	27809
65	2110	65536	131072
66	2110	66436	131972
67	738	67336	0
68	753	67536	132672
69	2570	67836	0
70	1995	68336	132972
71	0	68586	133122

It is possible to execute the eNodeB module in the same machine that runs the EPC module, on a different terminal window which starts the driver corresponding to the SDR device connected to the machine, a USRPB210 in the case shown in figure D.3. The module also contain a $bach$

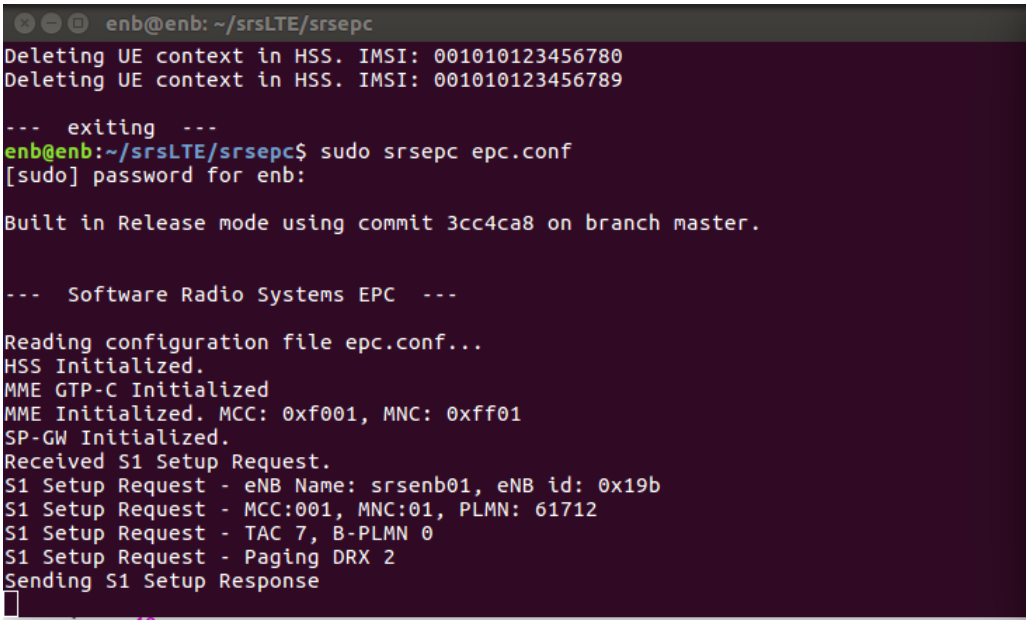

Figure D.2: EPC at machine one

through which it is possible to inform the configuration desired for the eNodeB. Several features can be informed through the configuration file, with the most relevant being:

- enb_id: Identifies the eNodeB via a 20-bits long number, represented in hexadecimal.
- MCC: MCC stands for Mobile Country Code which is specified as hexadecimal number that has the porpuse of identifying the country of the mobile subscriber [84]. This number is define as 1 in srsLTE, but it can be altered to any valid number.
- MNC: MNC stands for Mobile Network Code, which as a unique identification for the network, defined as 01 in srsLTE. The cobination of MCC and MNC constitutes the integrated mobile subscriber identity (IMSI) which is used to identify every subscriber in the network [85]
- n_prb: This parameter specifies the number of Physical Resource Blocks to be used by the eNodeB. It is through this parameter that the eNodeB identifies the bandwidth to be used.
- nof_ports: Specifies the number of antennas used for the transmissions (Tx). By default, in the case of the USRPB210 devices, activating one Tx antenna means that the reception (Rx) antenna of the corresponding channel will also be activated.
- dl_earfcn: This parameter specifies the E-Ultra Absolute Radio Frequency Channel Number which in LTE identifies the carrier frequency and its respective band, fallowing the definitions presented in Table D.1.
- tx_gain and rx_gain: Specifies the gain of the antennas, in dB.

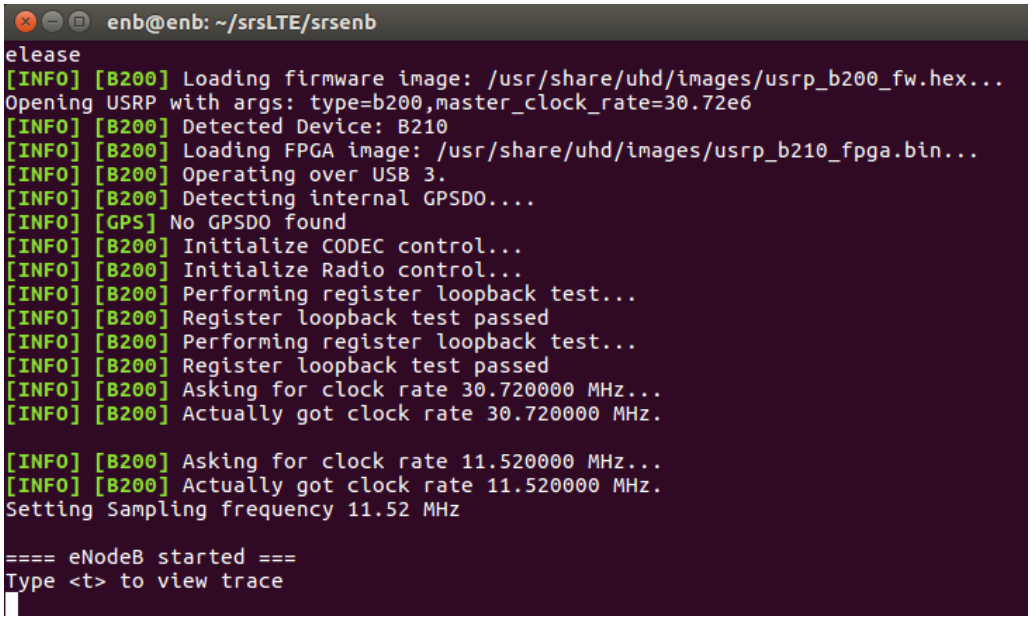

Figure D.3: eNODEB at machine one

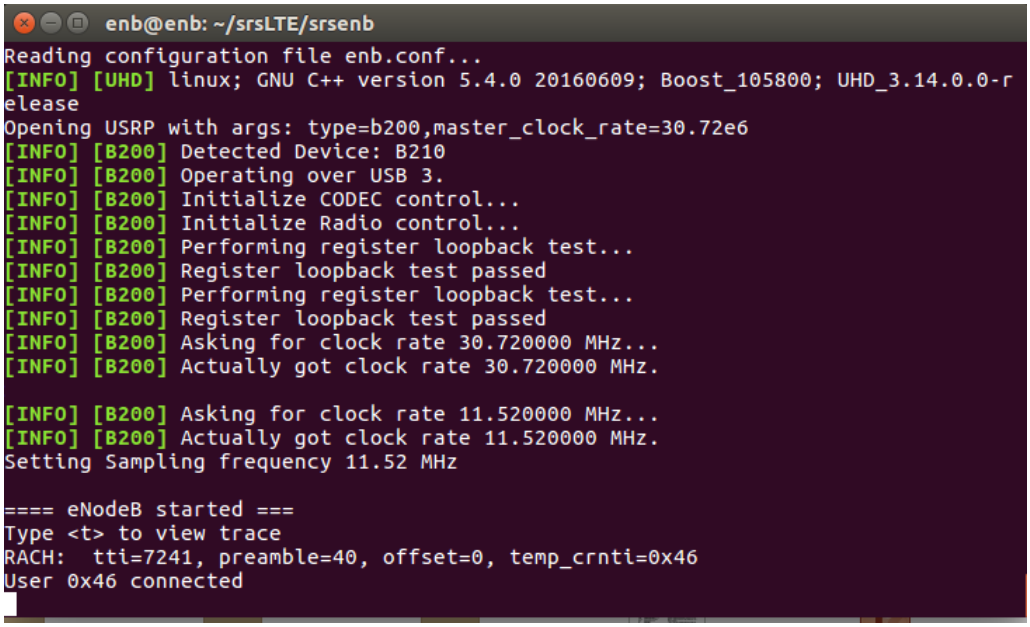

Figure D.4: Connection with UE running on machine two

The UE module should run on a different machine and it can also be used with a SRD device. In case there is a UE device connected to the machine in which the module is running, the device will be initialized and it will first search for active eNodeBs running on the same frequency. In case a cell network ins found, the UE will start the process of identification to perform the connection with the network and, after the connection process has finished, it is possible to visualize a series of information about the communication between the devices, as shown inf figure D.7.

Test field will be performed using the framework of srsLTE and the configurations established

```
==== eNodeB started ===
Type <t> to view trace
RACH:  tti=7241, preamble=40, offset=0, temp_crnti=0x46
User 0x46 connected
t
Enter t to stop trace.

------DL-----------------------------UL-----------------------------------
rnti  cqi    ri   mcs  brate   bler   snr   phr   mcs  brate   bler    bsr
46   9.56     0   0.0   0.0     0%  19.7  40.0  14.3  12.7k     0%    0.0
46   9.08     0   0.0   0.0     0%  20.1  39.3  15.0  12.8k     0%    0.0
46   6.28     0   0.0   0.0     0%  11.9  39.3  10.3  12.9k     0%    0.0
46   5.28     0   0.0   0.0     0%  11.8  37.7  7.67  13.0k     0%    0.0
46   5.88     0   0.0   0.0     0%  11.9  38.7  7.67  13.0k     0%    0.0
46   5.04     0   0.0   0.0     0%  11.7  37.7  8.33  12.9k     0%    0.0
46   5.92     0   0.0   0.0     0%  10.4  38.3  7.00  13.2k     0%    0.0
46   5.40     0   0.0   0.0     0%  9.23  39.7  4.00  9.72k     0%    0.0
46   6.00     0   0.0   0.0     0%  9.49  40.0  4.00  9.72k     0%    0.0
```

Figure D.5: Reading information from UE

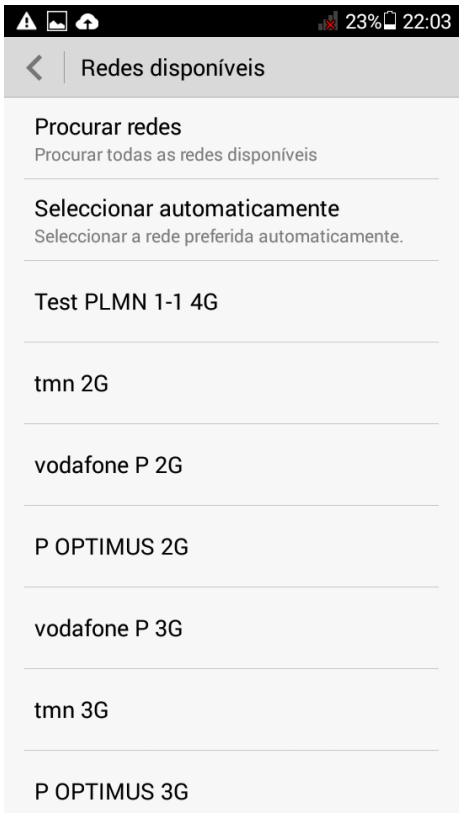

Figure D.6: LTE Test Network in mobile phone

so far to investigate the system´s performance. One will consider the existence of a BS and one interferer, that will be placed at different distances and their heights will be adjusted by means of adjustable shafts, fixed to mobile units to will allow for the quick reconfiguration of the scenario. BS and interferer will be connected to the same EPC, by means of a wireless connection. A USRPB210 will also be used as UE to characterize a scenario where the user is at different distances from the BS, where one will evaluate metrics such as PLR, BER and Throughput, following the methodology proposed in [74]. Results obtained from this analysis

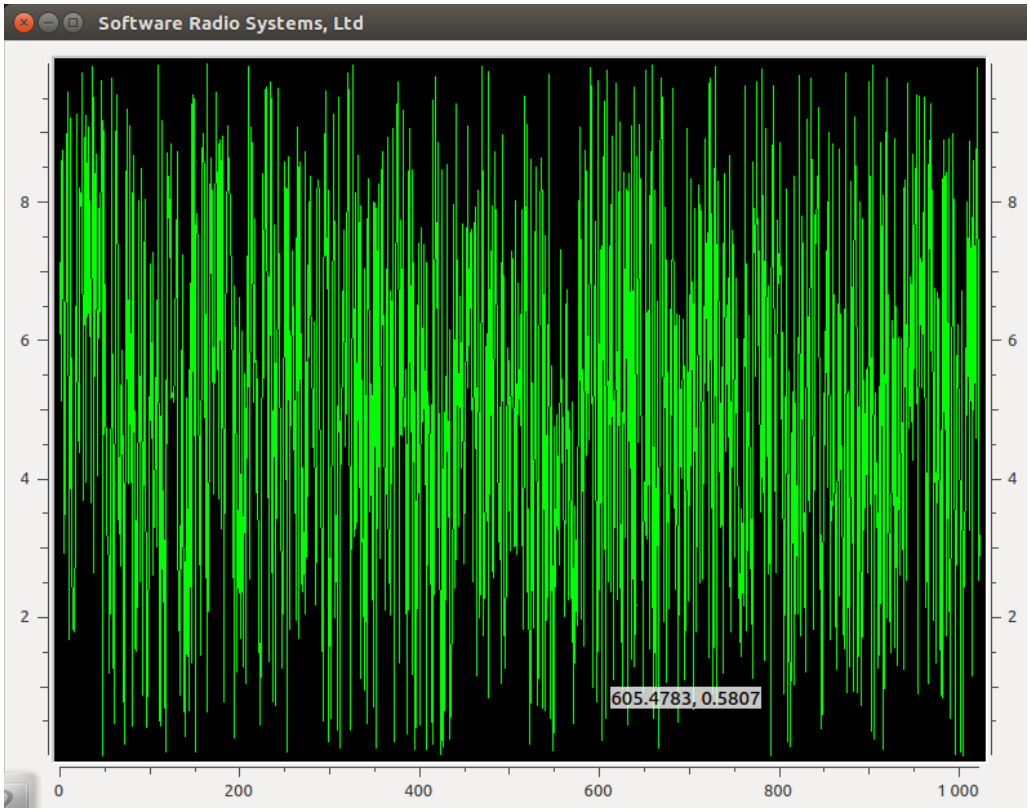

Figure D.7: Plot of signal with srsGUI

will be compared with the analytical results obtained for the Umi LoS propagation model.